CREEP-FEED SURFACE GRINDING

by

Stuart C. Salmon

A Dissertation Submitted for

the Degree of Doctor of Philosophy

at the University of Bristol. September 1979

There is nothing 'good enough'.

Sir Frederick Henry Royce, Bt., O.B.E., M.I.M.E., M.I.A.E.

MEMORANDUM

The accompanying dissertation "Creep-Feed Surface Grinding" is submitted in support of an application for the Degree of Doctor of Philosophy at the University of Bristol.

This work has not been submitted for any other degree at this University or for an award of a degree or diploma from any other institution.

The dissertation is based on independent work carried out by the candidate, all contributions from others are duly acknowledged in the text.

I hereby declare that the above statements are true.

Stuart C. Salmon

Stuart C Salmon

ACKNOWLEDGEMENTS

I wish to express my thanks to Prof. C Andrew and Dr. T D Howes for their assistance and guidance throughout the period of the research work. I am also indebted to all the members of the Grinding Group at the University of Bristol for their involvement in discussions and their constructive criticism.

Thanks are also due to the technical staff of the Mechanical Engineering Department, in particular Mr B Armstrong, Mr F Silk and Mr J Pendlay whose efforts in manufacturing test pieces and modifications to the test rig showed interest, but above all enthusiasm. A special word of thanks must be expressed in memory of Mr P Ackland who built the test rig designed by Dr T V Stuart and who died so tragically at Easter 1978.

I am most grateful to Rolls-Royce Limited for the opportunity given to me to carry out the research, along with their partial sponsorship. Thanks also to the Science Research Council for their sponsorship and the provision of my Industrial Studentship.

Lastly I wish to thank the staff at Rolls-Royce Limited, Derby, in particular Miss E Crampton and Miss Y Harris for draft typing and Mrs P Warrender, Miss J Martin and Miss C Ryan for typing the final version.

SYNOPSIS

The fundamentals of the creep-feed grinding process have been examined with a view to increasing the stock removal rate of superalloy materials.

A limitation of the creep-feed grinding process is workpiece burn. This is caused by 'wear flat areas' on the surface of the grinding wheel which generate rubbing energy, however the research shows that the 'wear flat areas' can be significantly reduced by continuously dressing the grinding wheel with a diamond roller dresser. The reduction in 'wear flat area' and the corresponding reduction in rubbing energy was found to change the partition of energy in the arc of cut, i.e. the proportion of the total grinding energy which is conducted into the workpiece, the chip and the cutting fluid. The majority of the rubbing energy is conducted into the workpiece whereas the remaining cutting and ploughing energy is mostly transferred to the chip and the cutting fluid. This change in the partition of energy allows a higher heat flux to be supported in the arc of cut. The research shows that by continuously dressing a creep-feed (induced porosity, fragile bond) grinding wheel the stock removal rate of the process can be increased by 25 times that of the existing manufacturing method and workpiece burn is completely eliminated. Grinding wheel breakdown becomes the new limitation of the process. Continuous dressing produced similar results with a conventional (no induced porosity) grinding wheel, however the limitation of workpiece burn remained.

A mathematical model of the 'warming-up effect' of the cutting fluid in the arc of cut is presented, based on data from a simulation of the grinding heat flux. The argument of the model is verified empirically showing that the bulk temperature of the cutting fluid has a significant effect on the stock removal capability of the process.

The work includes basic design details for a strain gauged grinding force dynamometer and a microscope-camera for inspecting the 'wear flat areas' on the surface of the grinding wheel.

LIST OF FIGURES

LIST OF PLATES

LIST OF APPENDICES

CONTENTS

CHAPTER 1

INTRODUCTION

One of the most spectacular advances in the development of today's technology is the advent of high strength, heat and corrosion resistant alloys. Their evolution took place to fit the particular requirements of the aerospace industry, however, their applications in other fields are now commonplace, eg., extrusion dies, steel mills and high performance engines. Even though these materials were introduced in the early fifties, many of the problems associated with their machineability still remain today. In general, these 'superalloys' have a tendency to work harden, and the workpiece adopts an abrasive nature due to carbides, which populate the grain boundaries and enhance tool wear (1).* Further to this, their inherent property of poor thermal conductivity causes high temperature gradients across the tool/chip interface and the surface of the workpiece, resulting in tool failure coupled with surface cracking. The metallurgical properties of these 'superalloys' combined with the demands for high surface integrity make conventional machining techniques (milling, drilling, turning and grinding) uneconomic and inadequate when compared with available unconventional methods.

Turbine blades for aero engines are typical superalloy components (see Plate 1). Today the forging of such components has been superceded by precision casting. The blades's aerofoil remains in the 'as cast' condition, however the root and shroud of the blade need to be of such high

---

*Numbers in brackets refer to references given at the end of the thesis.

precision and geometric accuracy that subsequent machining operations are necessary on the cast billet. It is for these reasons that Rolls-Royce Limited adopted creep-feed grinding to machine the blade features.

1.1 Creep-Feed Grinding

Creep-feed grinding is a high stock removal, abrasive machining process (see fig 1). A parallel may be drawn between creep-feed grinding and the milling process; creep-feed grinding replaces the milling cutter with a grinding wheel and takes large depths of cut (1 to 10mm) with a slow feed (around 90mm/minute) in one pass, resulting in high stock removal coupled with a high degree of surface integrity. Creep-feed grinding gains advantage over conventional (reciprocating) surface grinding in that the wheel suffers no intermittent cutting, and a form dressed on the wheel is maintained for a comparitively longer period. Creep-feed grinding is also more efficient than conventional grinding in terms of cutting time, firstly because reciprocating surface grinding suffers from unproductive time cutting air on the overrun at the end of each stroke of the slideway, when it is stopped and reversed. Secondly, with creep-feed grinding, the stock is usually removed in one pass of the workpiece, although it is common practice in the aero engine industry to take a final 'skimming-cut' after dressing the grinding wheel, to ensure a more accurate retention of form and a good surface finish.

Whilst the interest in creep-feed grinding shown by Rolls-Royce Limited is particularly concerned with the

1.1 application of machining superalloys, creep-feed grinding has also proved to be economically viable in the machining of other materials eg. sintered carbides and tool steels (2,3).

1.2 Limitations of the Creep-Feed Grinding Process

The limitation to the stock removal capability of creep-feed grinding superalloys has been shown to be thermal damage to the workpiece (20), sometimes referred to as workpiece burn.

Shafto (20) showed that at the onset of thermal damage there occurs a transition from nucleate boiling to film boiling of the cutting fluid in the arc of cut. This phenomenon has been studied, in the main, with relation to boiler design (95,96,99). The mechanism for nucleate boiling is such that bubbles grow and are shed from the hot surface creating turbulence which enhances the convection of heat into the fluid. A point is reached where the increasing heat flux triggers the transition from nucleate boiling to film boiling. When film boiling occurs the hot surface is completely shrouded by a vapour film and the heat transfer can only take place by radiation through that film. At this point of breakdown in heat transfer a large proportion of the heat generated by the grinding process is conducted into the workpiece and the workpiece burns. This limiting heat flux is often termed the 'burn-out heat flux'.

Malkin (5) postulated a theory for conventional grinding which suggests that the percentage 'wear flat area' on the surface of a grinding wheel dictates the

1.2 amount of energy entering the workpiece as heat. Malkin partitioned that energy into components of rubbing, cutting and ploughing energy and postulated that the cutting and ploughing components remain at a constant level, the rubbing energy increasing in direct proportion to the increase in 'wear flat area' until workpiece burn occurs (see fig 4).

It would seem from Malkins work that by controlling the 'wear flat area' on the surface of the grinding wheel the heat generated by the process can be influenced in order to minimise the heat flux in the arc of cut.

Stuart (4) showed that by continuously dressing a grinding wheel whilst grinding there is a significant drop in cutting forces, and postulated a corresponding drop in energy to the workpiece.

Combining the work of Shafto, Malkin and Stuart it might be expected that by using continuous dressing to control the 'wear flat area' on the grinding wheel, the heat flux could be reduced, allowing the stock removal rate to be increased.

Powell (6) has shown that the application of the cutting fluid into the porosity of the grinding wheel enhances the heat transfer capabilities of the fluid and that the correct application of the cutting fluid in the creep-feed grinding process is most important. Powell also showed, by simulation, that there exists a warming-up effect of the cutting fluid as it moves around the arc of cut. It would therefore seem that the heat flux at burn-out is likely to be influenced not only by the bulk temperature of the cutting fluid but also the length of the arc of cut, having a corresponding

1.2 effect on the stock removal capability of the process.

1.3 Objectives

The partition of energy, in particular the amount of the total grinding energy which flows into the work-piece, raising its temperature to the point of the onset of thermal damage, has been shown to be critical in the conventional grinding process (5). This partition of energy theory will be examined for the creep-feed grinding process, particularly when the grinding wheel is continuously dressed.

The application of the cutting fluid in creep-feed grinding has been studied theoretically and by simulation at the University of Bristol by Powell (6). This work will be mathematically modelled for the real grinding situation and used to provide guidelines for a series of grinding tests in order to examine the warming-up effect of the cutting fluid in the arc of cut.

It is the overall aim of the research work to examine the creep-feed grinding process with a view to removing superalloy stock faster than current industrial practice and still maintain a high degree of surface integrity.

An ecomomic case study of the creep-feed grinding process will be presented in order to highlight design features relevant to the next generation of creep-feed surface grinding machines.

CHAPTER 2

A SURVEY OF THE PUBLISHED LITERATURE

The object of the research work reported in this thesis is to investigate the creep-feed grinding of superalloys in order to increase the stock removal capability of the process. The limitation to high stock removal rates with these alloys is generally seen as thermal damage to the workpiece. This is especially so in cases where the workpiece material is sensitive to localized surface temperature changes which can cause deleterious effects in the micro-structure.

It is the intention of this chapter to discuss previous work concerned with the grinding process, in particular that related to high stock removal abrasive machining.

2.1 Thermal Aspects of Grinding

Many authors have mathematically modelled the thermal aspects and the energy balance of the grinding process. All bar a few (7) base their analysis on the 'moving heat source theory' of Jaeger (8). The model which is felt to be the most developed and therefore the closest representation of the 'real situation' is that of Des Ruisseaux and Zerkle (9,10,11). Their model considers the workpiece to be subjected to a continuously acting distributed heat source, rather than modelling the system at individual grit level (12), and accounts for the surface cooling of the workpiece. The model verified empirically, showed that a maximum 20 to 40% reduction in surface temperature is possible when using a water based cutting fluid, emphasizing the necessity

2.1 for the inclusion of the cooling term. Other models exist (15,16) along with theories concerning the cut-off process (17,18) which has been reported to be closely related to creep-feed grinding (19). The only model known to the author, directly related to the creep-feed grinding process is that of Shafto (20) where a finite element analysis was used to relate experimentally measured temperature profiles to the 'real situation'.

A number of authors have measured the 'temperatures in grinding' by a variety of techniques (21,22,23), however in many cases the temperatures which they sense are not clearly defined. It is possible that the 'temperatures in grinding' could be those in the shear zone at individual grit level, those of the abrasive grits themselves, the mean temperature in the arc of cut, the temperature of the surface layers of the workpiece or the bulk temperature of the workpiece. It is therefore difficult to realise which temperature is being measured (24,25,26,27,28,29), however the authors do discuss how the 'temperatures in grinding' that they measured, affect the surface and cause structural changes in the workpiece material.

Investigators have deliberated over the partition of energy in the cutting zone with little agreement. Outwater and Shaw tabled an energy split (see fig 2) which highlights a partition of energies that is crucial to any thermal analysis i.e., the amount of heat entering the workpiece and the amount of heat given up to the surroundings, grinding wheel, cutting fluid, chips etc. Maris et al (30) tabled six authors'

2.1 partition of energy figures (see fig 3). It will be seen later (section 2.3) from the work of Malkin that the 'wear flat area' on the grinding wheel is of prime importance when considering the amount of heat transferred to the workpiece. Hahn and Lindsay (31) showed that the real contact area between the grinding wheel and the arc of cut for the conventional grinding process, is around 1 to 3% of the geometric arc of contact.

2.2 The Cutting Fluid

The presence of a cooling medium in the arc of cut which has the ability to dissipate the heat, generated by the process, more efficiently than air, has been shown in theory to reduce significantly the surface temperature of the workpiece (9,10,11). Good heat dissipatability is not the only property of a cutting fluid by which to judge its suitability. The lubricating ability can reduce the generation of friction energy so that the intensity of the thermal energy in the arc of cut is low (32). This ~~dilema~~ dilemma is the root of the choice between the use of water based cutting fluids (good heat dissipatability) and neat oils (high lubricity) (33). Further to the argument is that of chemical reactions in the cutting zone (34) e.g. Duwell et al demonstrated that oxygen is essential to the grinding process, without it grinding is impossible (35). However in improving the grindability of some materials by chemical additions to the cutting fluid deleterious effects in the surface of the workpiece can arise (36, 37). Two detrimental effects away from the cutting

2.2 zone which also need careful consideration are firstly the dermatological reactions on the machine tool operator (38) and secondly the corrosive effects on the machine tool itself.

The cutting fluid chosen for the research undertaken in this thesis is a synthetic water based cutting fluid (Edgar Vaughans' Houghtogrind 55). All previous work on creep-feed grinding at Bristol has been conducted using this fluid, so for reasons of standardisation the cutting fluid used in the research was not changed (39,40).

Once the most favourable cutting fluid has been chosen the next question is how to apply it in order to ensure its presence in the cutting zone. Many authors report that a rotating grinding wheel drags a layer of air around its periphery which can act as an impenetrable barrier to flood application methods (41,42,43,44). The higher the wheel speed the more difficult becomes the application of cutting fluid. High pressure jets have been used to penetrate the 'air barrier' (45,46,47,48) and efforts have been made to scrape the layer of air away from the surface of the grinding wheel to assist the 'take-up' of cutting fluid into the surface pores of the grinding wheel. Further attempts to force the cutting fluid into the cutting zone have been to dress helical grooves in the grinding wheel (49,50). The advent of creep-feed grinding caused a special grinding wheel to be manufactured. A creep-feed grinding wheel is usually a very soft grade (E,F or G) with induced porosity to create swarf clearance for the long chip and allow a considerable amount of cutting fluid to be 'taken-up'

2.2 into the voids between the abrasive grits (see plate 2). Because of the inherent porosity of vitrified grinding wheels, more so with creep-feed grinding wheels, investigators endeavoured to introduce the cutting fluid into the pores of the wheel by a variety of methods (51,52, 53,54) with varying degrees of success. Following Powells example (6) it was decided to adopt the 'shoe system' (see plate 3 and 8) on the research rig used for the work reported in this thesis. Cutting fluid is supplied to the shoe at a pressure of around 2b with a flow rate of ~~6ls.~~ 6 ls^{-1}. Powell modelled the flow of the cutting fluid in the porosity of the grinding wheel and demonstrated that an accurate prediction for the 'patternation' of the grinding fluid in the shoe/wheel/arc of cut system can be made from fundamental fluid dynamic considerations. Powell explored the film boiling theory of Shafto using a heating element to simulate the energy released from the grinding process, and showed that with a block heat input to the arc of cut the cutting fluid appears to warm up as it moves around the arc of cut (56).

The implication of this aspect of Powell's work will be examined in the real grinding situation and reported later in the thesis.

2.3 Degeneration of the Grinding Wheel Surface

There are a number of reasons which might cause a grinding wheel surface to be unsuitable for grinding and result in workpiece burn: i) Poor application of the cutting fluid, leading to loading and clogging of the grinding wheel, ii) Dressing too finely or dwelling a diamond roller dresser on the grinding wheel creating

2.3 'glazing' of the grinding wheel surface, iii) Even a correctly dressed grinding wheel will eventually degrade (58) by the attritious wear of the abrasive grits themselves (59,60,61,62,63). Examining these deleterious effects it will become apparent that there exists a common denominator - 'flats' on the surface of the grinding wheel (5,64). Prior to any discussion on Malkins Wear Flat Area Theory, it will be useful to describe the mechanism of the grinding process.

The grinding mechanism at grit level, is composed of three basic components; cutting, rubbing and ploughing (65,66). If each grit behaves like the single tooth of a milling cutter then an analogy can be drawn between grinding and 'micro-milling' (see Appendix 3). From the analogy it can be seen that even in creep-feed grinding, the grit depth of cut is extremely small (in the order of 10^{-5}mm). The inhomogeneities within the bulk of a metal which are responsible for reducing the strength of the material e.g., grain boundaries, crystal defects and impurities, play a major part in the slip process by which they deform. However the individual grit depth of cut of the grinding process can be such that the deformation due to the shearing action takes place between the inhomogeneities, giving rise to a higher specific energy than would be expected from a macro-machining process e.g., single point turning where the cutting tool is performing a similar stock removal action but shearing within the bulk of the material. This is known as the 'Size Effect' and has been explored by a number of authors (67,68,69).

2.3 It has been shown (57) that a typical abrasive grit removes material in the following manner: As the infeed increases the force on the grit will take up any elastic deformation between the wheel and workpiece (14) until the force is great enough to rupture the surface of the workpiece. A groove is ploughed into the surface throwing up a burr on both sides of the groove (no material has yet been removed) (66). The increasing grit depth of cut and corresponding increasing force will reach a stage where a chip will form and shearing and cutting will take place. This diary of events will continue until the grit begins to wear and a flat will develop on the grit parallel to the arc of cut. From this point on, not only will cutting and ploughing take place but also rubbing of the 'wear flat' across the ground surface. With certain grinding wheel/workpiece combinations atomic affinities between elements can occur and cause the workpiece material to adhere to the abrasive grit. The workpiece material welds onto the grit and builds up in successive layers causing loading patches (70) to develop. These loading patches are seen as yet further flats on the active surface of the grinding wheel to enhance the rubbing energy.

Malkin (5) showed that the heat energy input to the workpiece was directly proportional to the 'wear flat area' on the surface of the grinding wheel (see fig 4). Two assumptions were made; i) that by extrapolating the linear relationship in figure 4 to zero percentage 'wear flat area', the result is a value for the cutting and ploughing energy separate from the rubbing energy, and

2.3 ii) that the amount of cutting and ploughing energy remains constant, however with increasing 'wear flat area' the amount of rubbing energy increases in proportion and adds to the cutting and ploughing energies. The total amount of energy entering the workpiece as heat increases as the wear flat area increases until workpiece burn occurs.

2.4 Dressing the Grinding Wheel

A grinding wheel surface can be prepared for grinding by a number of techniques (71,72). The 'micro-milling' analogy (Appendix 3) in combination with the wear flat theory can be used as a guide to the choice of dressing method. To achieve a good surface finish the stock removal rate has to be sacrificed. By allowing the grinding wheel to develop 'flats' the increased rubbing area will provide a high degree of finish as the active area of the grinding wheel is increased (73,74) for high stock removal the grit must be sharp, the presence of 'flats' will cause high rubbing energy and workpiece burn, however, equally important is the accurate retention of form on the surface of the grinding wheel.

Diamond roller dressers are widely used in industry to dress creep-feed grinding wheels particularly in the manufacture of turbine blades ~~where~~ where the form retention is essential. The grinding wheel is at its sharpest directly after dressing (75) and it would seem advantageous to maintain that sharpness by continuously dressing the grinding wheel whilst grinding. This was explored in the 1950's (76) when diamond roller dressers were in their infancy. The process was unsuccessful due to the inability

2.4 to hold the position of the diamonds within a fine tolerance during the sintering process when manufacturing the dressers. Hence the diamond roller dressers of the day could not produce a profile on the grinding wheel to the required standard of accuracy for use in the aerospace industry. The work of Stuart (4) has shown that continuous dressing and creep-feed grinding in the 1970's can provide a drop in the specific energy and therefore the potential to increase the stock removal capability of the process (see fig 5).

2.5 <u>High Stock Removal Grinding</u>

It has been shown that grinding with high peripheral wheel speeds reduces the grinding forces and produces a high degree of surface finish (77,78,79,80). Increasing wheel speed effectively decreases the chip depth of cut for a constant workpiece infeed rate, increasing the frequency of the number of active grits passing through the arc of cut. An increase in productivity can be achieved with high speed grinding by maintaining a constant cutting geometry. This can be done by increasing the workpiece infeed rate in direct proportion to the increase in wheel speed (81,82,83,84). Stuart however, showed that high wheel speeds associated with creep-feed grinding created more rubbing energy than lower wheel speeds and hence a lower stock removal rate before the onset of thermal damage to the workpiece (4). In the authors experience industry tends to adopt the slow wheel speed approach (85), most creep-feed grinding operations on difficult-to-machine materials are performed little above 18 ms^{-1}.

2.6 Summary

The literature survey has brought together, in the main, previous work of Shafto, Malkin, Stuart and Powell:

It would seem that by continuously dressing the grinding wheel whilst grinding, the stock removal rate of the creep feed grinding process can be increased in direct proportion to the drop in specific energy until the maximum heat flux is exceeded and thermal damage occurs, according to Shafto and Stuart. However, when a grinding wheel is sharp and has few 'wear flat areas', a greater percentage of the heat generated by the process goes off into the chip and to the surroundings so that the amount of the total grinding energy, conducted into the workpiece as heat, is small. A dull grinding wheel which has large 'wear flat areas' exhibits a particular partition of energy where a much greater proportion of the total grinding energy is conducted into the workpiece, this rapidly increases the surface temperature of the work-piece and results in workpiece burn. Should the 'wear flat area' theory apply to creep-feed grinding then it can be expected that the stock removal rate of the process, when combined with continuous dressing, will be even greater than the proportional drop in specific energy level expected from the work of Shafto and Stuart.

The simulation of the heat transfer characteristics in the arc of cut by Powell, showed a warming-up effect of the cutting fluid as it moves around the arc of cut, however, depending on the heat input profile around the arc of cut (Powell used a block profile) and the bulk temperature of the cutting fluid entering the grinding zone,

2.6 the burn-out heat flux (ref. Shafto) is likely to change and therefore influence the stock removal capability of the process.

The above summary therefore, provides the basis for the hypotheses of the research.

CHAPTER 3

EXPERIMENTAL APPARATUS AND MODIFICATIONS TO THE RESEARCH RIG

Figure 6 shows a block diagram centred on 'the grinding process' and surrounded by the factors which influence the process. The diagram has been completed with particular reference to the area of work reported in this thesis. It is the object of this chapter to discuss in detail, each of the block inputs to 'the grinding process' as shown in fig.6.

3.1 The High-speed Creep-feed Grinding Rig

The specification of the High-speed Creep-feed rig can be found in Appendix 1. Stuart (4) built a prototype high-speed creep-feed grinding rig of high stiffness for the purpose of investigating creep-feed grinding at high peripheral wheel speeds (see plate 4). The rig was not immediately suitable for the high stock removal test programme envisaged, and coupled with its poor reliability it was necessary to make a number of modifications to the rig. The details of these modifications are described in the following sections.

3.2 The Hydrostatic Bearings

The high-speed creep-feed rig suffered from heavy leakage of hydrostatic oil both into the cutting fluid and to the surroundings. In addition, for experiments which necessitate a high cutting fluid flow rate, the guard box would fill up with cutting fluid which would leak past the V-ring seals on the main spindle bearing and into the low pressure oil drain of the bearing, contaminating the hydrostatic oil.

3.2 The main spindle bearing was therefore dismantled and the V-ring seals, which were worn, were renewed. The build-up of cutting fluid in the guard box was alleviated by enlarging and re-routing the drainage path for the cutting fluid back to the supply tank. These modifications had a two fold benefit, not only were the leaks abated but the heavy oil contamination of the cutting fluid was eliminated. A close control was kept over the condition of the cutting fluid so that a consistent 60:1 dilution was used throughout the research programme.

After a series of high stock removal tests the slideway became tight to the point of seizure. The fault was thought to have been due to one of two reasons:

(i) the ball screw drive may have become contaminated with foreign matter, or

(ii) the hydrostatic slideway/thrust bearings may have seized.

The drive to the ball screw was dismantled. The ball screw and a nearby low pressure oil drain were contaminated however the ball screw functioned perfectly. There appeared to be signs of seizure on the faces of the hydrostatic thrust bearing, these were removed in situ using a fine hand file, thus avoiding a major dismantling of the rig. The hydrostatic slideway pad bearings were checked separately from the thrust bearing by disconnecting the high pressure oil supply to the thrust bearing and checking the movement of the slideway. The slideway functioned satisfactorily, however it was found that inspection of the hydrostatic restrictors was impossible without dismantling the main superstructure of the rig.

3.2 For this reason the restrictors were not examined. A second seizure of the thrust bearing towards the end of the research period prompted its replacement by a roller thrust bearing (see fig 7). The reason for designing the rig with a hydrostatic thrust bearing was to achieve a high dynamic stiffness. The pre-loaded roller thrust bearing which was substituted for the hydrostatic bearing detracts little from the overall stiffness yet substantially increases the reliability of the system. A test to check the repeatability of grinding test results showed no discernable difference between the type of bearing used on the slideway drive.

3.3 Transmission

The high-speed creep-feed grinding rig was designed with a range of work speeds (infeeds) from 1.8 to 81 mm/min. at 30 ms^{-1} wheel speed (at 1000 rev/minute). It was essential to keep the cutting geometry constant at a depth of cut of 3 mm for a series of high stock removal tests. This meant that the increase in stock removal rate could only be achieved by increasing the work speed. The maximum infeed rates required however were soon found to be outside the designed range of the rig.

The drive to the ball screw nut is achieved through a chain of gear boxes linked by toothed belts and pulleys to the wheel spindle (see plate 5). To alter the available range of speeds the toothed belts and pulleys had to be changed, this necessitated a different centre distance for each pulley down the line of gearboxes. Slider plates were manufactured and fitted beneath each gearbox to allow the centre distance to be varied and so

3.3 accommodate different combinations of belts and pulleys.

The slideway drive was originally transmitted from the gearbox through a "Bibbigard" torque limiting clutch to the ball screw nut. The clutch was a safety device. In the event of the slideway 'running-on' and imposing an excessive load on the ball screw or the thrust bearing, the torque limit on the clutch would be exceeded and the clutch would disengage, protecting the ball screw and the thrust bearing from damage. The clutch was found to be unreliable, especially at high speeds it would stick and not disengage leaving the ball screw and thrust bearing unprotected. The complete transmission of the drive from the gear boxes to the ball screw nut was redesigned.

The method used by Stuart to engage and disengage the feed at the start and end of each test was to run the rig with the slow speed gearbox selected 'between gears'. The feed would be started by crashing the gears into mesh and then out into the neutral, 'between gears' position at the end of the test. With the work speeds envisaged in this work to be in excess of 1m/minute, crashing the gears would be unsatisfactory. Typically, a high stock removal test would take only 4 seconds, allowing little time for engaging and disengaging the drive.

To protect the ball screw nut and thrust bearing an automatic cycle was designed using an electro-magnetic clutch and a system of limit switches to engage and disengage the slideway drive. The automatic cycle is achieved by two limit switches which cut the

3.3 supply to the clutch as the slideway approaches the end of its travel. Two manually operated switches control the cycle, one completes the circuit to engage the clutch at the beginning of a test and the other is an override for inching the bed to position the specimen with respect to the grinding wheel (see fig 8)

3.4 The Diamond Roller Dressing Unit

The original diamond roller dressing unit was prone to frequent seizures. Many modifications were carried out on the original unit. However the cost of repairs in time and money eventually led to the old unit being scrapped and a new one designed and manufactured.

The original dresser was mounted between two independent bearing housings, the DC driving motor was located in a fixed position remote from the dresser and transmitted the drive via a double universal jointed shaft which allowed for the misalignment in the system when the dresser fed into the grinding wheel. A possible reason for seizure of the dresser was excessive vibration from the shaft misalignment which caused the independent bearing housings to move, consequently the angular contact bearings ran out of line and ~~siezed~~ seized. There was also ingress of abrasive debris into the labyrinth seals which seized on the sealing lands. A new dressing unit was designed with the following points in mind:

(i) The bearing housings should be made from one block of material and be machined in line to ensure concentricity, parallelism and precision fits.

3.4 (ii) The driving motor should be mounted so that it runs in line with the dresser at all times.

(iii) V-ring seals should supercede the labyrinth type.

(iv) The new design should fit within the constraints of the existing rig with no alterations to the super-structure.

The new dresser unit (see plate 6) was machined from a single block of mild steel which was stress relieved after the machining operations prior to finish grinding. V-ring seals were used throughout the design in a stationary mode (i.e. fitted to the housing, not the shaft) so that they were unaffected by centrifugal force. However, the dresser consumed more power at high speeds using this method of sealing. Kluber grease, type NBU15 was used to lubricate the bearings for its high temperature, low drag, long life properties. The dresser was 'run-in' on a lathe and taken up to 6000 rev/minute where its stable running temperature was 70^{o}C in air, the bulk of the heat being generated by the V-ring seals. In service the dresser runs in an atmosphere cooled by the cutting fluid (see plate 7) so that thermal cycling is kept to a minimum. A more powerful motor was required to drive the new dresser because of the stationery V-ring seals, so the DC control circuit was rebuilt to cope with the increase in current.

3.5 The Cutting Fluid and its Application

The cutting fluid used throughout the research work has been Edgar Vaughan's Houghtogrind 55 diluted with tap water at 60:1. The filtration and delivery of the cutting fluid is performed by a Darenth system coupled to a Worthington-Simpson two stage centrifugal pump which delivers 6 ls^{-1} at 10b at full power. The tank capacity is 1025 litres. A complete turn over of the cutting fluid at full flow takes place every three minutes, hence the temperature of the cutting fluid is closely monitored as there is no refrigeration.

The cutting fluid is forced into the porosity of the grinding wheel by means of a shoe which is kept in intimate contact with the grinding wheel. The shoe length is of dimensions calculated to ensure flood conditions in the arc of cut (6). The original shoe tended to bounce on the surface of the grinding wheel and transmit a vibration to the force measuring equipment. A stiff and functional system is important especially when continuously dressing the grinding wheel. When continuously dressing, the wheel diameter is continuously decreasing therefore in order to maintain the pressure of cutting fluid in the shoe, the shoe must be kept in close contact with the grinding wheel surface. A new shoe holder and adjusting mechanism was therefore designed (see plate 8) which allowed the shoe to be fed into the grinding wheel whilst grinding.

3.5 The consumable shoe itself is new, designed for easy replacement with particular attention to safety and the ability to change a shoe without having to remove the grinding wheel. Within the constraints of the research rig the cutting fluid shoe was chosen to be consumable, however this need not be the case for a production machine tool.

3.6 Grinding Wheels

Two types of grinding wheel were used in the research work, both manufactured by the Universal Grinding Wheel Company Limited (see Appendix 1 and Plate 2).

(i) a creep feed grinding wheel - WA 60 80 FP2V and (ii) a standard wheel - WA 60 KV.

It is difficult to manufacture grinding wheels with large diameter/width ratios, especially when the bond is of the fragile nature associated with creep-feed grinding wheels. The grinding wheels supplied by the manufacturers were 50mm wide, however they were necked down to 25mm wide for a radial distance of 50mm around the wheel periphery. The maximum specimen width was 7mm and the dresser, for reasons of cost, was 28.47mm wide. Furthermore the cutting fluid is injected into the porosity of the grinding wheel, the power required to accelerate the cutting fluid to wheel speed at the entry from the shoe increases in proportion to the width of the shoe. Hence both the grinding wheel and shoe widths were restricted in order to keep the power consumption to a minimum.

3.6 The sides of the wheel at the 25mm width were coated with a silicon-rubber based compound, 'Marine' manufactured by Dow Corning. The compound prevents side leakage of the cutting fluid from the porosity of the wheel and conveniently makes the cutting fluid flow calculations two dimensional and therefore easier to manipulate.

The main difference between the two grinding wheels is that the creep-feed wheel has induced porosity brought about by the inclusion of naphthalene particles of a known size in the grit and bond mix. The wheel is pressed in the same way as an ordinary wheel however, the naphthalene is removed in an oven prior to firing the wheel. The result is a very porous structure wheel (see Plate 2).

3.7 Specimen Materials

Two specimen materials were used in the research, both superalloys, initially C1023, a Nimonic alloy was used. This had been a standard material used by previous researches (4,20,55) and was therefore a sound material for proving the rig modifications and re-establishing ~~datums~~ data. C1023 is not widely used now in aero engines whereas Mar M002 is the latest turbine blade material and reported to be the most awkward to machine. Mar M002 is almost totally machined by the creep-feed grinding process, there being few alternatives. Both materials are used in the 'as cast' condition, their specifications can be found in Appendix 1.

3.7 Although the main drive motor is rated at 35kW the amount of energy required to machine these materials means that a limit has to be put on the width of the specimens to avoid stalling the motor. Each nimonic type specimen was machined to 5mm $\pm$ 0,25mm wide although a 7mm width specimen was originally used by Stuart for tool steel specimens.

CHAPTER 4

INSTRUMENTATION AND MEASUREMENT

4.1 The Grinding Force Measurement System

A new dynamometer was designed and manufactured at the beginning of the research period. The need for a new dynamometer arose due to the inadequacies of the existing model. Stuart reported that the existing dynamometer suffered from the ingress of cutting fluid and the detachment of strain gauges. This caused spurious force values and the need to recalibrate the dynamometer at frequent intervals. Inspection of the dynamometer and its location in the rig revealed that the loading and setting of specimens could be inaccurate. The operator was required to place a hand inside the guard box and behind the grinding wheel in order to tighten the specimen. The cramped nature of the guard box made the securing of the specimen a difficult and hazardous task. The specimen was located in the dynamometer using packing pieces to set the depth of cut and a jig to position the specimen with respect to the load beams. When tightening the specimen in the dynamometer the specimen could rock due to the twisting motion of the securing bolts (see fig 9). Hence, the dynamometer, being a fundamental instrument in the research programme, was redesigned with the following points in mind:-

(i) Reliability; the dynamometer should function without fear of ingress of cutting fluid or the need to calibrate at frequent intervals.

4.1 (ii) Accuracy; the specimen should be pre-set in a fixture outside the rig and located in a known datum position in the rig.

(iii) Safety; the loading and securing of the specimen should be performed from the front of the rig and should not require any adjustment from behind the grinding wheel.

(iv) Performance; a dynamometer for measuring cutting forces should have high stiffness and a high natural frequency (91,92). Improvements along these lines would be an extra bonus.

For high stiffness and minimal cross coupling, piezo-electric load cells are ideal, however their cost and the cost of their associated instrumentation would have been prohibitive. The gain in stiffness offset against cost and sophistication would not necessarily offer an equivalently better dynamometer. It was decided to manufacture the load cells as short necked beams with strain gauges of the foil type to measure the strain in each beam. The bridge amplifiers and associated instrumentation necessary for this system of measurement were already in existence and previous experience in the field of strain gauged systems was greater than that for piezo-electric load cells (1).

The tests carried out by Stuart gave good estimates for the expected force values, hence the dynamometer beams could be designed to be as stiff as practically possible. Should a similar failure rate of load beams exist due to the ingress of cutting fluid with the new design as with the old, the removal and replacement of

4.1 load beams was designed to be quick and easy. Each beam was sealed against the ingress of cutting fluid and the bombardment of grinding debris with an aluminium can and 'O' ring (see Appendix 2 and fig 10). Five identical beams were manufactured and all were installed with foil strain gauges of the EA 06 125 TG 350 type manufactured by Micro Measurements Incorporated. After the gauges had been attached the beams were thermally cycled to check their installation. Thermal cycling expands any air trapped beneath the strain gauge matrix. Monitoring the strain gauge output during the thermal cycle will show non linearity and a zero shift if the strain gauge is badly installed. The insulation of the strain gauges was checked to ensure that a resistance in excess of 1MΩ existed between the strain gauge and the load beam at a potential of 12 V. The strain gauges were connected to form a temperature compensating 4-way bridge with the active strain gauges positioned on the centre lines of the load beams (see Appendix 2).

The mechanics of the new dynamometer are such that the specimen is loaded into a shuttle and pre-set on a dummy dynamometer platform identical to the real dynamometer but remote from the working area. The specimen is clamped in the directions of the forces being measured, which was not the case for the original dynamometer. The shuttle is then loaded into the dynamometer and tightened against a wedge. Access is required from the front of the rig only (see Plate 3).

4.2 Calibration of the Dynamometer

It is not practicable to calibrate the dynamometer inside the rig due to the confined space in which to apply the load. The dynamometer was therefore clamped on a mock machine bed which was a very stiff steel beam. ~~A mock machine bed was a very stiff steel beam on which the dynamometer was clamped~~. The calibration loads were applied to a dummy workpiece clamped in position on the dynamometer platform (see fig 11). A cradle carried the weights, and the load was transferred to the dummy workpiece via a hardened steel ball on a linkage located on the vertical centre line of each beam so that purely vertical loads were applied. The dynamometer was set in the horizontal position with a spirit level and the two vertical beams were calibrated. The dynamometer was then clamped to an angle plate and turned through 90^{o} where the horizontal beam was calibrated. A stabilized bridge input voltage of 10V was used and the ouput was monitored on a micro-voltmeter which eliminated any amplifier/filter instrumentation interference.

The dynamometer was calibrated for both compressive and tensile forces. The first calibration did not prove successful as the slopes of the force/deflection relationship between the tensile and compressive readings differed. The likely cause of the difference was felt to be due to non linear joint stiffness. It was therefore decided to eliminate as many joint surfaces as possible. The aluminium cans were removed, the dynamometer modified and reassembled with jointing compound. The benefits were slight, so a thin shim was inserted between the surfaces of the dynamometer and

4.2 each load beam to act as a pre-load on tightening the fixing screws. The mismatch in calibration between compressive and tensile strains was still present. It was decided to sacrifice the 4 screw system and increase the number of fixing screws/surface area ratio. As a precaution provision had been made for the dynamometer and load beams to take a 12 screw system instead of the newly designed, "quick beam change" system of 4. The modified dynamometer then calibrated satisfactorily to a mismatch in compressive to tensile strain of slightly over 4%. The ingress of cutting fluid was again a potential problem as the aluminium cans had been sacrificed. The load beams were coated with a Bostik coating - Bostik 2114; a polysulphide synthetic rubber which is a tenacious compound with a great deal of flexibility and resistance to edge-peeling. The load beams were then packed with 'Marine' - a silicone rubber compound manufactured by Dow Corning. The whole dynamometer was then given a liberal spray of Holts 'Damp Start'. A recalibration showed that the protective packing had not affected the dynamometer characteristics.

The dynamometer was recalibrated three times during the research period to check for drift, and showed less than 2% drift over the complete test programme.

4.3 The Grinding Force Data Recording Instrumentation

The dynamometer, having been calibrated to a micro-voltmeter was linked to the Amplifier/Filter system used by Stuart. The force trace on a U-V recorder exhibited a low signal to noise ratio. A series

4.3 of earth loops were eliminated and the strain gauge leads were screened. It was found that the DC Amplifiers with their own built-in bridge supply were interacting with each other through the filter unit. It was the changing of the bridge supply voltage to one beam that caused the remaining two beams to react sympathetically. It was therefore decided to reinstrument the complete Data Recording System so that each load beam was totally independent of its neighbour (see Appendix 2). New active filters were designed and made. The original filter was a 1Hz low pass filter and thought to have a slow response time for the envisaged test programme, hence both 1Hz and 10Hz low pass filters were built. The frequency responses for the filters are shown in Appendix 2. The strain gauge bridges were provided with individual 10V stabilized supplies and their outputs were fed to separate DC Amplifiers. The voltage amplified signal was passed through the 10Hz filter and back into the amplifier for current amplification. The current amplified signal was displayed on a U-V recorder. A satisfactory calibration of the dynamometer was made with the data recording system connected through a 10Hz filter. The natural frequency of the dynamometer was found to be 1.1KHz by the 'tap test' method using the data recording system, unfiltered (see Appendix 2).

4.4 Rig Measurement

The measurement of the grinding energy is sensitive to a number of parameters. The following section describes

4.4 the methods of measurement and their accuracy.

1. Wheel Diameter

The wheel diameter is a crucial dimension for setting the correct depth of cut and also the peripheral speed of the grinding wheel on which the work speed and dresser infeed rate depend. The dynamometer was set on the machine bed to within 0,005mm flatness. The distance from the dynamometer platform to the centre of the grinding wheel spindle was measured using end-bar standards. The distance was 329,82mm $\pm$ 0,01mm. Once the grinding wheel was in position the wheel diameter was measured indirectly from the gap between the dynamometer platform and the lowest point on the wheel periphery. This was carried out using slip gauges with keepers to protect the surface of the gauges from the abrasive.

2. Wheel Speed

Stuart used a toothed wheel and photo-cell system with a visual readout on a Racal counter to measure the wheel speed. It was observed that the counter would also count an interference signal from electrical apparatus operating in the laboratory, this was unsatisfactory. The grinding wheel spindle was driven directly from a motor with tacho feed back control. By tapping into the tacho feed back circuit and entering the signal into a digital voltmeter the wheel speed could be read directly. The signal was calibrated to the actual wheel speed by a Haslar hand held tachometer, there being

4.4 2. a slight volt drop across the feed back loop. In earlier tests the signal was fed into a Data Logger which allowed the frequent sampling of the wheel speed during a test. It was observed that even under high loads the motor would maintain speed to within ± 3%. Only when stalling did the control on the wheel speed breakdown, in which case the quick-blow fuses always blew. For tests where the Data Logger was not used it was assumed that the tacho signal was still representative of the rotational speeds.

3. Dresser Speed

The speed control on the dresser motor was open loop and initially suffered from lack of power.

A new 1.1kW motor was required to drive the new dresser as extra power was needed to overcome the rubbing of the stationery V-ring seals. The more powerful motor then held 0.8 speed ratio within ± 5% for both wheel grades. A Rank-Pullin tacho was used to monitor the dresser speed linked to a Data Logger as above.

4. Work Speed

The drive to the ball screw nut on the machine bed is connected to the grinding wheel spindle motor through a series of gear boxes and toothed belts (see plate 5). By changing the ratios of the gear boxes the bed speed can be varied. The speed and accuracy of speed holding is a function of the wheel speed described above.

4.4 5. Dresser Infeed Rate

The dresser infeed mechanism is not a simple one to calibrate (see fig 12). The system was drawn to scale and calibrated geometrically. The dresser moves in an arc, however for small movement it can be assumed linear. The geometric calibration was checked using a dial indicator to measure the infeed of the dresser for given distances travelled by the machine bed. Again the accuracy depends upon the spindle speed as the wedge is driven from the slideway via the main spindle.

6. Fluid Flow Rate, Pressure and Temperature

The cutting fluid is delivered to the rig via a centrifugal pump, there is a metering orifice in the delivery line calibrated to a Mercury U-tube manometer, the flow rate being proportional to the differential pressure in the manometer. The temperature of the cutting fluid was measured in the delivery line by a Mercury in glass thermometer. A Bourdon-tube type pressure gauge was tapped into the 'shoe' to measure the pressure of the cutting fluid on entry into the pores of the grinding wheel.

7. Grinding Wheel Surface Measurement

The grinding wheel required two surface measurements to be carried out:-

4.4 7. (i) Wheelwear

The wheel wear was easily measured for the continuously dressed tests, calculated from the dresser infeed rate. However when grinding conventionally the wheel wear measurement was more difficult. A thin shim of steel was held tightly between two blocks and only a small length of shim was allowed to protrude. The shim was then plunged normally into the wheel surface whilst the wheel was rotating and then quickly withdrawn. A profile of the wheel surface was then found on the shim. Using a shadow graph projector the wheel profile image can be inspected and the radial wheel wear measured. This method is open to a number of inaccuracies.

(a) The shim is likely to bend on contact with the wheel, due to the grinding forces.

(b) For a standard test only 900mm^3 are removed from the workpiece and for a G ratio of 10, that is a radius change of 0.0095mm in 300mm.

(c) The amount of grinding wheel dressed away prior to grinding can only be measured by the change in wheel diameter.

Little confidence can be put in individual wheel wear results, however a trend can be observed over a number of tests.

4.4 7. (ii) Wear Flat Area

A microscope-camera was purpose built to measure the wear flat area on the surface of the grinding wheel (see plate 9) using a similar method to that of Malkin (60;68). The microscope was set up on the rig and adjusted for exact vertical illumination using a mirror to reflect light normal to the wheels surface back up the microscope (see plate 10). The photographic analysis was statistically sampled and the accuracy assessed. For a set of photographs of a sample greater than 81 and with a 95% confidence limit the system should be accurate to 0.05% of wear flat area (see Appendix 4). The photographs were analysed on a Quantimet 720 (courtesy of Rolls-Royce Limited, Filton), which counts the light to dark areas on the photographs within pre-set levels of light and dark, its sample size is 500,000 (see sect. 5.4.).

8. Specimen Measurement

The specimens were measured before and after grinding with micrometers to calculate the actual depth of cut. These measurements were made to the nearest 0,01mm. Surface finish CLA values were measured using a calibrated Rank Taylor Hobson 'Surtronic'.

4.5 Computer Program

The raw test data are in the form of three U-V traces recorded continuously over the duration of a test from the output of the horizontal and the two vertical strain gauged beams on the dynamometer. The speed of the U-V paper is time related to the speed of the machine slideway and the specimen is set to a datum start position on the dynamometer with respect to the strain gauged beams and the grinding wheel. The U-V traces are measured at equal time intervals and entered into the computer program which, from the datum information, calculates the grinding forces, energy and power flux for each data point in time. The computer program also takes into account the change in grinding wheel diameter whilst continuously dressing and compensates for the DC drift in the amplification system (see Appendix 7).

CHAPTER 5

EXPERIMENTAL METHOD AND RESULTS

The experiments reported in this thesis fall into 5 separate categories:

1. High stock removal by continuous dressing.
2. The 'Burn Barrier' found with conventional creep feed grinding.
3. The 'Wear Flat Area' theory related to creep feed grinding.
4. The thermal effects of the cutting fluid on the creep feed grinding process.
5. The metallurgical and surface finish characteristics of down grinding when continuously dressing.

It is the intention of this chapter to combine the experimental method and the results from each category of tests, presenting them, in order, to form the sequential pattern of the research programme. The collective results of the research work will be discussed later in the thesis.

The first section will outline the typical creep feed grinding test procedure. Departure from this procedure in order to carry out special tests will be described under the separate category headings of the subsequent sections.

5.1. General Test Procedure

The hydrostatic supply to the test rig was always run for at least an hour prior to testing so that thermal equilibrium of the hydrostatic bearings could be reached and a steady hydrostatic pressure established.

5.1. The grinding wheel surface was prepared by diamond roller dressing; the same diamond roller dresser was used throughout the research programme (see Appendix 1). A standard dressing procedure was adopted so that the grinding wheel conditions were the same at the start of every test. This procedure is the same as that used by Stuart, for the purpose of standardisation. The grinding wheel was dressed at a speed of $12ms^{-1}$, the dresser running at a surface speed ratio of 0.8 to that of the grinding wheel. A slideway speed was selected in conjunction with the wedge angle to give a dresser infeed rate of 0.5mm/min. (see sect. 4.4.5.). A jet of cutting fluid was injected into the nip between the grinding wheel and the dresser at a pressure of 1b to provide cooling and lubrication. The table feed was engaged until 0.3mm on radius had been dressed from the grinding wheel, the dresser was then retracted quickly so that the spark-out time of the dresser on the grinding wheel was minimal. Previous work has shown that the sharpest wheel results from a dresser dwell time of zero (73).

The grinding wheel diameter was measured after dressing (see sect. 4.4.1. for the method of measurement) and along with the desired wheel speed, slideway speed, and chosen maximum normal infeed rate*, was entered into the computer program for the calculation of the rig settings. The specimen for testing was then mounted on the dynamometer shuttle with the relevant amount of packing to set the correct depth of cut.

---

*The Maximum Normal Infeed Rate is the infeed rate of the workpiece normal to the grinding wheel at the top of the arc of cut.

5.1. The pre-set assembly was checked for size and flatness on an inspection table using a dial indicator. The shuttle carrying the specimen was then fitted onto the dynamometer platform in the rig. The gear ratios were selected for the slideway feed required, and the guard box closed.

The power to the main spindle motor was switched on and the grinding wheel brought up to speed. The dresser was run at all times to ensure that abrasive debris and cutting fluid did not contaminate the bearing seal chambers. The dresser was seen to be clear of the grinding wheel and therefore not interfere with the test run. The cutting fluid pumping system was purged and the dresser nozzle control valve was opened and set to a pressure of 1b, the main delivery line was then opened and the shoe pressure set (1.5b for the WA 60 80 FP2V and 2.5b for the WA 60 KV grinding wheels). The system was allowed to come to equilibrium whilst the instrumentation was adjusted; approx. 2 to 3 mins.

The strain gauge bridges on each of the load beams on the dynamometer were brought to the null position using a 1kΩ offset potentiometer. The U-V recorder was set in motion and the electromagnetic clutch energised. At the end of the test the clutch automatically disengages the infeed (see sect 3.3).

The test completed, the U-V recorder was stopped and the cutting fluid pumps shut down, the main spindle motor was switched off along with the dresser.

Once the spindle was seen to have stopped the guard box was opened and the specimen taken from the dynamometer platform. The specimen was measured to check the actual depth of cut and a wheel wear shim replica was taken (see sect. 4.4.7). The U-V trace was analysed and the data fed into the analytical part of the computer program. The surface finish of the test piece was measured using a Rank Taylor Hobson 'Surtronic', this is a portable surface measuring machine.

5.1.1. Control Tests and Conventional Creep Feed Grinding Limitation

A series of tests were carried out in accordance with the general procedure (see sect. 5.1.) to re-establish the data characteristics of the High-Speed Creep-Feed Grinding Rig with relation to the process limitations established by Stuart.

The limiting maximum normal infeed rate and corresponding specific energy was determined at the onset of thermal damage for all combinations of wheels (WA 60 80 FP2V and WA 60 KV) and workpiece materials (C1023 and Mar M002). The results are shown in tabular form in fig. 13. and agree with the data established by Stuart.

5.2. High Stock Removal Rates by Continuous Dressing

Stuart (4) showed that continuously dressing the grinding wheel whilst grinding, results in a significant drop in grinding force with a corresponding decrease in the specific energy (see fig. 5.).

5.2. Shafto (20) showed that there exists a relationship between the specific energy and the maximum normal infeed rate for the creep feed grinding process. The maximum heat flux (the product of the specific energy and the maximum normal infeed rate), was shown to reach a peak (32 to 36 MWm^{-2}) above which film boiling occurs and causes thermal damage to the workpiece.

It would seem that by continuously dressing the grinding wheel whilst grinding, the stock removal rate of the creep feed grinding process can be increased in direct proportion to the drop in specific energy until the maximum heat flux is exceeded and thermal damage occurs. However other authors have postulated theories for conventional grinding (5,64) regarding the partition of energy in the grinding zone; i.e. When a grinding wheel is sharp and has few 'wear flat areas', a greater percentage of the heat generated by the process goes off into the chip and to the surroundings so that the amount of the total grinding energy, conducted into the workpiece as heat, is small. A dull grinding wheel which has large 'wear flat areas' exhibits a partition of energy where a much greater proportion of the total grinding energy is conducted into the workpiece, this rapidly increases the surface temperature of the workpiece and results in work-piece burn. Should the 'wear flat area' theory apply to creep-feed grinding then it can be expected that the stock removal rate of the process, when combined with continuous dressing, will be even greater than the proportional drop in specific energy level due to in-process dressing shown by Stuart (4) (see fig. 5.).

5.2.1. Experiment to Determine the Relationship between the Specific Energy and the Dresser Infeed Rate (Method)

The object of the experiment was to perform a series of creep-feed grinding tests with constant cutting geometry at a constant stock removal rate where each test was continuously dressed at different dresser infeed rates. A relationship between the specific energy of the process and the dresser infeed rate resulted.

The dresser was rotated in the same peripheral direction as the grinding wheel at a speed ratio of 0.8, and the grinding wheel was run at $30ms^{-1}$. The ratio of dresser to wheel speed of 0.8 was chosen after the work of Meyer et al (93). This work showed that the lowest specific energy results from a grinding wheel dressed with a diamond roller dresser at synchronous speed, however the 'plucking action' of the abrasive grits at the diamonds in the diamond roller dresser matrix causes heavy wear and damage to the dresser. The relationship between specific energy and dresser speed ratio shows that a ratio of 0.8 has little effect on the increase in specific energy (see fig. 14.), yet there is sufficient mismatch in speed to prevent plucking and therefore preserve the life of the dresser. Pearce (98) explains the need for a variation in speed ratio between the dresser and the grinding wheel in order to avoid replication of the dresser surface on the grinding wheel which can result in poor surface finish.

5.2.1. When a grinding wheel is continuously dressed it becomes progressively smaller in diameter, therefore as the machine bed moves beneath the grinding wheel a taper is ground onto the workpiece. In order to ensure that the cutting geometry and the stock removal rate remain constant, the computer program calculates the rig settings and in ~~going~~ doing so calculates the necessary angle to be ground on the specimen prior to testing so that the cutting geometry and the stock removal rate is constant throughout the test (see fig. 15.).

The setting up of a continuous dressing test is more tedious than a conventional creep feed grinding test as it is necessary to have the diamond roller dresser 'spark out' on the grinding wheel and the corner of the specimen touching the grinding wheel when the infeed is engaged at the beginning of a test. This is to ensure that the grinding is coincident with the dressing, in order to achieve the set depth of cut.

Tests were carried out using both C1023 and Mar M002 materials and WA 60 80 FP2V and WA 60 KV wheel combinations.

5.2.2. <u>Experiment to Determine the Relationship between the Specific Energy and the Dresser Infeed Rate (Results)</u>

The results are shown in figs 16 and 17. The characteristic is identical for all the wheel/work-piece combinations tested. There appears to be a point on the dresser infeed rate axis where the

5.2.2. specific energy curve 'levels out'; no matter how much the dresser infeed rate is increased beyond that limit the specific energy remains the same. This is therefore the point where the grinding wheel surface geometry reaches a state of maximum sharpness. Further evidence of this is shown in the relationship between surface finish and the dresser infeed rate (see fig. 18). The surface finish becomes progressively worse as the dresser Infeed rate increases until, coincident with the point of maximum sharpness, it remains constant.

With the grinding wheel maintained at optimum sharpness (i.e. selecting a dresser infeed rate which yields the lowest specific energy) the stock removal rate should be able to be increased to the limit of workpiece burn, in line with the maximum heat flux criterion by Shafto.

5.2.3. <u>Experiment to Determine the Limitations to the Continuously Dressed Creep-Feed Grinding Process (Method)</u>

The same wheel and workpiece combinations were used as in section 5.2.1. However, the test procedure was changed; the cutting geometry and dresser infeed rate were kept constant, but the work speed was increased until the limit of the stock removal capability of the process was reached.

5.2.4. Experiment to Determine the Limitation to the Continuously Dressed Creep-Feed Grinding Process (Results)

The results are shown in figs. 19 and 20. There are two effects which have shown significant improvement in the process by the use of continuous dressing. Firstly the gain in stock removal rate is over and above that which is predicted by the Shafto criterion for conventional creep feed grinding (see sect. 5.2). Secondly it was found to be impossible to burn the workpiece materials (C1023 or Mar M002) using the combination of a high dresser infeed rate (1.7 and 2.5 mm/min. respectively), and a weakly bonded creep feed grinding wheel (WA 60 80 FP2V). The stock removal rates achieved here were in the order of 25 times faster than existing methods of grinding in industry.

The limitation to the stock removal rate in this case was wheel breakdown, the high infeed rate of the workpiece crushed away the abrasive ahead of the dresser (see plate 11). In the case of the WA 60 KV grinding wheel (a much stronger bond), thermal damage was still the limiting factor.

5.3. The 'Burn Barrier' found with Conventional Creep Feed Grinding

The previous set of tests showed a departure from the Shafto criterion for conventional creep feed grinding in that a larger maximum heat flux was supported at the onset of burn whilst continuously dressing.

5.3. The Shafto model (94) includes a term which represents the fraction of the mechanical energy of the grinding process that enters the workpiece as heat. This partition of energy fraction was chosen to be 0.6 by Shafto, after the work of Malkin et al (5,30) and was considered to remain constant. In the surface temperature formula, Shafto shows that the ratio of the partition of energy fraction to the heat transfer coefficient in the arc of cut, is the major factor influencing the temperature in the arc of cut. Thus, it was felt that the partition of energy was being affected by the action of continuous dressing on the grinding mechanism. Without continuous dressing thermal damage is caused by the collective cutting, ploughing and rubbing energies (5), whereas with continuous dressing the 'wear flat area' on the grinding wheel is greatly reduced. The very low percentage 'wear flat area' associated with continuous dressing at a high dresser infeed rate results in a minimal amount of rubbing energy being generated. When continuously dressing the grinding wheel, the energy transferred to the workpiece surface is largely due to cutting and ploughing as the grinding wheel is in a state of constant sharpness.

It was decided to conduct an experiment to test for the proposed difference in the partition of energy when continuously dressing and when conventionally creep feed grinding. It has already been established that the onset of thermal damage for conventional creep feed grinding occurs at a maximum normal infeed rate of 8mm/minute for

5.3. the wheel/workpiece combination WA 60 80 FP2V/Mar M002 (see fig. 13), at 3mm depth of cut. To ensure workpiece burn would occur, a fairly high maximum normal infeed rate was chosen; 30mm/minute. Keeping the cutting geometry constant at 3mm depth of cut and 30mm/minute maximum normal infeed rate, a high dresser infeed rate was selected and gradually backed off to zero dresser infeed rate (i.e. a conventional creep-feed process with the dresser not in contact with the grinding wheel) over a series of tests, until the onset of thermal damage. A most unexpected result transpired - workpiece burn never occurred (see fig. 21). The critical maximum normal infeed rate was exceeded yet the workpiece showed no signs of thermal damage.

The test produced an unexpected result which led to the hypothesis that a 'burn barrier' must exist, both sides of which the workpiece can be ground without suffering thermal damage. There must also be separate mechanisms acting before and after the 'burn barrier' which affect the partition of energy fraction thus explaining the departure from the Shafto criterion for conventional creep feed grinding.

It was decided to repeat the method of testing adopted by Shafto and Stuart but to proceed on through the 'burn barrier' and out the other side, all the time observing the process for change.

5.3.1. Experimental Method for Increasing the Feed Rate beyond the 'Burn Barrier'

A series of conventional creep feed grinding tests were carried out with constant geometry, at a depth of

5.3.1. cut of 3 mm. Each test saw the grinding wheel dressed to the same standard before proceding on to the next test. This method is that described in section 5.1. for conventional creep feed grinding tests, the maximum normal infeed rate was varied from 4 to 100 mm/min. Selected tests before, during and after the 'burn barrier' saw the surface of the grinding wheel photographed and assessed using the microscope-camera.

5.3.2. Results of the 'Burn Barrier' Experiments

The results were plotted on a graph of specific energy against maximum normal infeed rate (see fig. 22), along with previous results of Shafto and Stuart.

A graph of mean power flux against maximum normal infeed rate was plotted as each test was performed (see fig. 23). The graph followed a curious yet repeatable shape. It is felt that with the support of work by Rubenstein et al (14,57) the graph might be explained in terms of a wheel wear pattern which is fundamental to the creep feed grinding process (see sect. 6.1.).

Two important aspects of the 'burn barrier' experiments lead into the next series of tests. It was photographic evidence, using the microscope-camera which revealed that two differently formed grinding wheel surfaces were equivalent in terms of 'wear flat area'. The first, by conventionally creep-feed grinding with a maxium normal infeed rate in excess of

5.3.2. 50 mm/min. and secondly, tests carried out using continuous dressing with high dresser infeed rates (in excess of 2 um/rev). Both processes were photographically shown to result in very low percentage 'wear flat areas'. This result suggests that the high maximum normal infeed rate which causes self dressing to take place ~~is synonomous with~~ resembling an uncontrolled continuous dressing process.

At this stage in the research the manufacturing industry requested that slow peripheral wheel speed creep-feed grinding be explored. Industrial safety regulations tend to force companies towards lower grinding wheel speeds, however Rolls-Royce Limited adopted low speed creep-feed grinding because thermal damage was being caused at $30ms^{-1}$. Appendix 3 shows that the effect of decreasing the grinding wheel speed is to make the grinding wheel appear softer. The increase in the grit depth of cut at low grinding wheel speeds exerts a high force on the individual grits breaking them from their bond. In effect this is uncontrolled continuous dressing. Stuart (4) conducted a number of tests at high wheel speeds; 30, 45 and 60 ms^{-1}, hence the author carried out a series of creep feed grinding tests at $10ms^{-1}$ (see fig. 24). Workpiece burn did not occur at $10ms^{-1}$, however the workpiece feed rate was limited as the rig was prone to stalling because of the low speed, low torque, characteristic of the main spindle motor.

5.3.2. This series of tests confirmed that thermal damage can be alleviated by in-process dressing which can be brought about by increasing the infeed of the workpiece (see fig. 23), decreasing the grinding wheel speed, (see fig 24) both of which promote self dressing, or by ~~continuous~~ continuously dressing the grinding wheel with a diamond roller dresser. The advantage in using a diamond roller dresser is that the form is held precisely throughout the process, a self dressing grinding wheel rapidly loses its form.

5.4. The 'Wear Flat Area' Theory Related to Creep Feed Grinding

The continuous dressing tests (section 5.2.) showed that a marked drop in specific energy results from continuously dressing the grinding wheel whilst grinding, allowing a substantial increase in the stock removal rate prior to the onset of thermal damage or grinding wheel breakdown. Similarly the 'burn barrier' experiments showed that high stock removal rates are attainable with conventional creep feed grinding in the regime of self dressing. Photographic evidence has verified that a common factor contributing to the high stock removal rates achievable without thermal damage, by the processes described in section 5.3.2., is the elimination of 'wear flat areas' which generate the deleterious rubbing energy.

Using the continuous dressing technique as a research tool to control the 'wear flat area' on the grinding wheel surface, the applicability of Malkins 'wear flat area' theory to creep feed grinding, will be investigated.

5.4.1. Experiment to Establish the Relationship between the 'Wear Flat Area' on the Grinding Wheel and its Corresponding Specific Energy (Method)

. The test procedure was identical to that for the 'specific energy v dresser infeed rate' series of tests reported in section 5.2.1. It has been demonstrated that should the grinding wheel 'spark out' on the workpiece or the dresser dwell on the grinding wheel then the surface characteristics of the grinding wheel are radically altered e.g. loading patches removed (70). It was therefore imperative to reverse the table feed at high speed immediately the automatic clutch disengaged at the end of a test. A strict routine was adopted for this procedure which ensured ~~consistancy~~ consistency from test to test.

The grinding wheel was photographed using the microscope-camera, described in section 4.4.7., at a minimum of 81 stations, distributed randomly around the grinding wheel periphery. After developing, the printed pictures were analysed using a Quantimet and the percentage 'wear flat area' calculated from the data. Further tests were carried out without continuous dressing, this allowed the grinding wheel surface to degenerate in the conventional creep feed grinding mode. The grinding wheel deteriorates very quickly under these conditions, so in order to record low levels of 'wear flat area' a constant geometry was adopted throughout the test. As a grinding wheel feeds into a rectilinear workpiece the corner of the

5.4.1. workpiece is removed first. The amount of material removed per revolution of the grinding wheel increases until at full depth of cut, constant geometry is achieved. A specimen was pre-machined to remove that material from the rectilinear workpiece so that the cutting geometry remained constant from the beginning of the test. Both WA 60 80 FP 2V and WA 60 KV grinding wheels were tested.

5.4.2. Results of the 'Wear Flat Area' Experiments

The results of the testing carried out as above, are shown in figs. 25 and 26. Both continuously dressed and conventionally creep-feed ground tests are represented on the same graph, also see plate 12. The conventionally ground results take on a linear relationship whereas the continuously dressed results, at low 'wear flat area', bend the straight line relationship to intersect the specific energy axis at a much lower level than the linear extrapolation. The partition of energy fraction pertaining to the creep-feed grinding process can be estimated by taking first, the value of specific energy at the onset of burn for a conventional creep-feed grinding process E_c. Secondly, using the same cutting geometry, the specific energy at the onset of burn for a continuously dressed creep-feed grinding process is measured E_d. It has been stated (see sect. 5.3.2.) that the energy at burn for conventional creep-feed grinding is made up of cutting, ploughing and rubbing energies whereas with continuous dressing, the energy is made up of predominantly cutting and ploughing energy with minimal rubbing energy.

5.4.2. Using the assumptions of Malkin (5), that rubbing, cutting and ploughing energies can be summed, and that the cutting and ploughing energy is independent of 'wear flat area' and also independent of the rubbing energy, then the amount of cutting and ploughing energy can be assumed to be the same for both continuous dressing and conventional grinding processes. Subtracting E_d from E_c will give the quantity of energy caused by rubbing E_r. The partition of energy fraction is then calculated as follows:

E_r/E_c = the percentage rubbing energy P.

and therefore 100 - P = the percentage cutting and ploughing energy.

On this basis, over all the combinations of wheel and workpiece tested for conventional creep-feed grinding, the partition of energy is calculated to be 97% rubbing and 3% cutting and ploughing energy. It is important to note that the percentage 'wear flat area' has not been reduced to zero, therefore the rubbing energy has not been totally eliminated, hence the 3% cutting and ploughing energy is a conservative estimate.

5.5 The Effects of Arc Length and Cutting Fluid Bulk Temperature on the Stock Removal Rate of the Process

At this stage in the research it would seem that the problem of workpiece burn and the consequential scrapping of components has been eliminated by the use of the continuous dressing technique coupled with the optimal application of the cutting fluid, at least for plain forms. Furthermore, the stock removal rate has

5.5 has been increased by 25 times that of the conventional creep-feed grinding process. However it would seem that even higher stock removal rates could be achieved by using a stronger bonded grinding wheel somewhere between the grades WA 60 80 FP 2V and WA 60 KV used in this research. The weakly bonded grinding wheel broke down at the limiting stock removal rate whereas the stronger bonded grinding wheel maintained its form yet resulted in workpiece burn because of excess rubbing energy.

Little attention has been paid to the role of the cutting fluid in affecting the stock removal capability of the process, however the work of Shafto and Powell shows that the cutting fluid plays a significant part in transferring the heat away from the cutting zone in order to prevent workpiece burn. The work carried out by Powell (6) in which the application of the cutting fluid and its ability to dissipate heat from the working zone was studied, used a heating element to represent the grinding power flux and the fusing of that element to signify the onset of film boiling - the phenomenon established by Shafto (20).

Powells findings have been collated and presented in the form of a mathematical model which attempts to represent the real situation, see Appendix 5.

The investigation which follows is a study of the effects suggested by the model which makes a significant contribution to the stock removal capability of the process. No attempt has been made to verify the model quantitatively, it has simply been used to highlight the effects which are likely to provide 'triggers' that might improve the stock removal capability of the creep-feed grinding process.

5.5.1. Experiments to Determine the Effect of the Bulk Temperature of the Cutting Fluid and the Arc Length of Cut on the Stock Removal Rate of the Creep-Feed Grinding Process

A number of tests were carried out in this series of experiments to establish the thermal conditions in the grinding wheel/arc of cut interface. It was important that the grinding wheel surface did not radically change from test to test and affect the thermal characteristics of the process. From the 'wear flat area' experiments it was shown that a freshly dressed grinding wheel would degrade very quickly, especially at large depths of cut, whereas a dull grinding wheel would change to a lesser extent as the great majority of the energy generated would be rubbing energy. Hence all the tests in this series of experiments were performed using dull grinding wheels. The 'wear flat area' was checked for each test using the microscope-camera technique (see sect. 4.4.7.).

The object of the first series of tests was to conventionally creep-feed grind as in section 5.1 but without dressing the grinding wheel, in order to establish the relationship between the maximum normal infeed rate at which workpiece burn occurs and the depth of cut set for each test. The cutting fluid was kept at nominal ambient temperature, 20^{o}C. A second series of tests were carried out whereby the temperature of the cutting fluid was varied and the heat flux at burn was observed for different depths of cut in order to compare the real situation with the results from Powells simulation. One of the

5.5.1. assumptions from the model in Appendix 5 is that it would be advantageous to cool the cutting fluid and deleterious to raise its temperature. The cost of refrigerating the cutting fluid at a flow rate of $6ls^{-1}$ from a tank capacity of 1025 litres is very high. It was therefore decided to examine the deleterious effects of heating the cutting fluid using electric immersion heaters, being a much cheaper method. The temperature boundaries chosen were ambient, 20°C, 35°C and 40°C. The temperatures were controlled to within 1°C. The manufacturers of the cutting fluid (Edgar Vaughan - Houghtogrind 55) gave an assurance that prolonged exposure to temperatures up to 50°C would not affect the chemical properties of the fluid. However the 60:1 dilution was carefully monitored and corrected due to the increase in evaporation rate of the water at elevated temperature.

All the tests in this series of experiments were carried out using the porous WA 60 80 FP 2V creep-feed grinding wheel and Mar M002 specimen material.

5.5.2. <u>Results of the Effects of Arc Length and Cutting Fluid Bulk Temperature on the Stock Removal Rate</u>

Figure 27 shows the relationship between the depth of cut and the maximum normal infeed rate at the onset of workpiece burn, illustrating that there exists a significant 'depth of cut' effect. Figure 28 shows the relationship between the arc length and the mean power flux at the onset of burn for different bulk temperatures of the cutting fluid and figure 29 shows how the combination of the arc length (dictated by the depth of cut) and the bulk temperature of the cutting fluid affect the overall stock removal rate of the process.

5.6 The Surface Integrity Examination of the Continuously Dressed Creep-Feed Ground Surface

The research has illustrated where the limitations to the stock removal capability of the process lie in terms of avoiding the onset of thermal damage, however the manufacturing industry is not only concerned with high stock removal but also in attaining a high degree of surface integrity. A continuously dressed specimen exhibits a matt surface finish which becomes worse as the dresser infeed rate increases (see fig. 18). Better surface finish CLA values can be achieved using lower dresser infeed rates but to the detriment of high stock removal rates. It is the object of this series of tests to establish a cause for the surface abuse and propose remedial action.

The surface integrity of continuously dressed components is generally worse than that for conventionally ground workpieces. In conventional grinding, where self dressing is minimal, the pattern of active grits on the surface of the grinding wheel is virtually unchanged throughout the process. The active grits wear attritiously and workpiece material loads and clogs around them growing from the nucleus of the active grit. A continuously dressed grinding wheel surface however, changes the distribution of its active grits for every pass that the grinding wheel makes of the dresser, causing the distinctive matt surface finish associated with continuous dressing. A series of tests was devised to give a qualitative assessment of the surface integrity of continuously dressed specimens by metallurgical examination.

5.6 Although a continuously dressed creep-feed ground surface appears matt, unlike a typical precision finish, the main concern was the surface indentations or pits which appear secondary to the matt finish (see plate 13). This was thought to be caused by one or both of the following effects:

(i) The surface of the workpiece is bombarded with loose grits and grinding debris breaking free from the grinding wheel surface.

(ii) Particularly at high stock removal rates and when down cutting, the workpiece suffers from redeposition of material emerging from the nip at the bottom of the arc of cut.

To test the above theory a composite specimen was made from brass and Mar M002 (see fig. 30) along with a standard Mar M002 control specimen. It was felt that there might be a discolouration on the surface of the brass if redeposition occurred.

5.6.1. <u>The Inspection of the Surface of the Composite Specimens</u>

The specimens of brass and Mar M002 were carefully sectioned and mounted for inspection in a scanning electron beam microscope. All of the surfaces appeared pitted with craters (see plate 13). A steel specimen similarly ground was also inspected. Using a micro-probe analyser it was found that every crater in the surface of the steel specimen exhibited the presence of an abrasive grit, whereas few of the craters in the surface of the Mar M002 showed any grits. Mar M002 is a harder material than the steel used hence it is possible

5.6.1. that the abrasive grits bounced off the surface of the Mar M002 and merely left a crater; literally a 'grit blasting' effect.

The question of redeposition of material must remain a subject for further work as although there was a visible indication on the surface of the brass the micro-probe analyser was unable to detect any nickel on the brass.

It was shown by a further test that the pitted surface, and all evidence of the surface having been creep-feed ground by continuous dressing, could be removed in a single pass of the grinding wheel in the conventional mode at a depth of cut of 0.02mm.

CHAPTER 6

DISCUSSION

The research work reported in this thesis has explored a closely defined area of the general creep-feed grinding process, in particular two 'difficult to grind', superalloy materials were tested, (C1023 and Mar M002) using two different grinding wheels with properties comparatively in the extreme of hardness and porosity. With support from previous work the results of the present research have helped to establish fundamental principles for the creep-feed grinding process which have been applied to the process and resulted in a substantial increase in the stock removal capability.

It is the object of this chapter to collate the results of the research work and using the previous work of other authors, discuss the points relevant to the creep feed grinding process in general.

6.1 The Mechanics of the Creep Feed Grinding Process

The 'Burn Barrier' experiments (see sect. 5.3) were an important series of tests which, although unexpected, provided evidence for a fundamental grinding mechanism theory, supported by the work of Rubenstein and Hahn (14,57).

The mechanics of the conventional precision grinding process can be divided into three stages according to Rubenstein:

1) Initally the grinding wheel wears quickly, depending on the severity of the dressing technique. The proportion of ploughing to cutting grits reduces and

6.1 1) the grits, weakened by the dressing action, fracture or break from the bond. Eventually the grinding wheel wear stabilises.

2) The second stage of the grinding wheel wear pattern is characterised by a uniform wear rate, much less than that of the first stage. This is attributed to the attritious wear of the abrasive grits.

3) The third stage of the wear pattern is a function of the bulk properties of the grinding wheel, independent of the dressing technique. Excessive grinding wheel wear occurs due to the 'pull-out' of grits from the bond, along with the catastrophic failure of the bond bridges. The grinding wheel wear rate becomes extremely high.

The three stage model of the grinding wheel wear as described by Rubenstein, above, was similarly observed by Yoshikawa (58), however creep feed grinding 'difficult to grind' superalloys produced the pattern characterised by figure 23 and described as follows:-

A) This is the region of conventional creep-feed grinding up to the onset of thermal damage. (The letters A to C represent the three stages of the process illustrated in figure 23). Here the grit depth of cut is very small, indicated by the maximum normal infeed rate; typically between 1 and 6 μm/rev of the 600mm diameter grinding wheel. It is assumed that the grinding wheel has been freshly dressed prior to grinding so that the rubbing energy component is minimal. At very low

6.1 A) grit depths of cut, the abrasive will be predominantly in the ploughing mode, however the process progresses into the cutting mode with an increase in infeed. Hahn discusses the 'ploughing-cutting transition' and using the Mises yield criterion on the grit/workpiece surface interface, argues that above a critical tensile stress, fracture of the 'free plastic surface' allows a build up of material in front of the cutting edge, creating a shear zone ahead of the grit which promotes the formation of a chip. It is the increase in infeed mentioned above which increases the tensile stress described by Hahn and so causes the 'ploughing-cutting transition' to take place.

The highest specific energy occurs in the ploughing mode and decreases with increasing maximum normal infeed rate (see fig. 22). The reason for this is explained by Backer et al (67) and is termed the 'Size Effect'. Infinitesimally small grit depths of cut will operate within the surface layers of the workpiece deforming the material on a molecular level. The shearing forces on a molecular scale are far greater than those of the bulk material, hence the specific energy is larger with smaller grit depths of cut.

As the maximum normal infeed rate increases a greater load is imposed on the individual grits, causing attritious wear of the abrasive which develops 'wear flats' on the grinding wheel surface. The 'wear flat area' reaches critical proportions and the rubbing energy increases the input of heat to the workpiece surface, resulting in thermal damage.

6.1 B) This is a region of workpiece burn where the maximum normal infeed rate between 6 and 30 μm/rev of the grinding wheel for a 3 mm depth of cut. The 'wear flat area' is above its critical limit and the workpiece exhibits thermal damage. Malkin showed that a change in the tangential/normal grinding force ratio occurred in the burn region (5,53). This held true in region B where the force ratio was 0.18 whereas the force ratio in regions A and C was 0.22.

The fluctuation of the mean power flux in this region might be explained by thermal softening of the material which takes place when the workpiece burns, however the author offers no further explanation except to emphasize the repeatability of the power flux/infeed rate relationship in this region.

C) In this region where the maximum normal infeed rate is in excess of 30 μm/rev of the grinding wheel, the mechanism is one of complete self dressing. The grinding forces at individual grit level are of such magnitude that the grits fracture and break freely from the vitreous bond, causing high wheel wear yet discouraging the formation of 'wear flat areas' which cause the deleterious rubbing energy to be generated.

In region C, the process appears to have reverted to a predominantly cutting mode, verified by the normal/tangential force ratio returning to a value of 0.22.

6.1 C) A series of photographs were taken using the microscope-camera in each of the areas designated A, B and C, they showed that the distribution of 'wear flats' coincide with the change in force ratio associated with the rubbing energy phenomenon; large 'wear flat areas' being the cause of workpiece burn and low 'wear flat areas' allowing the work-piece to be free from thermal damage.

It is region C which is of most interest since it is the region which supports the largest power flux and yet suffers no thermal damage. This is due to the change in the partition of energy which takes place in the transition between rubbing and cutting.

The reason postulated for the grinding wheel breakdown is the large grit depth of cut imposing high forces on the individual grits, breaking them from the bond. The self-dressing action is in effect re-sharpening the grinding wheel giving the individual grits a keen edge which promotes a return to shearing and hence cutting. It would seem that the same effect is experienced with low peripheral wheel speed grinding, used in industry today; lowering the peripheral speed of the grinding wheel whilst keeping the infeed constant, in effect, increases the grit depth of cut. The grinding wheel appears softer as it takes on the self dressing action observed in region C (refer sect. 5.3.2).

The results discussed above are particular to the combination of Mar M002, a tough super-alloy, and the weakly bonded WA 60 80 FP 2V grinding wheel, therefore only certain features of the three phases of the creep feed grinding process are true to the general case. The region C, where the abrasive grit breaks freely from the bond may not occur with a stronger bonded grinding wheel.

6.2 The Effect of 'Wear Flat Area' on the Creep Feed Grinding Process

Many researchers (5,64,65,66) have observed the 'wear flat area' phenomenon, Malkin in particular developed a partition of energy relationship (5) which showed that for a conventional precision grinding operation, without cutting fluid, the total grinding energy was split into components of ploughing, cutting and rubbing energies.

Malkin (5) postulated a partition of energy theory which says that if the total grinding energy were divided into its component ploughing, cutting and rubbing energies, then 75% of the ploughing energy, 45% of the cutting energy and 100% of the rubbing energy enters the workpiece as heat. The shear strain rate of the grinding process is high due to the fast cutting velocities and large shear strains. Because the shear strain rate is so high the cutting action may be considered to be adiabatic; the metal removal at grit level occurs so rapidly that heat from the shear zone cannot escape during the cutting process. Malkin argues that it would be reasonable to expect that for a process which functions in a predominatly cutting mode,

6.2 the minimum specific energy of the process would approach the specific melting energy of the workpiece material, assuming adiabatic shear. Coes and Shaw (5) have shown this to be so and indeed the continuous dressing experiments (sect. 5.2) and the high stock removal tests (sect. 5.2.4), reported in this thesis, have also supported the argument. The specific melting energy of the materials tested is approximately 9 J mm^{-3} and the lowest specific energy recorded, whilst grinding in a predominantly cutting mode is 16 and 13 J mm^{-3} for C1023 and Mar M002 respectively.

To establish the proportion of cutting energy Malkin linearly extrapolated the 'energy/wear flat area' relationship to zero wear flat area, on the assumption that at zero wear flat area there can be no rubbing energy, only energy due to cutting and ploughing (see fig. 4). In doing so it would seem that Malkin might have over-estimated the amount of cutting and ploughing energy, as the result in section 5.4.2 showed. The intercept on the energy axis at zero wear flat area is much lower than that assumed by linear extrapolation. The proportion of cutting and ploughing energy to rubbing energy has been shown to be approximately 97% rubbing to 3% cutting and ploughing (see sect. 5.4.2). The 3% proportion of cutting energy errs on the conservative side as the tests reported in the thesis were never totally free from wear flats, the lowest being 0.015% wear flat area. Therefore the percentage of the total grinding energy which is cutting energy is likely to be less than 3%.

6.2 In creep feed grinding the work speed is much slower than that for precision grinding, hence the speed of the moving heat source is correspondingly slower. The grinding process model of Des Ruisseaux and Zerkle uses the basic Jaeger model for moving heat sources which is dependent on the speed of the moving heat source. The Des Ruisseaux and Zerkle model particularly takes account of surface cooling, and for the case of a slower moving heat source the model is radically affected. It is reasonable to assume that Malkins 'partition of energy' is similarly affected, in that almost 100% of the ploughing and rubbing energy is conducted into the workpiece.

Malkin measured the total grinding energy at the dynamometer, and using a calorimetry technique, measured the heat energy conducted into the workpiece for each test. The ratio of the heat conducted into the work-piece/total grinding energy, was plotted against the specific energy (see fig. 31). Malkin assumed that at the lowest specific energy the process was cutting and at higher specific energy was ploughing, hence Malkins partition of energy gives: 45% of the cutting energy and 75% of the ploughing energy is conducted into the workpiece. It is felt that the results from the research work suggest that the amount of heat conducted into the workpiece is much less than Malkin shows when in a predominantly cutting mode, thus the curve shown in figure 31 should increase more steeply as the specific energy increases.

6.2 To verify the relationship will necessitate a further series of tests with continuous dressing and a means of accurately measuring the amount of heat conducted into the workpiece.

It has been popular to compare creep-feed grinding with the abrasive cut-off process (30) especially in the light of the above mentioned 'adiabatic shear'. The abrasive cut-off process relies on the workpiece being pre-heated in front of the grinding wheel by rubbing energy, the very fast infeed then 'blows away' the molten material before the heat can be conducted into the machined surface. This is not the case for creep feed grinding. The maximum slideway travel on the research rig is approximately 90 mm and the length of all the specimens ground was over 125 mm. This means that every test was terminated in a full depth of cut situation. If the creep feed grinding process was operating in the domain of 'abrasive cut-off' then the heat affected zone ahead of the grinding wheel would have been apparent in the arc of cut. Except in the case of thermal damage, initiated by the film boiling of the cutting fluid, no specimens exhibited any indication that the process ~~was synonomous with~~ resembled the cut-off process.

6.3 <u>The Thermal Effects of the Cutting Fluid</u>

Many researchers (43,44,52,53) have shown that in order to conduct heat away from the arc of cut, to prevent thermal damage of the workpiece, it is critical that a water based cutting fluid is effectively applied to the cutting zone. Powell (6) showed by simulation, that

6.3 the length of the arc of cut has a pronounced effect on the maximum heat flux dissipated at the onset of workpiece burn (see fig. 32). This was shown to be due to the cutting fluid warming up around the arc of cut. Powell simulated the heat flux in the arc of cut with an electrically heated 'heating element'. The heat input profile was a block profile. With the grinding wheel in intimate contact with the heating element and under flood cooling condition, the heat intensity was controlled by increasing the current to the low voltage, high current heating element, until the element fused. The fusing of the element signified a breakdown in the heat dissipatibility of the cutting fluid. A double element, connected in series, was then tested so that the initial point of burn-out in the arc of cut could be located. The heater current was increased as before, until the element fused. In every case the element downstream of the simulated maximum normal infeed failed, indicating that the cutting fluid temperature is elevated as the cutting fluid progresses around the arc of cut. The research showed that under actual grinding conditions the cutting fluid model of Powell (6) held true for the creep-feed grinding process.

Figure 28 shows the relationship between the mean power flux and the depth of cut for a predominantly rubbing situation. Shafto postulated that for creep-feed grinding the maximum power flux remains constant for all depths of cut (94). As a general case this is not entirely true. Figure 28 shows a significant

6.3 change in the maximum power flux dissipated at depths of cut below 1mm whereas the Shafto criterion is only valid for depths of cut in excess of 1mm, the range which he investigated. This can be explained by the warming-up effect. Shafto showed that a maximum heat flux of 32-36 MW m^{-2} was the limit for the creep-feed grinding process. This is a terminal point due to the transition from nucleate to film boiling. Heat is transferred to the cutting fluid as it moves around the arc of cut, therefore it would seem that the maximum heat flux, generated at the top of the arc of cut, must be below a critical value so that the transition from nucleate to film boiling does not occur before the cutting fluid reaches the bottom of the arc of cut. It is this phenomenon which is responsible for the 'depth of cut' effect. An increase in depth of cut brings about an increase in arc length for a constant grinding wheel diameter. It has been suggested that the cutting fluid warms up around the arc of cut as it conducts the heat away from the work-piece surface, a short arc length can therefore cope with a high flux at the top of the arc of cut as the cutting fluid has to travel only a short distance. The maximum heat flux is high, yet the period of time that the cutting fluid is exposed to the heat flux is short. Hence a much larger maximum heat flux can be supported prior to the transition from nucleate to film boiling. Considering a longer arc length, the cutting fluid can reach the transition point before it leaves the arc of cut and film boiling will be

6.3 initiated resulting in workpiece burn.

Comparisons drawn across the work of Shafto must be made with caution, as his research rig used grinding wheels $\frac{1}{3}$ the diameter of those used by Stuart and the author. The generality of the Shafto criterion is influenced by the fact that the cutting geometry is not consistent across all diameters of grinding wheel for equivalent maximum normal infeed rates. A change in cutting geometry could affect the partition of energy for the same maximum normal infeed rate.

It is common workshop knowledge that refrigerating the cutting fluid helps to maintain dimensional stability of the machine tool structure as well as the workpiece. The above discussion and the experimental results (see fig. 29) have shown the importance of the effect of the temperature of the cutting fluid on the stock removal capability of the creep-feed grinding process.

6.4 The Metallurgical Aspects of the Creep-Feed Grinding Process

A major concern with the creep-feed grinding process, particularly when continuously dressing, is the surface integrity of the finished component. Microscopic and micro-probe analysis was carried out and showed the surface to be metallurgically and structurally sound with no surface cracks, however the surface texture was notably poor and showed evidence of the occasional embedded grit coupled with a pitted surface, 'grit blasted' by loose abrasive particles

6.4 flung from the wheel periphery. Visual inspection of the workpiece shows a matt finish, but rigorous creep and fatigue testing of this surface is necessary to establish the degree of machining abuse and its effects on the life of components machined by this process.

6.5 The Economics of Creep-Feed Grinding

It might seem that continuous dressing would result in a high usage of grinding wheels and hence a low G ratio when compared with the existing method. This is not the case. The economic study reported in Appendix 6 shows for a particular component, that its present machining time can be reduced by almost 40 times with continuous dressing for no increase in grinding wheel usage.

Already machine tool manufacturers are applying the knowledge gained from the research to build a new generation of grinding machines (88). With the future possibility of high peripheral wheel speed grinding, micro-processor control, multi-station grinding machines (89) and energy adaptive control (90), increases in the stock removal capability of the process could be by orders of magnitude.

CHAPTER 7

CONCLUSIONS

The object of the research work has been to explore the fundamental aspects of the creep feed grinding process, in particular the machining of 'superalloys', C1023 and Mar M002, in order to increase the stock removal capability of the process. Workpiece burn was previously the limitation to the stock removal rate of the process however, the research has shown that workpiece burn can be completely eliminated by combining the action of continuous dressing with a fragile bonded creep-feed grinding wheel, at least when grinding a plain form in superalloy materials. The presence of workpiece burn causes an aero engine component to be scrapped, however the limitation to the creep-feed grinding process with continuous dressing is wheel breakdown, hence the component is ground over-size and can be reclaimed without total loss.

In conventional grinding the 'wear flat area' on the active surface of a grinding wheel is the prime cause of rubbing energy which is almost wholly transferred to the workpiece as heat, increasing its temperature and initiating the onset of thermal damage. The research showed that the 'wear flat area' associated with the creep-feed grinding process can be controlled by continuously dressing the grinding wheel with a diamond roller dresser, or similarly by increasing the workpiece infeed rate to a level where a fragile bonded grinding wheel takes on a self dressing action. In the case of the latter there is a gross loss of form from the grinding wheel, whereas continuous dressing maintains the form precisely. Both methods result in much higher stock removal rates than the conventional process.

The research showed that the 'partition of energy' theory as put forward by Malkin does not generally apply to the creep feed grinding of superalloy materials. The empirical results of the research showed that the amount of cutting and ploughing energy generated by the process at very low 'wear flat areas' is much less than Malkin's theory would suggest. Hence a grinding wheel which is mainly cutting and ploughing supports a higher heat flux prior to the onset of thermal damage than one which is predominantly rubbing.

The proper application of the cutting fluid is critical to the creep feed grinding process. Tests showed that the bulk temperature of the cutting fluid has a marked effect on the stock removal rate of the process. A cooler cutting fluid has a beneficial effect in its ability to conduct more heat away from the cutting zone prior to the onset of thermal damage. Larger depths of cut, which mean longer arc length, cannot cope with high maximum heat fluxes, since it appears that the cutting fluid warms-up as it moves through the arc of cut. It would seem that the cutting fluid temperature increases around the arc of cut until it reaches the burn-out temperature and results in workpiece burn.

Continuous dressing played a most important part in the research work, allowing 'superalloy' stock to be machined faster than ever before using creep-feed grinding wheels. Even conventional grinding wheels, which otherwise would not be considered for creep-feed grinding, exhibited very high stock removal rates when continuously dressed. The combination of continuous dressing and the application of the cutting fluid has increased the stock removal rate of the creep-feed grinding process by 25 times that of conventional creep-feed grinding.

Supported by the economic study in Appendix 6 the research has prompted a leading British machine tool manufacturer to adopt the two main principles highlighted in this work (continuous dressing and the effective application of the cutting fluid) for a new generation of creep feed grinding machines.(88)

CHAPTER 8

FURTHER WORK

The research work reported in this thesis has exhibited the potential of the creep-feed grinding process for the high stock removal of two 'superalloy' materials. The grinding of a complex form e.g. the fir-tree root of a turbine blade, is a typical creep-feed grinding operation, however the research programme has been conducted using a plain form only. The specific energy profile is constant across a plain form whereas across a complex form the specific energy profile would be expected to vary. The effect of grinding a form on the stock removal capability of the process is economically an essential area for further investigation.

The creep-feed grinding process showed a potential for high stock removal by the action of continuously dressing the grinding wheel. The wear on the diamond roller dresser is an important consideration for the overall economics of the process. The cost of a hand set diamond roller dresser, essential for maintaining accurate forms and low specific energy, is extremely high. Two diamond roller dresser manufacturers were consulted and were of the opinion that the life of a dresser could possibly be extended by the action of continuous dressing as the dresser will not suffer the cyclic and intermittent dressing action associated with the conventional creep-feed grinding process. Many factors affect the life of a diamond roller dresser e.g. the distribution and size of the diamonds as well as in-process vibration and thermal shock; it would seem that these areas need close examination.

The choice of the grinding wheel grade for use with continuous dressing has been shown to affect the transition from thermal damage to grinding wheel breakdown. An optimum grade presumably lies between the extremes of the WA 60 KV and the WA 60 80 FP2V grades used in the research. Further work to find optimum grinding wheel grades, in particular the effects of grit size, bond strength and the achievable surface finish, would appear to have the capability of reducing the vast selection of grinding wheel grades on the market today, that is if continuous dressing were more generally applied.

The action and application of a water based cutting fluid has been observed by the author and others in the Grinding Group at Bristol. Particular interest has been the way in which the cutting fluid conducts the heat generated by the grinding process, away from the workpiece to avoid thermal damage. Neat oils could prove to be a preferable alternative to water based cutting fluids in that they are commonly accepted to be significantly better lubricating agents and therefore generate less heat by friction, reducing the deleterious effects of the rubbing energy. There are a number of effects which can be attributed to the type of cutting fluid used when grinding e.g. loading of the grinding wheel, redeposition of material and metallurgical changes in the workpiece surface. In order to quantify these effects a comparison between the performance of the creep-feed grinding process when neat oils are used and when water based cutting fluids are used, would therefore seem useful.

In this work, a mathematical model was formulated to give further insight into the warming-up effect of the cutting fluid on the performance of the creep-feed grinding process, however a more detailed study of the model, determining empirically each individual assumption, and verifying the behaviour of the model in its entirety, would seem worthwhile.

The research work highlighted a possible discrepancy in Malkins partition of energy theory, relating to the amount of the total grinding energy that enters the workpiece. Using a similar calorimetry technique to that used by Malkin, the energy transferred to the workpiece during creep-feed grinding with continuous dressing could be measured and if needs be, a correction made to Malkins partition of energy model.

The continuously dressed creep-feed grinding process gives rise to a matt surface finish. This suggests two avenues for further work; i) To evaluate the surface by a programme of creep and fatigue testing, supported by simulated in-service component assessment, and ii) To determine the underlying cause of the effect in order to prevent it occuring so that the process becomes a single-pass process. Should the continuously dressed surface prove unsatisfactory then a 'skimming cut' would be necessary after the bulk stock has been removed, in order to clean up the surface. In any case, it is usual, in the aero engine industry, when conventionally creep feed grinding to take a 'skimming cut' after the bulk stock has been removed to ensure the accurate retention of form.

The economic study of the creep feed grinding process with continuous dressing illustrates a potential advantage in terms of faster machining times with less grinding wheel wear by

adopting large grinding wheel diameters and large batch production. A future bonus lies in the fact that continuous dressing removes the majority of rubbing energy which detracts from the use of high peripheral speed, creep-feed grinding. It is feasable that the combination of high peripheral wheel speeds with the continuous dressing of large diameter grinding wheels could lead to stock removal rates in the order of 100 times faster than existing methods in production. Further work in this area has an obvious potential.

REFERENCES

1. The Surface Integrity of High Temperature Alloys.
S C Salmon, B Tech, Thesis Loughborough Univ. of Tech, 1975.

2. The advent of Creep Feed Profile Grinding.
C H Wick, Manufacturing Eng. and Management, June 1975 pp 44-46.

3. Elb Machines for Single-pass Grinding of Profile Shape on Flat Parts.
Editorial, Mach. and Prod. Eng, October 1969 pp 688-692.

4. High Speed Creep Feed Grinding.
T V Stuart, Ph D, Thesis University of Bristol, 1977.

5. Thermal Aspects of Grinding - Parts 1 and 2.
S Malkin et al, Trans ASME, Jnl of Eng. Ind, November 1974, pp 1177-1191.

6. Application of Cutting Fluid in Creep Feed Grinding.
J W Powell, Ph D, Thesis University of Bristol, 1979.

7. Temperature Field in a Workpiece During Peripheral Surface Grinding.
J Gazda et al, Strojirenstvi, 24, 1974, pp 347-351 (in Czech).

8. Moving Sources of Heat and the Temperature at Sliding Contacts.
J C Jaeger, Proc. Roy. Soc N S W, Vol 76, 1946, pp 203-224.

9. Some Thermal Aspects of the Grinding Process.
N R DesRuisseaux et al. ASTME February 1969, MR69-570.

10. Temperature in Semi-infinite and Cylindrical Bodies Subjected to Moving Heat Sources and Surface Cooling.
N R DesRuisseaux et al. Jnl. Heat Trans. Trans ASME Vol. 92, 1970, pp 456-464.

11. Thermal Analysis of the Grinding Process.
N R Des Ruisseaux et al. Jnl. Eng. Ind. Trans. ASME Vol 92, 1970, pp 428-434.

12. Surface Temperatures in Grinding.
Outwater and Shaw, Trans, ASME January 1952, pp 73-86.

13. Thermal Aspects of Surface Grinding.
W J Sauer, Ph D, Thesis, Carnegie-Mellon University, Pitts, Penn 1971.

14. On the Nature of the Grinding Process.
R S Hahn, Proc 3rd MTDR Conf. 1962, pp 129-154.

15. Temperature Calculations for Grinding Operations.
N N Khanzhin. Mach. and Tooling Vol. 62 No. 8, pp 36-38.

16. Thermal Effects Connected with Surface Grinding.
M Gallay, Mechanique No. 298, October 1974, pp 14-18
(in French).

17. Thermal Aspects of the Abrasive Cut-Off Operation -
Part 1.
S. Eshghy, Trans ASME, May 1967, pp 356-360.

18. Thermal Aspects of the Abrasive Cut-Off Operation - Part 2.
S Eshghy, Trans ASME, May 1967, pp 360-364.

19. Thermally Induced Damage in Grinding.
R Snoeys et al. CIRP, Vol 27, February 1978, pp 571-581.

20. Creep-Feed Grinding.
R G Shafto, Ph D Thesis. University of Bristol, 1975.

21. Temperature Determination in Grinding.
J Panhorst et al. Ind. Dia. Review, September 1976, pp
320-325.

22. An Investigation on Instantaneous Temperatures in the
Grinding of Alloy Steels.
D E Anel'chick, Ind. Dia. Review, December 1965, pp 539-543.

23. Contactless Method of Temperature Measurement in Grinding.
S A Popov. Russ. Eng. Jnl. Vol 59 No. 1 pp 74-77.

24. The influence of the Grinding Process on the Structure
of Hardened Steel.
Littmann and Wulff Trans. ASME Vol 47 1955 pp 693-714.

25. Thermal Aspects of the Grinding Operation.
K Takazawa Ind. Dia. Review, April 1972, pp 143-149.

26. Grinding Temperature.
K Sato Bull, JSGE, No. 1, 1961, pp 31-33.

27. Effects of Grinding Variables on Surface Structure of
Hardened Steel.
K Takazawa Bull, JSPE Vol. 2, No.1, April 1966, p 14.

28. The Relation between Grinding Conditions and Thermal
Damage to the Workpiece.
R S Hahn, Trans. ASME, May 1956, pp 807-812.

29. High Speed Grinding.
Optiz etal, CIRP Vol. 16, 1968, pp 61-73.

30. Heat Affected Zone in Grinding Operations.
Maris et al. 14th MTDR Conf, 1973.

31. On the Effects of Real Area of Contact and Normal Stresses
in Grinding.
Hahn and Lindsay CIRP, Vol 15, 1967.

32. Grinding Fluids.
R E Schofield et al, Prod. Eng., September 1973, pp 313-315.

33. Advances in Grinding Fluids.
P D Oates, Ind. Dia. Review, January 1972, pp 12-14.

34. The Role of Chemical Reactions in the Preparation of Metal Surfaces by Abrasion.
Duwell et al, Wear 9 1966, pp 417-424.

35. The Effect of Oxygen and Water on the Dynamics of Chip Formation During Grinding.
Duwell et al, ASLE 68-LC-19

36. Fluorides and Silico-fluorides as Cutting and Grinding Lubricants for Titanium.
Shapiro, ASLE 68-LC-20.

37. Exotics and Chlorinated Fluids do Mix.
K Gettleman, Modern Machine Shop, May 1974, pp 94-99.

38. Oil Cancer Kills.
Metalworking Production, November 1968, p 54.

39. Heat Transfer Characteristics of Grinding Coolants in Quenching.
Holton and Underwood, B.Sc Thesis, University of Bristol, 1978

40. Transient Boiling Heat Transfer in Simulated Grinding.
Clewlow and Lewis, B.Sc Thesis, University of Bristol 1979.

41. A Better Way to Apply Grinding Coolant.
T C Morris, Metalworking Production, November 1966, pp 86-89.

42. How Wet is Your Wet Grinding?
R C Fisher, Amer. Machinist, Vol 107, No. 7, April 1963, pp 114-115.

43. Coolant Supply for High Speed Grinding.
Palmer-Lewis, Metalworking Production, December 1968, pp 34-35.

44. Grinding Fluids Break the Air Barrier.
MTIRA, Metalworking Production, January 1974, pp 68-73.

45. High Speed Grinding.
M C Shaw, ASME 7oWA/Prod. 27

46. Influence of Supply Condition of Grinding Fluids on Grinding Performance of free In-feed Plunge Grinding.
R Furuichi Bull. JSME Vol.24 1971 pp 275-280.

47. A Survey of the Present State of High Speed Grinding.
Konig et al. CIRP Vol.24 1971 pp 275-280.

48. Effectiveness of High Pressure Jet Cooling in In-feed Grinding.
Khudobin et al. Russ Jnl.Eng. Vol.68 No.5 pp 67-69

49. Grinding Wheel with Helical Grooves - An Attempt to .Improve the Grinding Performance.
Nakayama et al. CIRP Vol.25 1977 pp 133-138

50. Characterisation of Wheel Wear in Plunge Grinding.
Verkerk. CIRP Vol.25 1977 pp 127-131.

51. Influence of Cooling Method on Grinding Zone Temperature
I P Karaim. Machines and Tooling. Vol.60 No.6 1969 PP 42-43.

52. Coolant Application in Creep Feed Grinding. - Interim Report
J W Powell. Univ. of Bristol. Jan. 1976.

53. Lubrication by Grinding Fluids at Normal and High Wheel Speeds
Osman and Malkin. Trans. ASLE Vol.15,4 pp 261-268.

54. Grinding Operations with Coolant Delivery from Inside and Outside the Grinding Wheel.
Martynov et al. Machines and Tooling No.9 1959.

55. Workpiece Damage Produced by Creep Feed Grinding.
W J Plumbridge et al. Dedt.Mech.Eng. Univ. of Bristol.

56. A Study of the Heat Flux at Which Burn Occurs in Creep Feed Grinding.
J W Powell et al. 19th MTDR. Conf. 1978.

57. The Mechanics of Grinding.
C Rubnstein. Int.Jnl MTDR Vol.12 Jun.1972 pp 127-139½

58. Criterion of Grinding Wheel Tool Life.
Yoshikawa. Bull. JSGE Vol.3 1963 pp 29-32

59. Scanning Electron Microscopy and Microprobe Investigation of High Speed Sliding Wear of Aluminium Oxide.
J A Kirk et al Wear. 27 (1974) pp 367-381.

60. The Wear of Grinding Wheels. Pt.1 Attritious Wear.
S Malkin et al. Trans. ASME Nov. 1971 pp 1120-1128.

61. The Wear of Grinding Wheels. Pt,2 Fracture Wear.
S Malkin et al. Trans. ASME Nov. 1971 pp 1129-1133.

62. The Wear Mechanisms of Grinding Wheels.
S Malkin. Trans. ASME MR69-566.

63. On the Wear by Attririon of Abrasive Grains.
H Tsuwa et al. Bull JSPE No.2 1966 pp40-46.

64. Wear Flats Generated during Grinding With Various Grinding Fluids.
M E Foerster et al. Proc.2nd North Amer. Metalworking Conf. May 1974 P601.

65. Mechanism of Rubbing and Biting of Cutting Edge on Work Surface in Grinding Process.
Shonozaki et al. Bull. JSPE Vol.2 No.1 1966 pp8-13.

66. Rubbing of Abrasive Grains in the Grinding Process.
Y Tanaka. Bull. JSPE Vol.1 No.3 1965 pp177-181.

67. The Size Effect in Metal Cutting.
W R Backer et al. Trans. ASME Jan. 1952 pp 61-72

68. Effects of Grain Size and Operating Parameter on the Mechanics of Grinding.
S Kannappan et al. Trans. ASME Jnl.Eng.Ind. Aug.1972 pp 833-842

69. Size Effects in Abrasive Processes.
S Malkin et al. 13th MTDR Conf. 1972.

70. M Frost University of Bristol. Private Communication.

71. Cutting Characteristics of Grinding Wheels Dressed by Different Methods.
Z Kornberger et al. Mach. & Prod. Eng. Mar 1971 pp 490-494.

72. Dressing Abrasive Grinding Wheels with Diamond Tools.
J S Selby. Tooling Mar 1970 pp 35-48.

73. Effects of Rotary Dressing on Grinding Wheel Performance.
T Murray et al. Trans. ASME Jnl.Eng.Ind. Jan 1978 pp 1-6

74. The Effect of Dressing Techniques on Grinding Wheel Wear.
E J Pattinson et al. Int.Conf.Manuf.Tech.Univ. of Michigan. Amer. Soc. Tool and Manuf. Eng. 1967 pp 601-617.

75. The Influence of the Dressing Depth of Cut on the Performance of a Single Point Diamond Dressed Alumina Grinding Wheel.
V Pacitti et al. Int. Jnl MTDR Vol.12 1972 pp 267-279.

76. Continuous Dress Grinding
A Ashburn. Metalworking Production Jun 1957 pp 1106-1108.

77. The Influence of High Wheel Speed on Grinding Performance
I J Stewart. Trans. ASME MR69-206.

78. Investigation of the Effectiveness of High Speed Grinding
S N Korchak. Machines and Tooling No.9 pp 48-50.

79. High Efficiency Grinding.
H Opitz. Amer. Machinist. Dec 1968 pp 127-128.

80. What is Gained by High Speed Grinding?
MTIRA Metalworking Production Nov.1968 pp 51-54.

81. High Speed Grinding
R H Dahlin. Amer. Machinist. Feb. 1971 pp 76-81.

82. Increased Output in High Speed Grinding.
L N Filimonov. Russ. Eng. Jnl. Vol.55 No.5 pp 70-72.

83. High Speed Grinding and Productivity
J N Brecker. Carnegie-Mellon Univ. Pitts. Penn.

84. Surface Grinding with High Wheel Speeds and Metal Removal Rates.
W Konig et al.

85. Lower Wheel Speeds in Creep Feed Grinding.
K B Southwell et al. Universal Grinding Wheel Co. Ltd.

86. What the Future Holds for Grinding.
Editorial. Metalworking Production. Dec. 1974 pp 48-55.

87. Grinding Will Meet Tomorrows Demands.
Editorial. Metalworking Production. Apr. 1976. pp 95-103

88. Forming Prompts New Shapes in Grinding.
J Taylor. Metalworking Production. Feb.1979. pp 90-91.

89. GM'S Concept for Increased Grinding Productivity.
Editorial. Manuf. Eng. & Mang. Jun.1975 pp 36-37.

90. Energy Adaptive Grinding.
Editorial. American Machinist. Jul.1977 pp 115-119.

91. Dynamics and Design of Dynamometer
Shiozaki et al. CIRP Vol.18 1976 pp 663-675.

92. A Metal Cutting Dynamometer
G Boothroyd. The Engineer. Feb 1962.

93. Diamond Roller Dressers.
~~H R Meyer et al. Ind.Dia. Review Mar 1975 p89.~~
R L Howard. Mach.and Prod.Eng. 10 March 1976 pp 218-222.

94. Thermal aspects of creep feed grinding.
G R Shafto et al. Dept. Mech. Eng. University of Bristol.

95. Heat Transfer at High Rates to Water with Surface Boiling
W H McAdams et al. Ind. & Eng. Chem. Vol.41 No.9
Sept. 1949 pp 1945-1953.

96. Photographic Study of Surface-Boiling Heat Transfer to Water With Forced Convection.
F C Gunter. Trans. ASME Feb. 1951 pp 115-123.

97. Diamond Roller Dressers: their design and application considerations in Europe.
H R Meyer et al. Ind. Dia. Review Mar. 1975 pp 89-95.

98. Crush Dressing at Full Wheel Speed.
T R A Pearce et al. 19th MTDR Conf. 1978.

99. Forced Convective Boiling and Condensation.
J G Collier. McGraw-Hill, 1972.

FIGURES

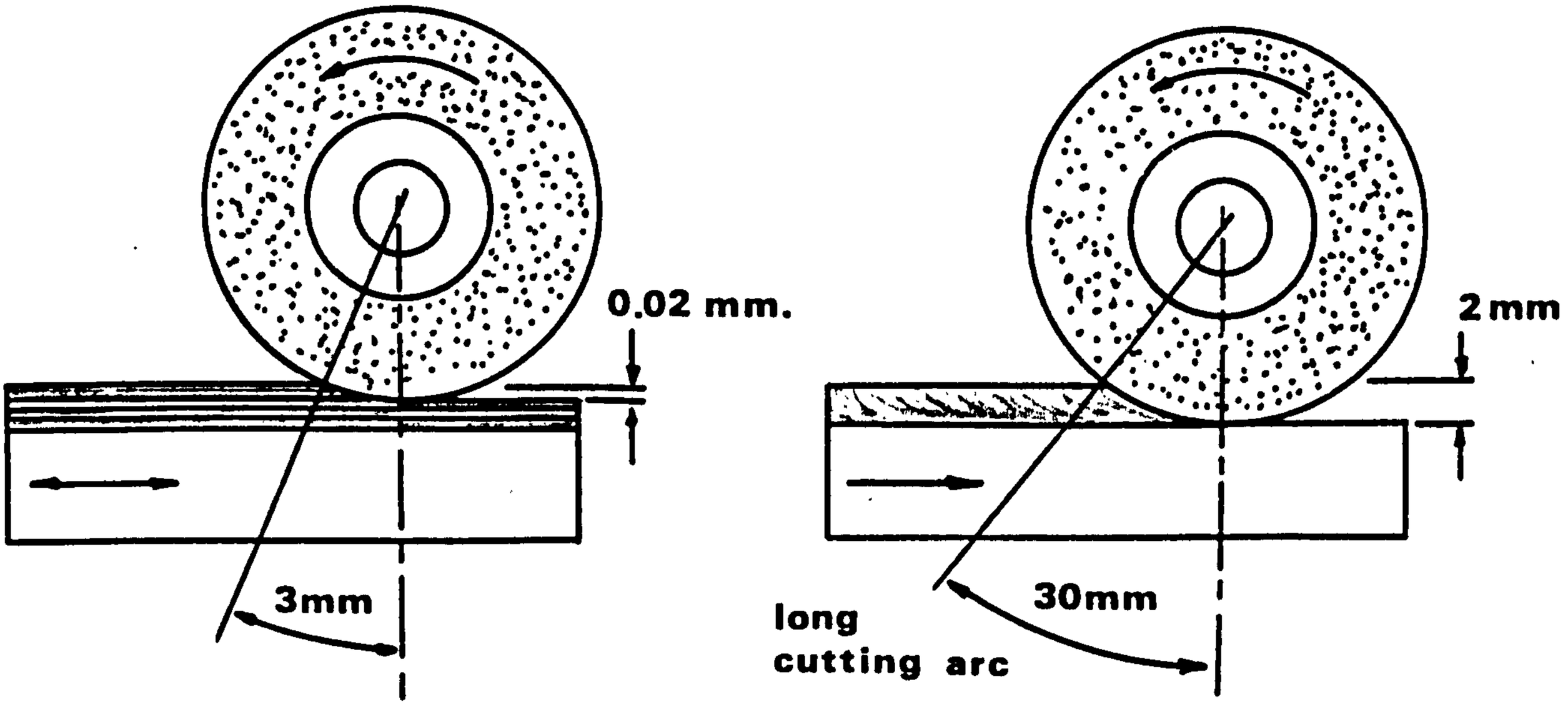

CONVENTIONAL RECIPROCATING GRINDING

CREEP FEED GRINDING

The Creep-Feed Grinding process is a high stock removal process and differs from conventional reciprocating grinding as shown above. The grinding wheel depth of cut is large and the table feed slow. The creep-feed grinding process has therefore demanded special grinding wheels which have induced porosity to allow more efficient cooling of the workpiece and give large chip clearance. Thermal damage has been a limitation to the process due to the heat input to the workpiece surface over the long arc length of cut.

FIGURE 1.

FIGURE 2

ENERGY CONSIDERATIONS

The total specific energy of the grinding process will appear in several forms which include the following:-

1. Heating of the workpiece
2. Heating of the grinding wheel
3. Kinetic energy of the chips
4. Heating of the chips
5. Radiation to the surroundings
6. Generation of a new surface
7. Residual energy remaining in the lattice of the ground surface and the chip

FIGURE 3

HEAT BALANCE BASED ON EXPERIMENTAL WORK OR ANALYTICAL DERIVATIONS BY VARIOUS AUTHORS (MARIS ET AL)

Author	Ref.	Percentage of Energy to Workpiece	Percentage of Energy to Chip and Wheel	Comments
Sauer	13	30 - 70	70 - 30	Experimental
Lee	97	80	20	Experimental
Malkin	5	60 - 80	40 - 20	Experimental
Sato	26	84	16	Experimental
Outwater and Shaw	12	35	65	Analytical (shear Energy)
Eshghy	17	10	90	Analytical (cut-off)

THE RELATIONSHIP BETWEEN THE ENERGY CONDUCTED INTO THE WORKPIECE AND THE PERCENTAGE WEAR FLAT AREA by Malkin.

Test Data (ref 5)

Wheel Grade	32A-46 (G,I,K) 8VBE
Wheel Speed	30 ms^{-1}
Work Speed	4.572 m/min.
Depth of cut	0.025 mm.
Material	A1S1 1095

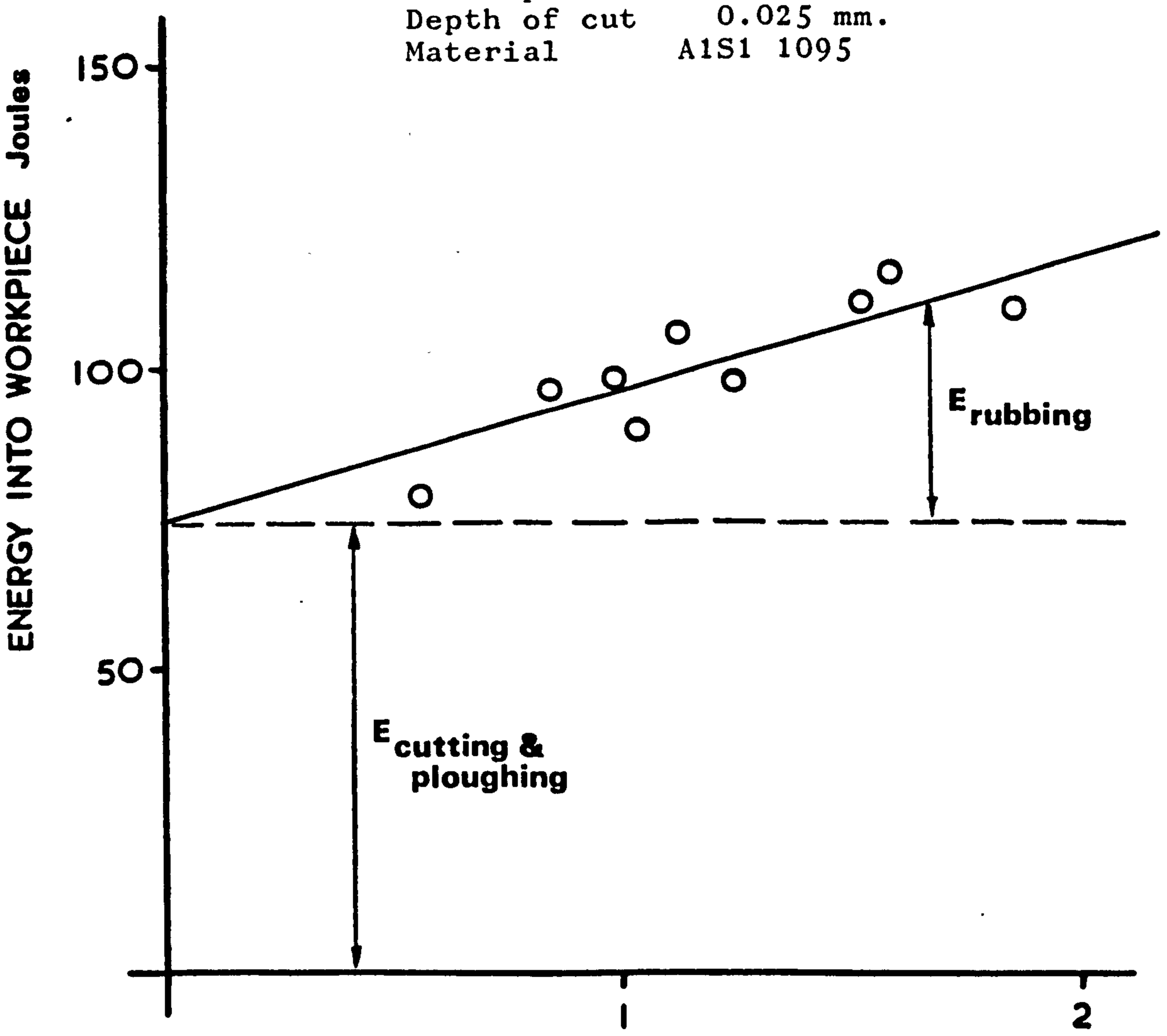

FIGURE 4

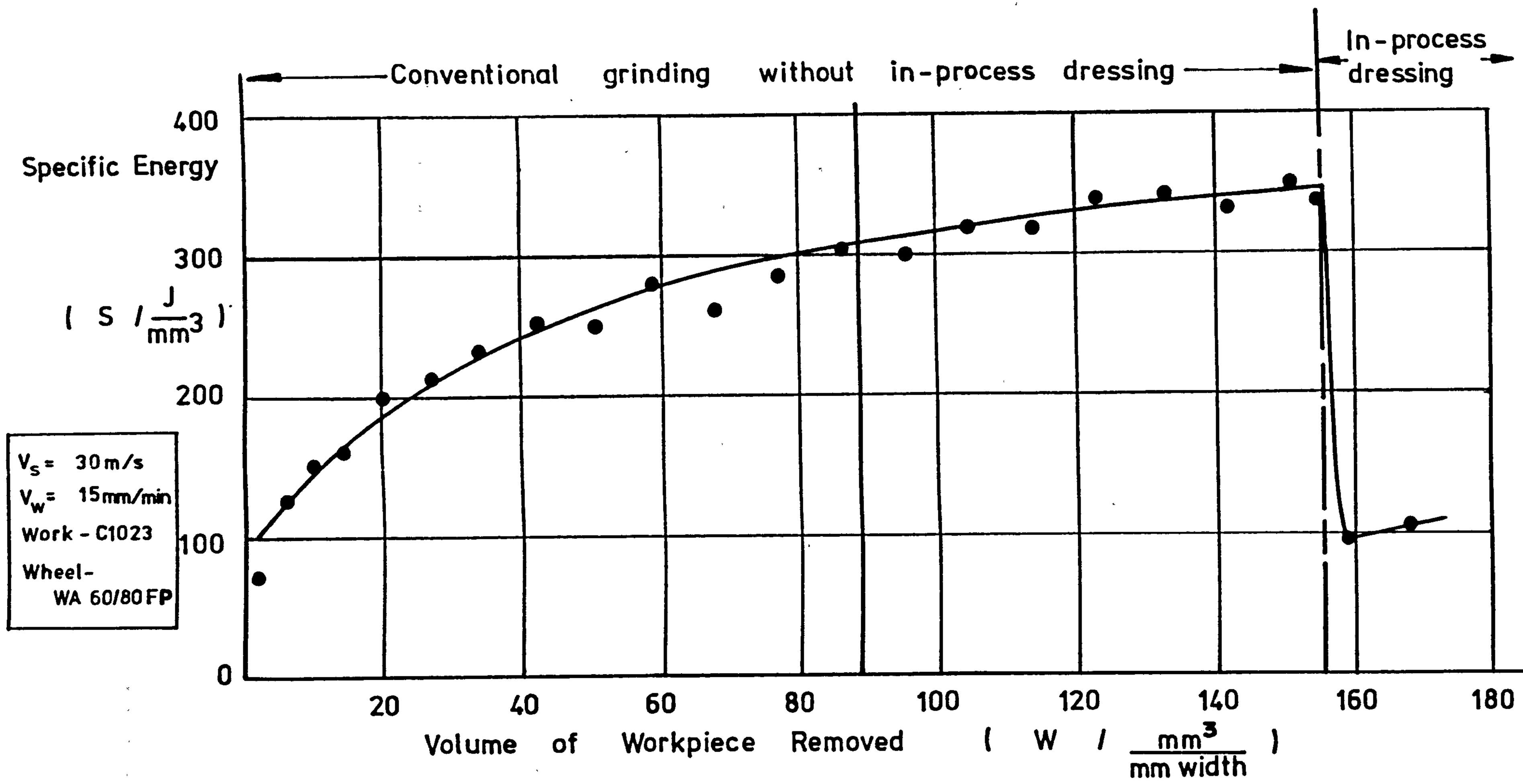

SUDDEN DROP IN SPECIFIC ENERGY CAUSED BY IN - PROCESS DRESSING. (By Stuart. Ref. 4) **fig 5.**

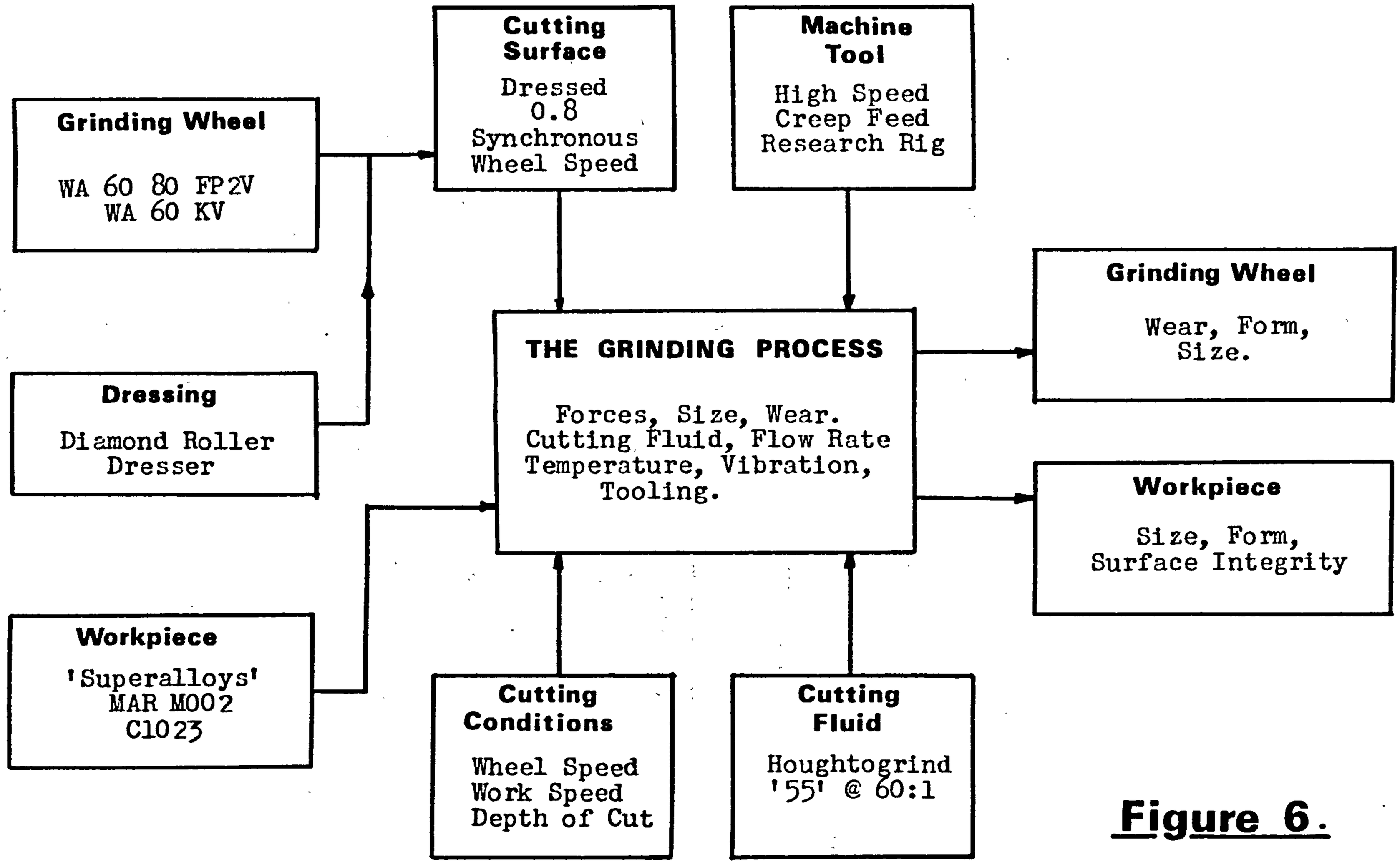
Grinding Wheel
WA 60 80 FP2V
WA 60 KV
Cutting Surface
Dressed
0.8
Synchronous
Wheel Speed
Machine Tool
High Speed
Creep Feed
Research Rig
Grinding Wheel
Wear, Form,
Size.
Dressing
Diamond Roller
Dresser
THE GRINDING PROCESS
Forces, Size, Wear.
Cutting Fluid, Flow Rate
Temperature, Vibration,
Tooling.
Workpiece
Size, Form,
Surface Integrity
Workpiece
'Superalloys'
MAR M002
C1023
Cutting Conditions
Wheel Speed
Work Speed
Depth of Cut
Cutting Fluid
Houghtogrind
'55' @ 60:1

Figure 6.

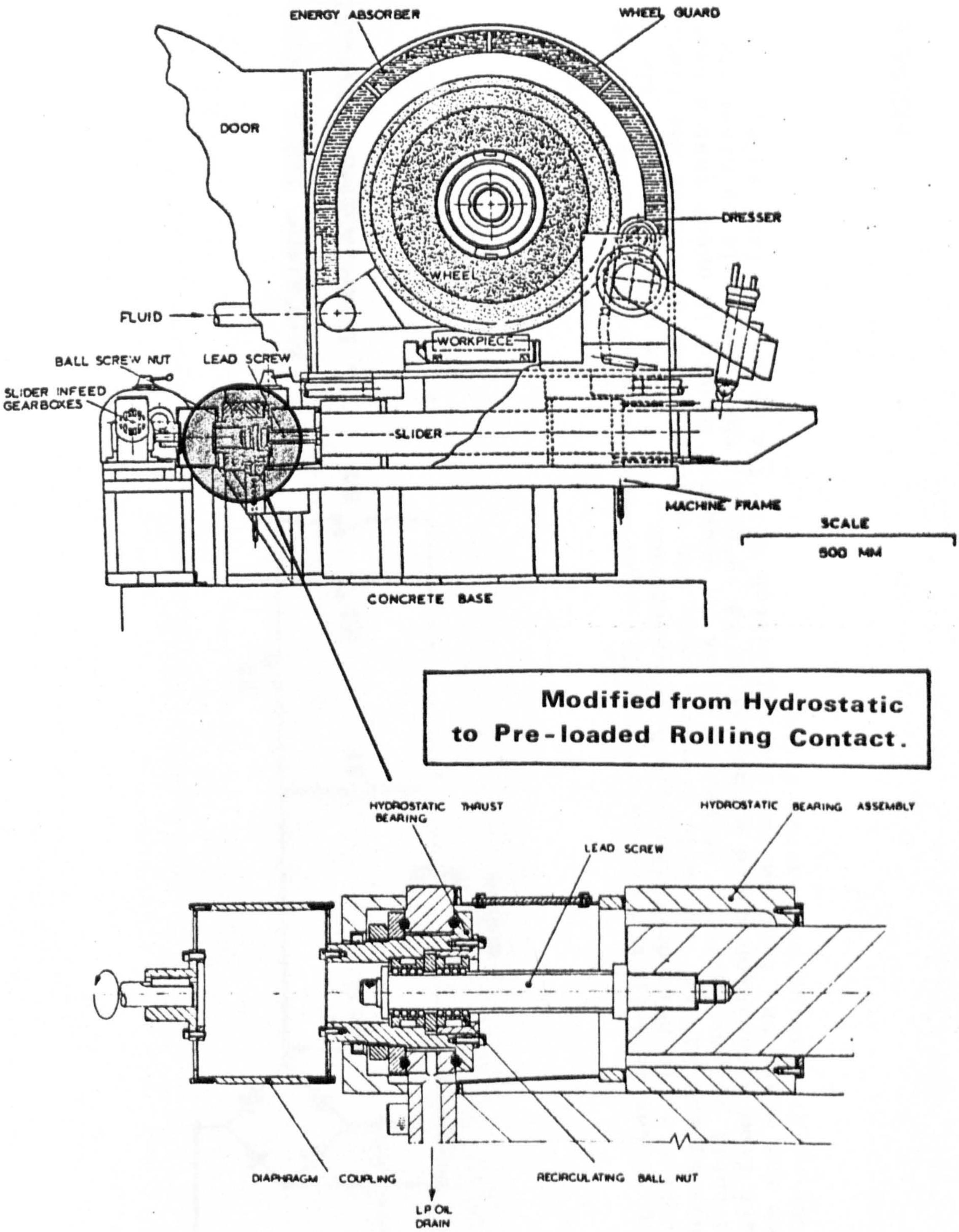
ENERGY ABSORBER
WHEEL GUARD
DOOR
DRESSER
WHEEL
FLUID
WORKPIECE
BALL SCREW NUT
LEAD SCREW
SLIDER INFEED GEARBOXES
SLIDER
MACHINE FRAME
SCALE
500 MM
CONCRETE BASE
Modified from Hydrostatic to Pre-loaded Rolling Contact.
HYDROSTATIC THRUST BEARING
HYDROSTATIC BEARING ASSEMBLY
LEAD SCREW
DIAPHRAGM COUPLING
L.P. OIL DRAIN
RECIRCULATING BALL NUT

FIGURE 7.

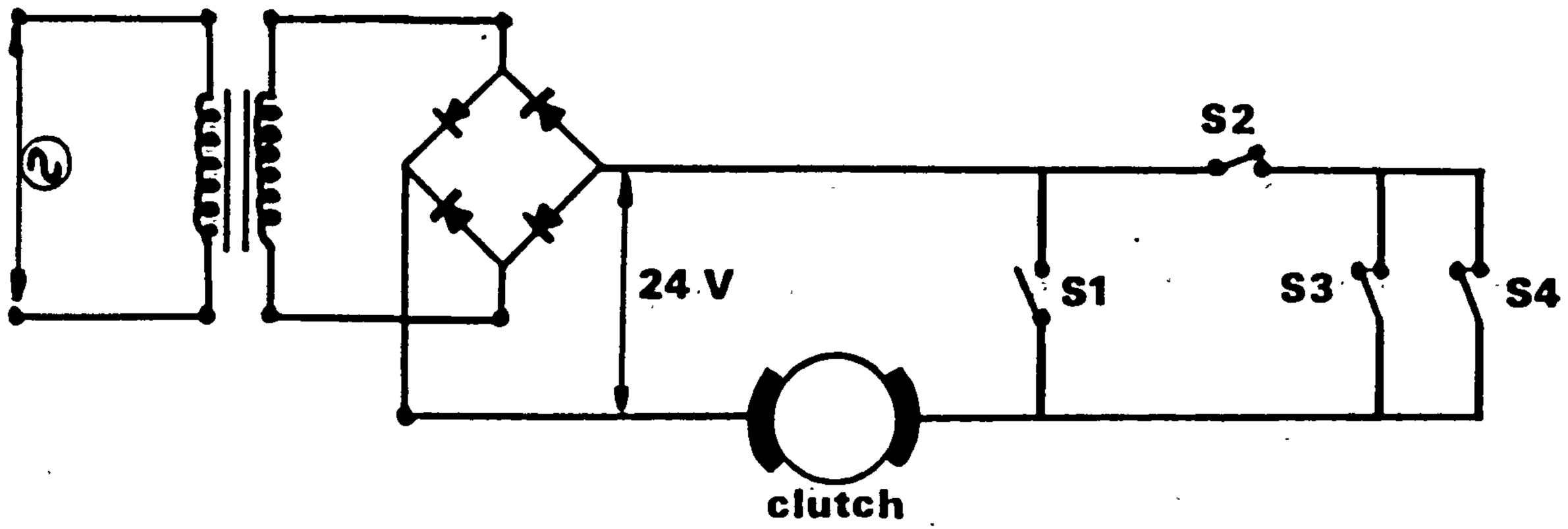

AUTOMATIC TABLE INFEED DISENGAGEMENT CIRCUIT

The switching system is such that S1 is a 'normally open' switch which provides an inching facility. Whilst S1 is held down the clutch is energised. S2 is the master switch, the limit switches S3 and S4 are 'normally closed', once the master switch is closed the clutch is energised until a limit switch, either S3 or S4 is opened. Should it occur that a test needs to start from a position where either S3 or S4 is open, the routine is to close the master switch and start the test on the inching switch S1. The system is fail safe, protecting the recirculating ball-screw drive.

FIGURE 8

This diagram shows how the clamping of the specimen, in the original dynamometer was not in the direction of the forces being measured. Due to the twisting of the tightening bolts it was possible for the specimen to move from its set position.

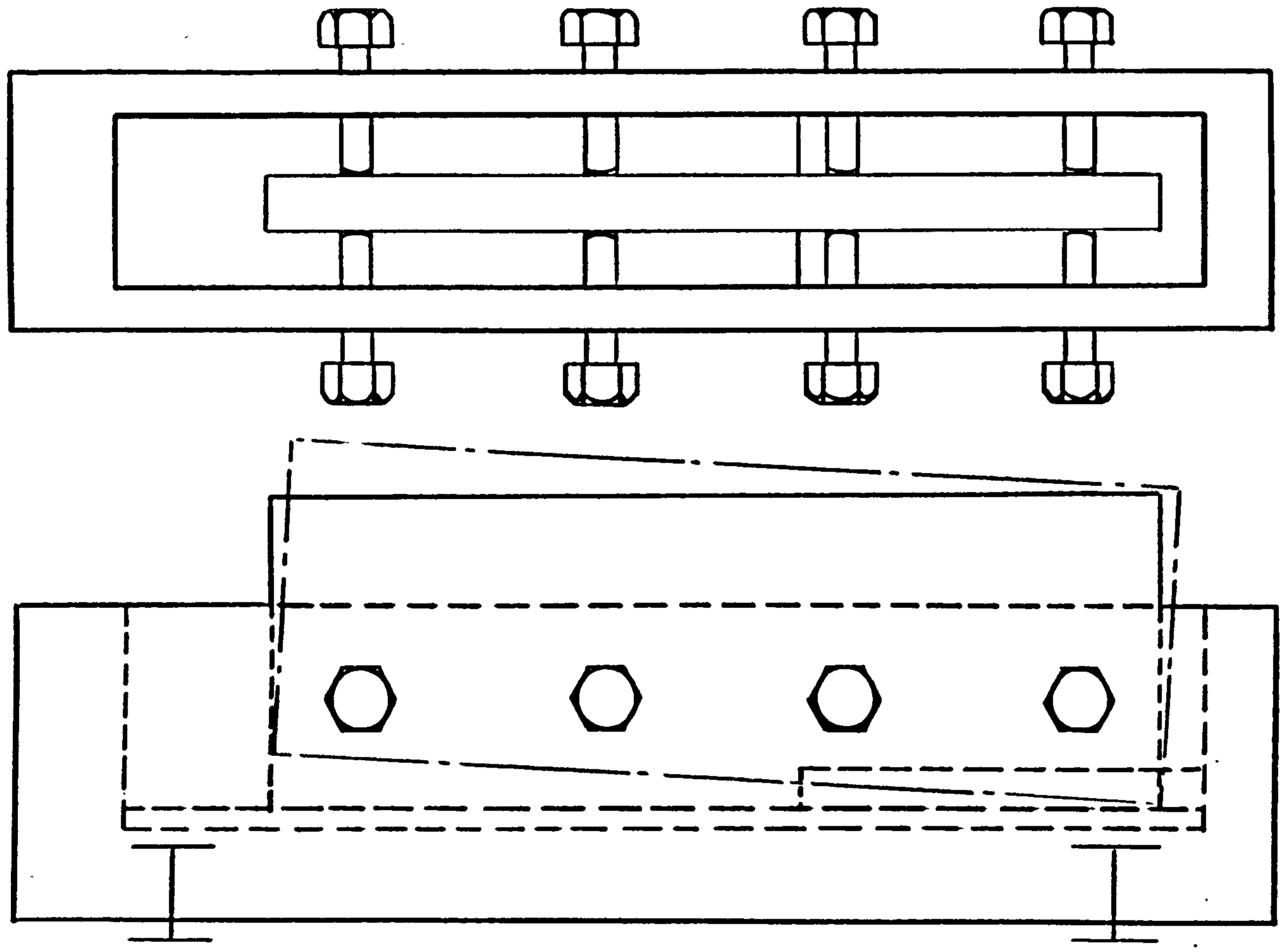

ORIGINAL METHOD OF LOCATING A SPECIMEN IN THE DYNAMOMETER. FIGURE 9.

DESIGN OF DYNAMOMETER LOAD BEAMS

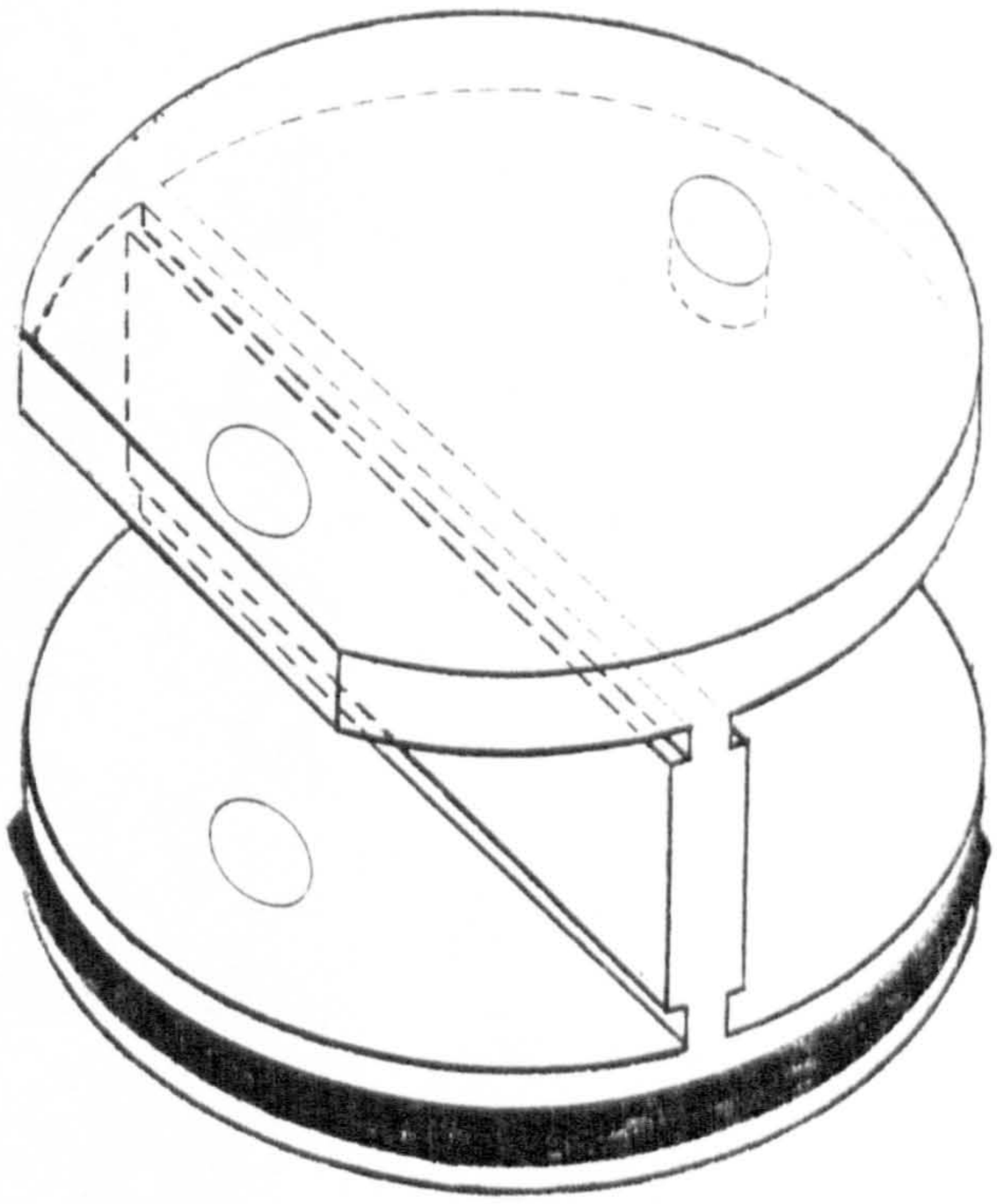

The I-beam section was designed between two circular flanges (right) with an O-ring groove in the base flange. An aluminium can fitted over the beam and sealed on the O-ring (below).

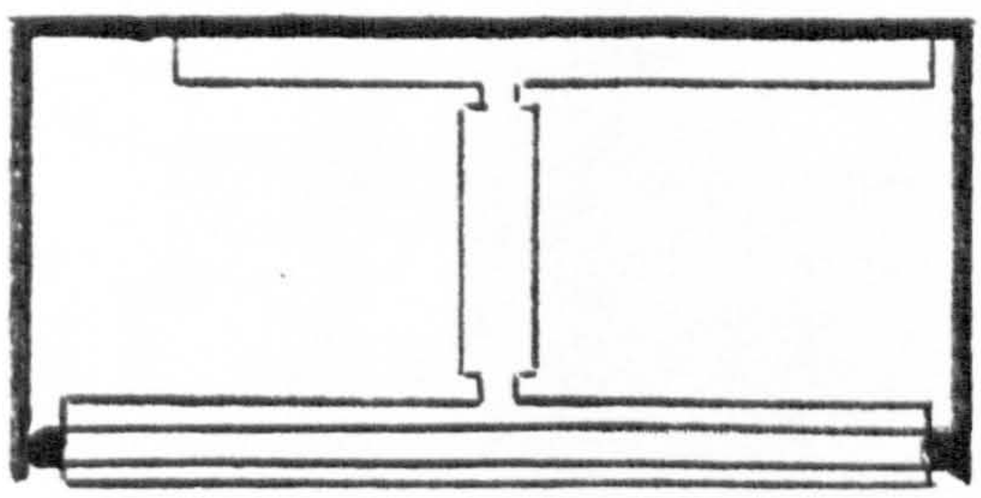

The complete 'quick change' beam assembly and screened strain gauge leads are shown below.

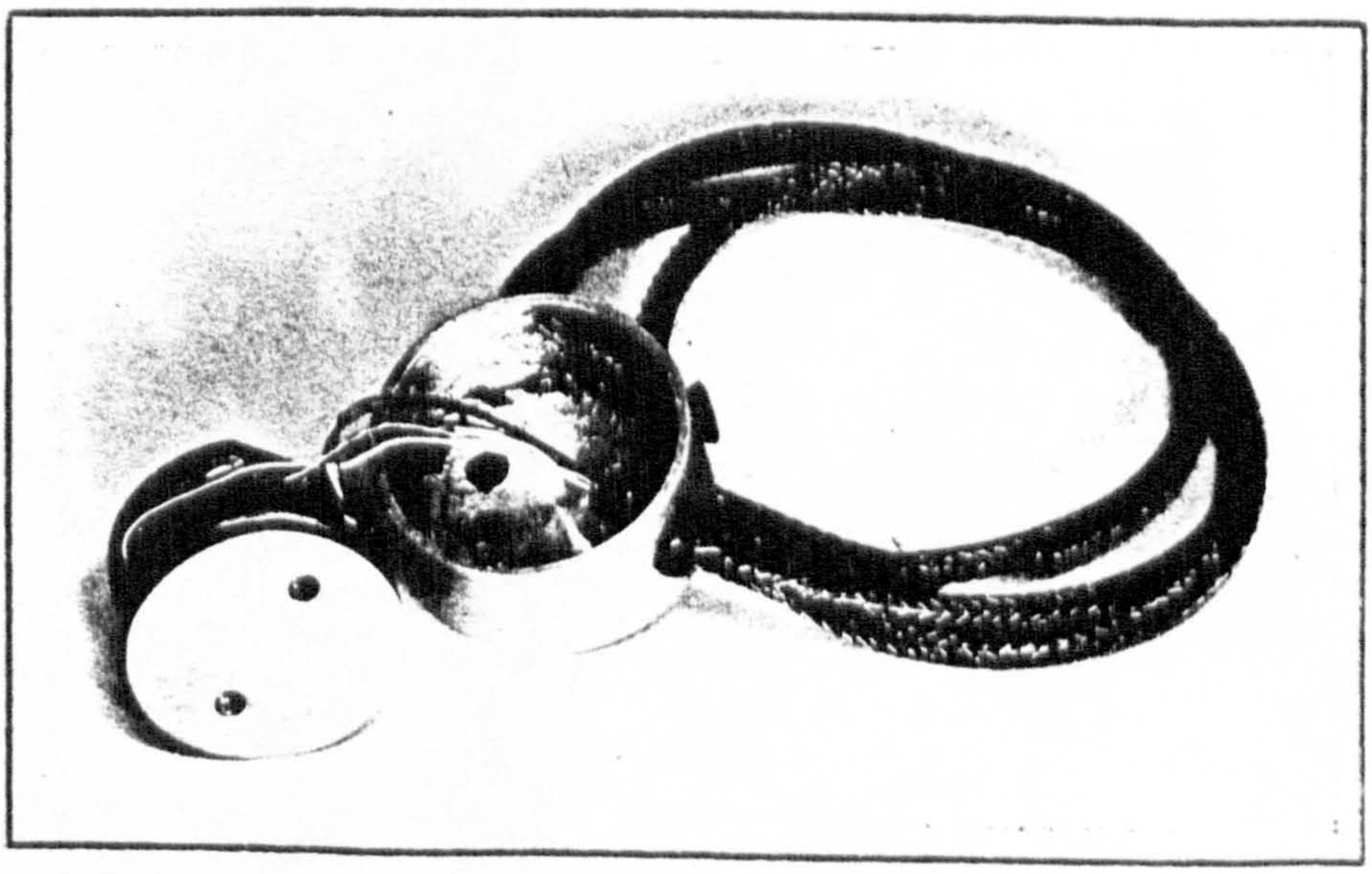

FIGURE 10

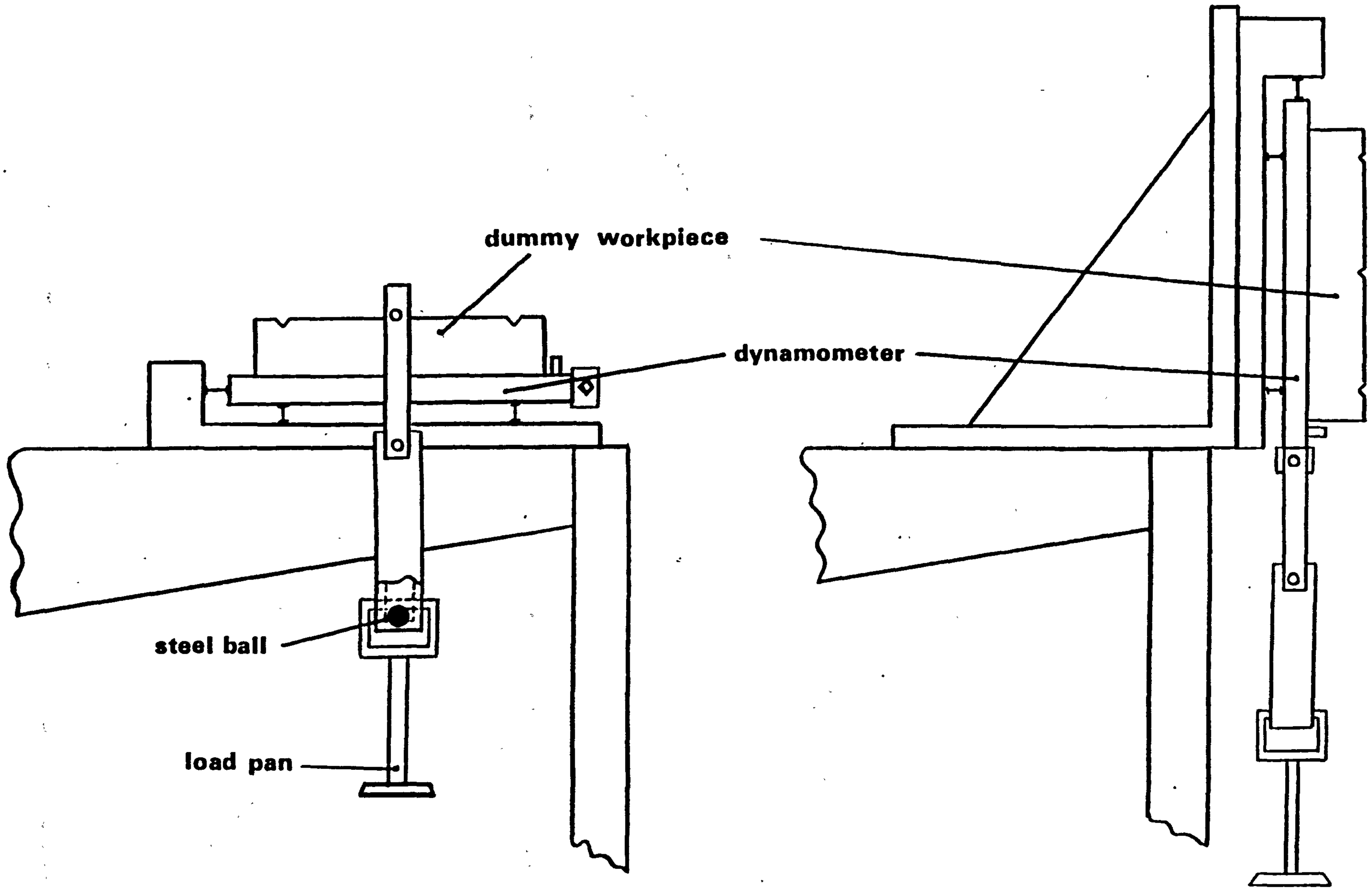

CALIBRATING THE NEW DYNAMOMETER.

FIGURE 11.

THE DRESSER INFEED MECHANISM AND CALIBRATION GRAPHS

FIGURE 12

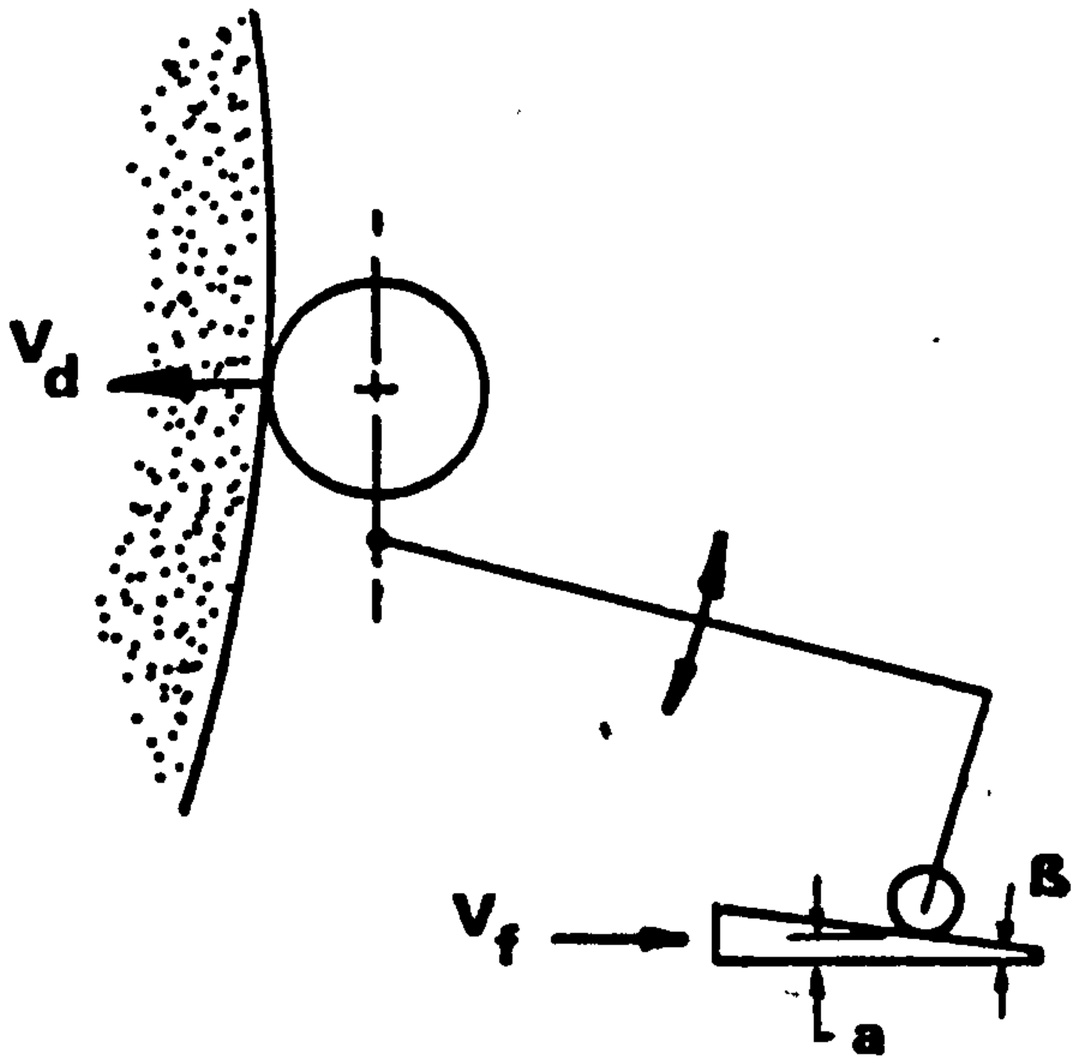

$$V_d = \frac{C_w V_f \tan ß}{1 + \frac{\tan ß}{\tan \theta}}$$

LIMITING STOCK REMOVAL RATES OF THE CONVENTIONAL AND CONTINUOUSLY DRESSED CREEP-FEED GRINDING PROCESS

For Wheel Grade: WA 60 80 FP2V; Depth of Cut: 3 mm; Cutting Fluid: Houghtogrind 55 (60:1) 6 ls^{-1} @ 1.5 bar.

	CONVENTIONAL			CONTINUOUSLY DRESSED		
Material	Work Speed mm/min.	Max. Power Flux MW m^{-2}	Limitation	Work Speed mm/min.	Max. Power Flux MW m^{-2}	Limitation
C 1023	60	40	Burn	1060	55	Wheel Breakdown
Mar M002	55	35	Burn	1350	45	Wheel Breakdown

For Wheel Grade: WA 60 KV; Depth of Cut: 3 mm; Cutting Fluid: Houghtogrind 55 (60:1) 6 ls^{-1} @ 2.5 bar.

	CONVENTIONAL			CONTINUOUSLY DRESSED		
Material	Work Speed mm/min.	Max. Power Flux MW m^{-2}	Limitation	Work Speed mm/min.	Max. Power Flux MW m^{-2}	Limitation
C 1023	10	20	Burn	1060	55	Burn
Mar M002	10	15	Burn	1170	45	Burn

FIGURE 13

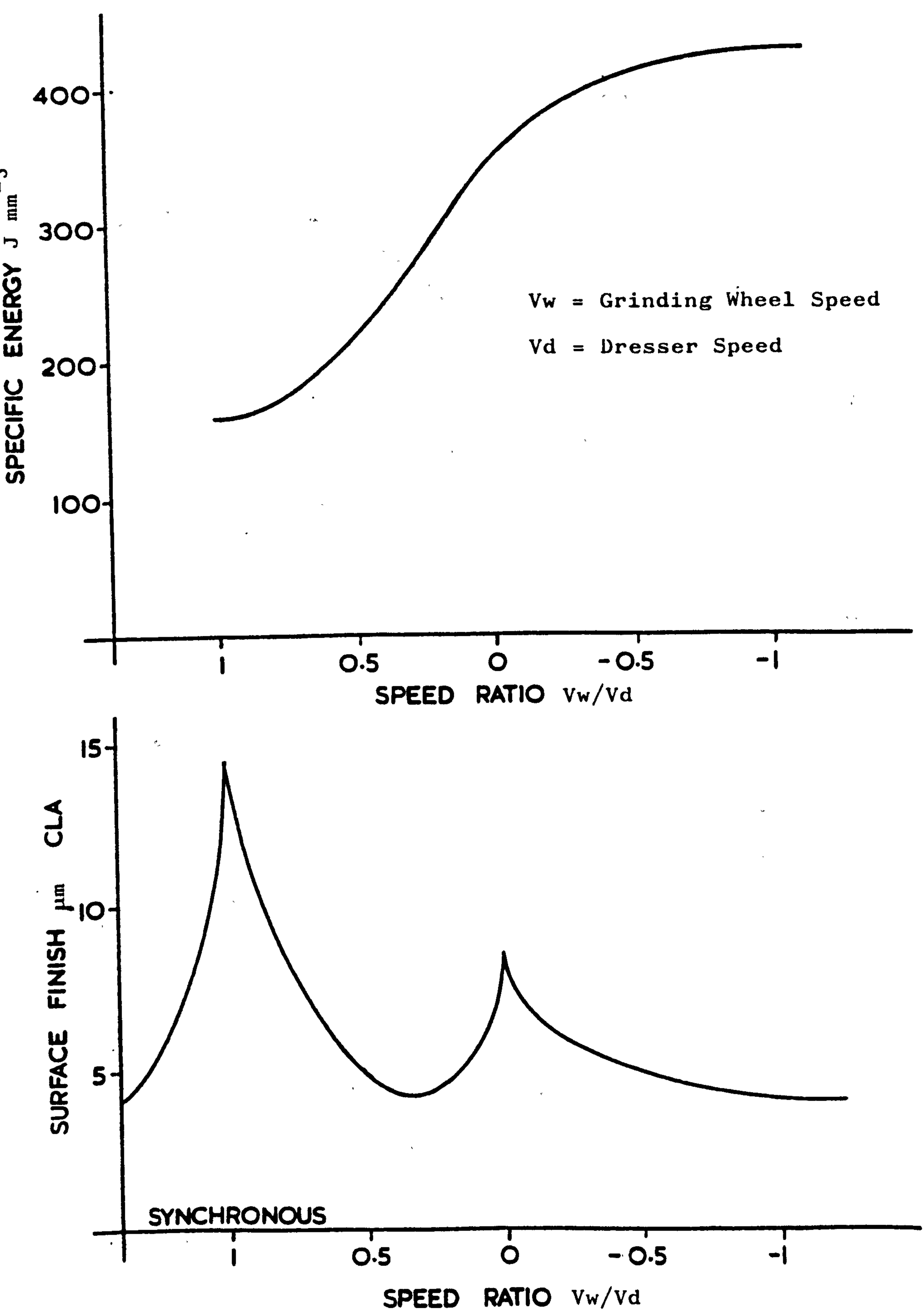

VARIATION OF SPECIFIC ENERGY AND SURFACE FINISH WITH SPEED RATIO OF THE GRINDING WEEL AND DRESSER. REF. 97.

FIGURE 14

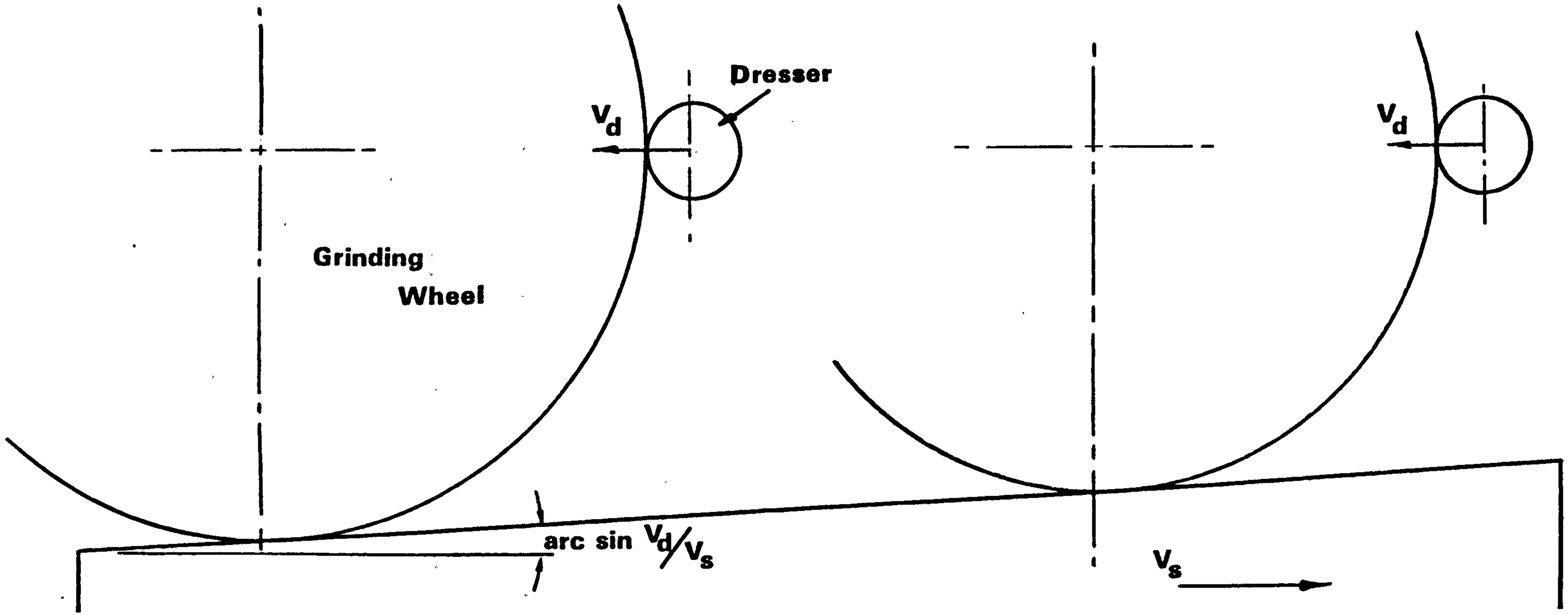

The grinding wheel diameter decreases continuously throughout a continuously dressed creep-feed grinding process (shown). To avoid a taper being ground on the workpiece the slideway or a fixture could be tilted at an angle which is the arc sin Vd/Vs where Vd is the dresser infeed rate in mm/min. and Vs is the slideway speed in mm/min. The taper however, could be used to advantage when grinding broaches. The speeds of the dresser infeed and the slideway could be synchronized in order to achieve the required 'rise per tooth' of the broach.

FIGURE-15.

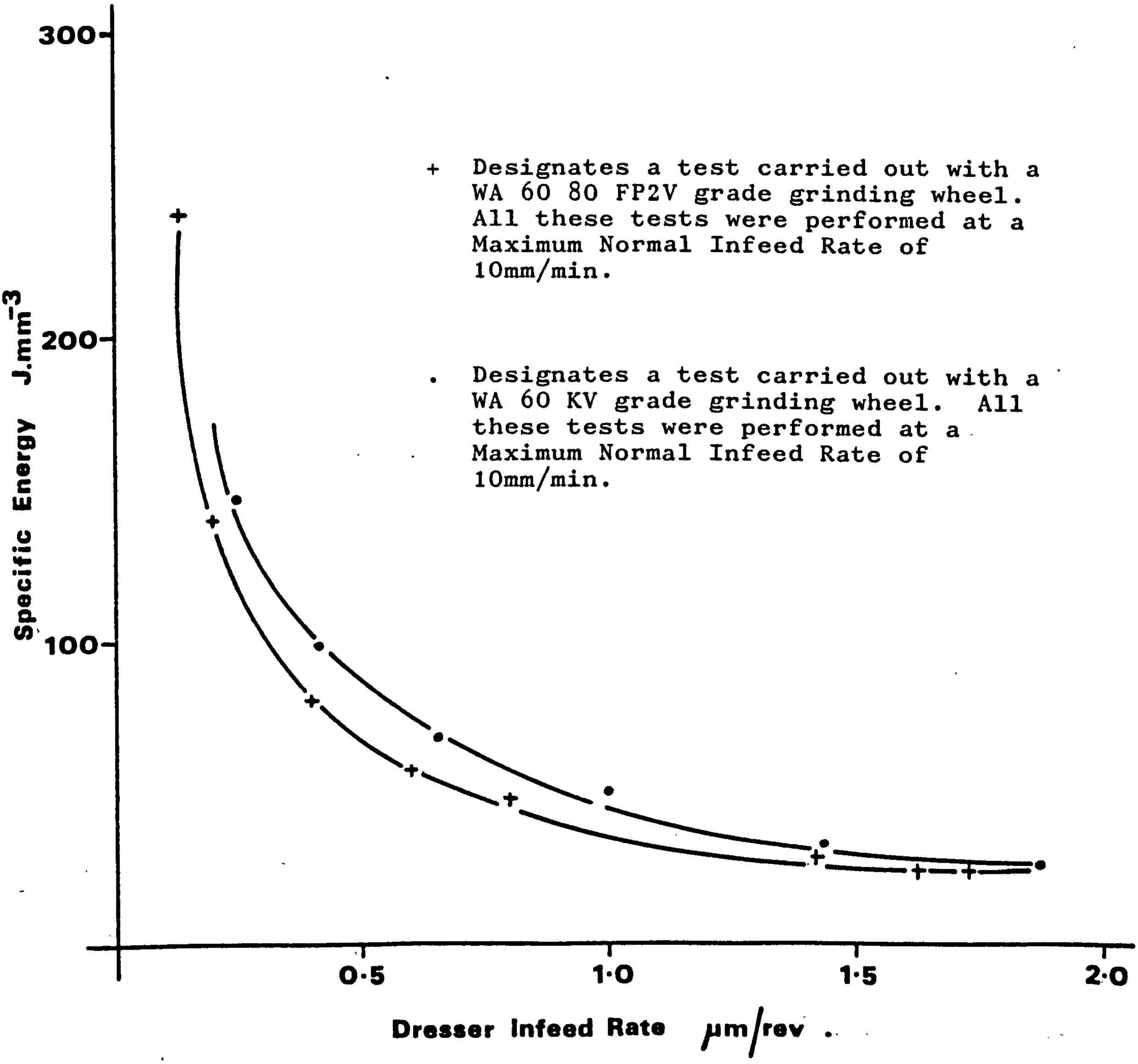

GRAPH OF SPECIFIC ENERGY v DRESSER INFEED RATE FOR C1023

FIGURE 16

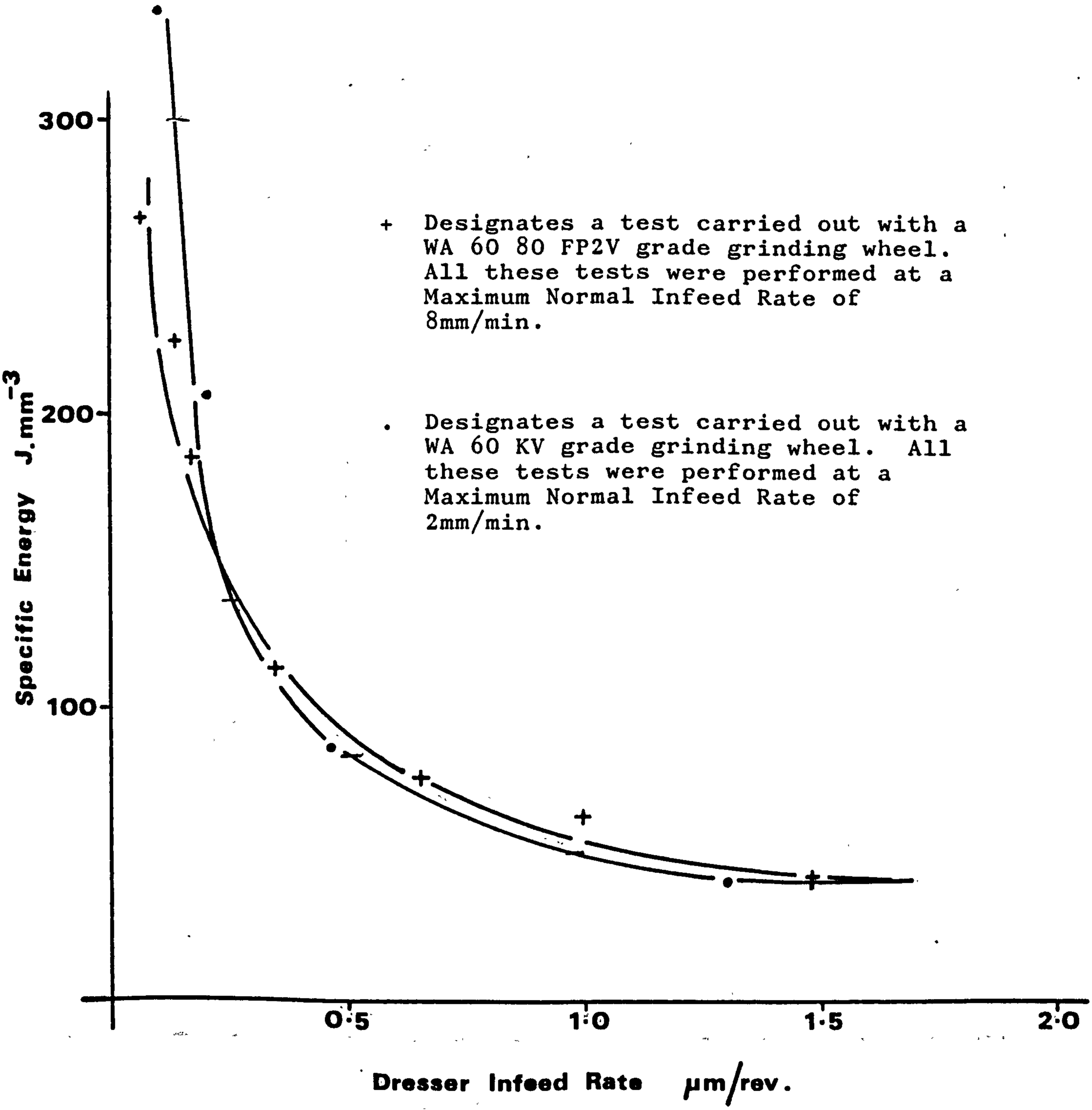

+ Designates a test carried out with a WA 60 80 FP2V grade grinding wheel. All these tests were performed at a Maximum Normal Infeed Rate of 8mm/min.

. Designates a test carried out with a WA 60 KV grade grinding wheel. All these tests were performed at a Maximum Normal Infeed Rate of 2mm/min.

GRAPH OF SPECIFIC ENERGY v DRESSER INFEED RATE FOR MAR MOO2

FIGURE 17

GRINDING WHEELS - WA 60 8O FP 2V
WA 60 KV

MATERIAL - MAR MOO2

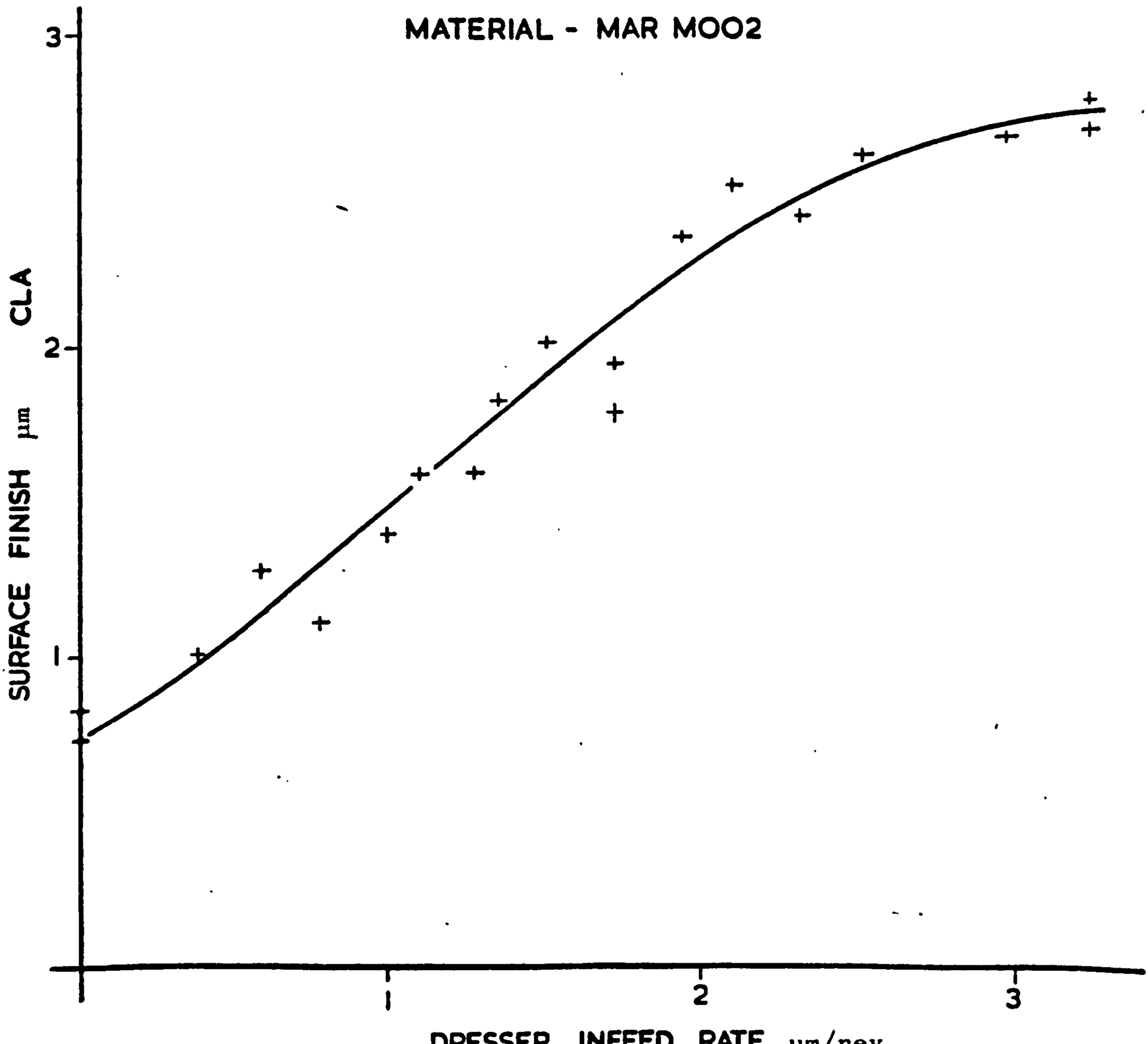

VARIATION OF SURFACE FINISH WITH DRESSER INFEED RATE.

FIGURE 18.

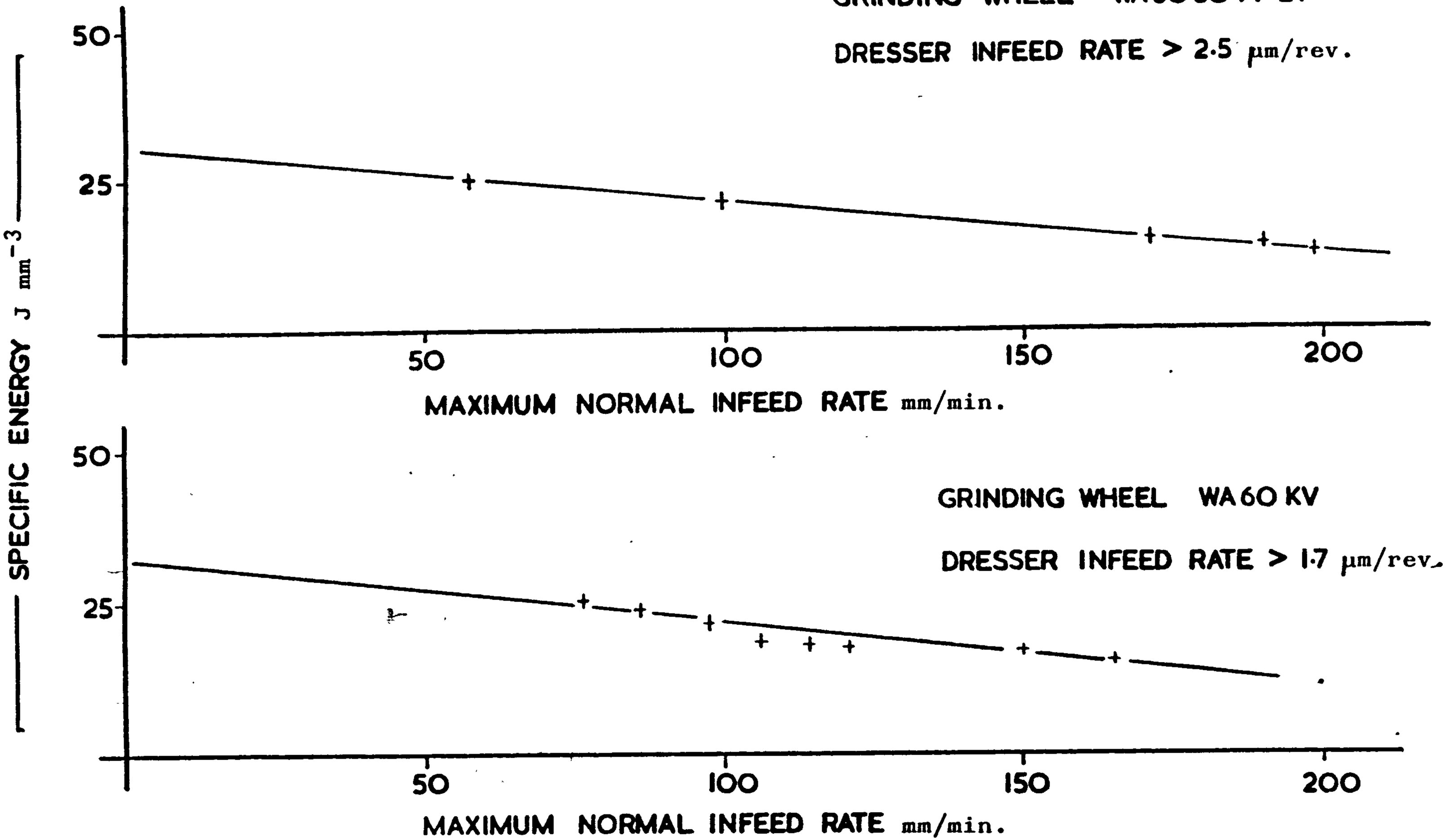

VARIATION OF SPECIFIC ENERGY WITH MAXIMUM NORMAL INFEED RATE FOR MAR M002.

FIGURE 19.

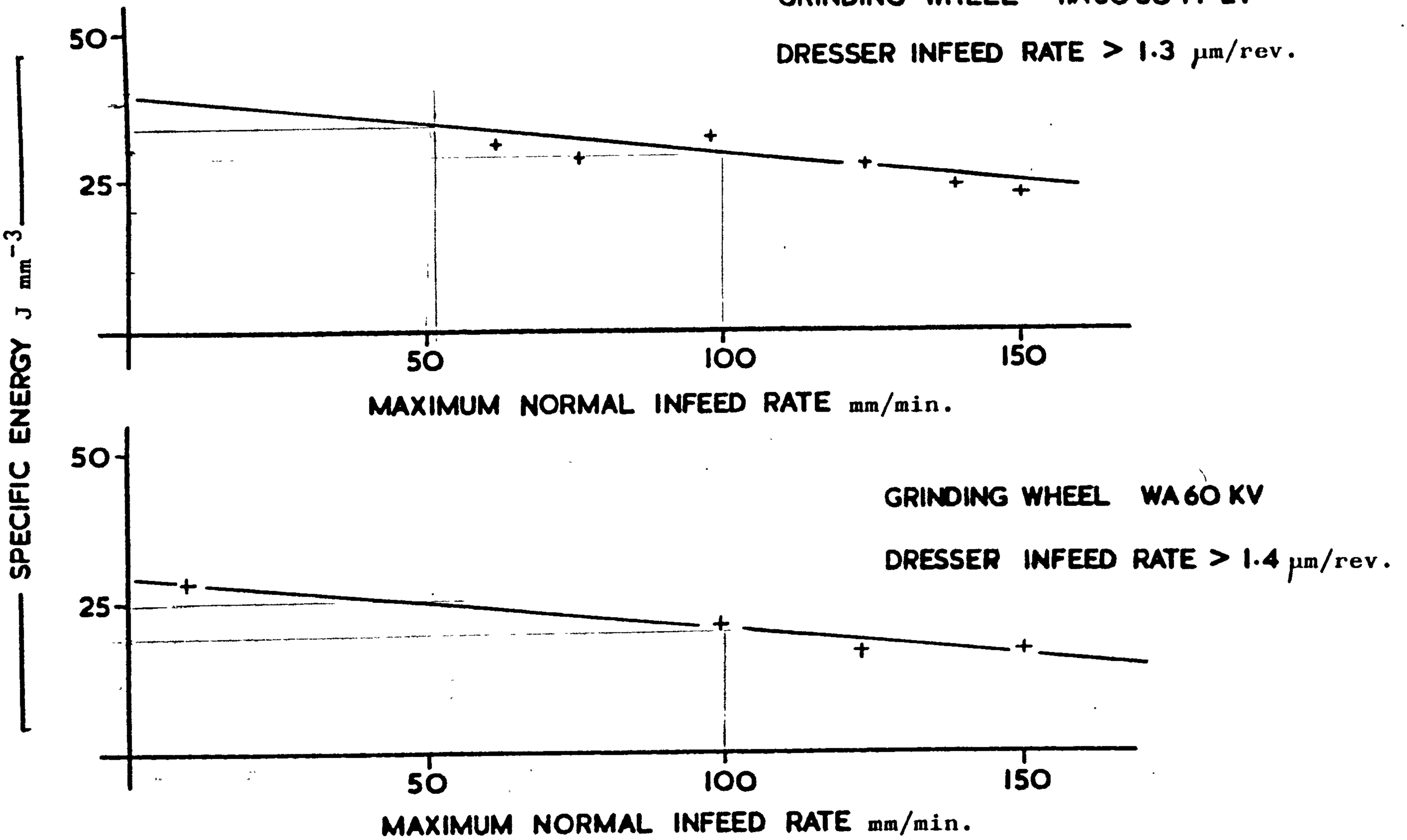

VARIATION OF SPECIFIC ENERGY WITH MAXIMUM NORMAL INFEED RATE FOR C1023.

FIGURE 20.

VARIATION OF SPECIFIC ENERGY WITH DRESSER INFEED RATE FOR MAR MOO2

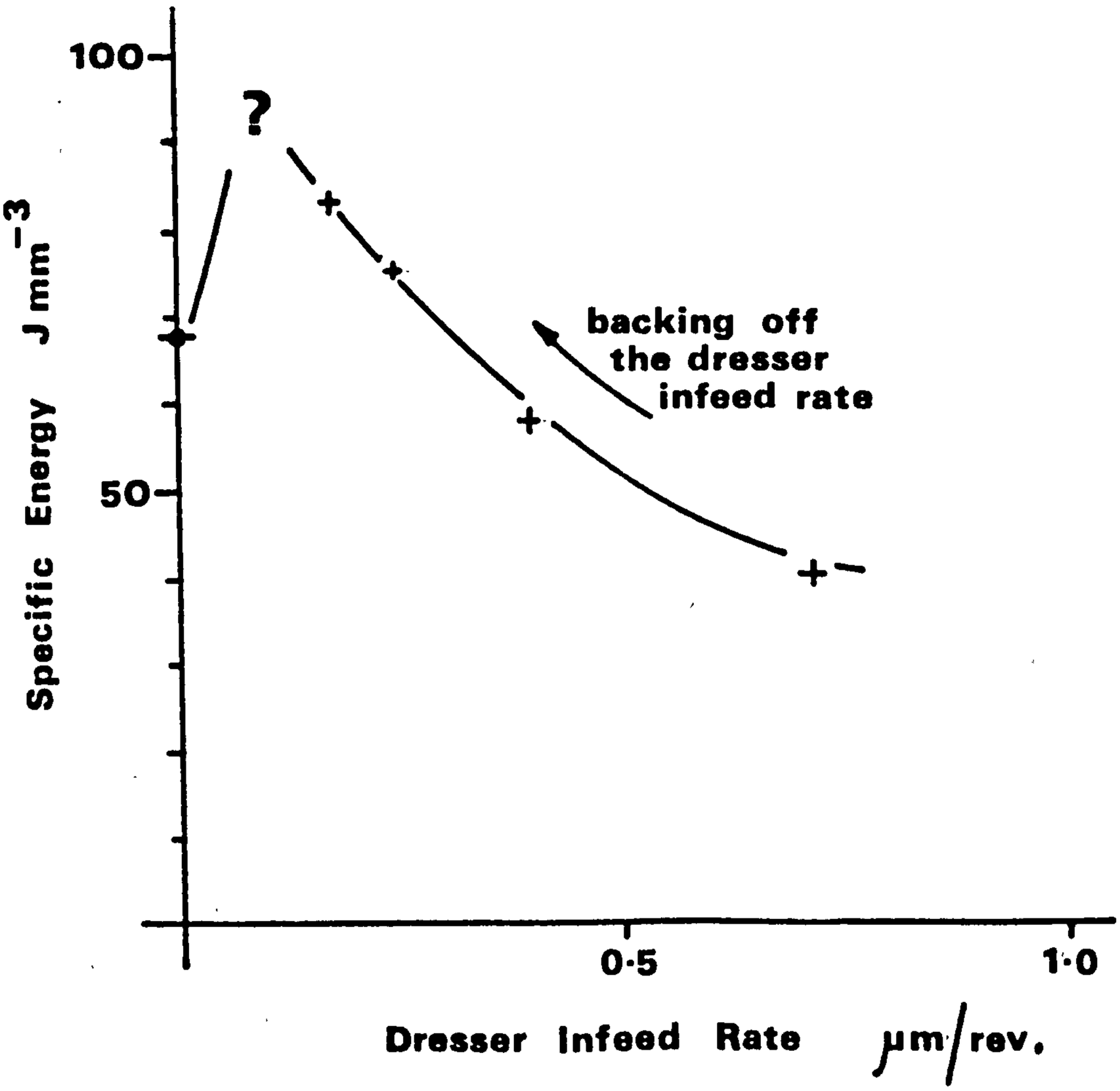

It was hoped, in this instance, that with a maximum normal infeed rate of 30mm/min (which is in excess of the limiting feed rate at the onset of thermal damage), the dresser infeed rate could be backed off until the specific energy increased to the point where the workpiece would burn. However this was not the case. At zero dresser infeed rate (conventional creep-feed grinding) the grinding wheel adopted a self-dressing action and although there was a gross loss of form workpiece burn never occurred.

FIGURE 21

VARIATION OF SPECIFIC ENERGY WITH THE AMOUNT OF STOCK REMOVED IN ONE REVOLUTION OF THE GRINDING WHEEL

Δ by SHAFTO & STUART

\+ BURN FREE

• BURNT

REFER TO FIGURE 23.

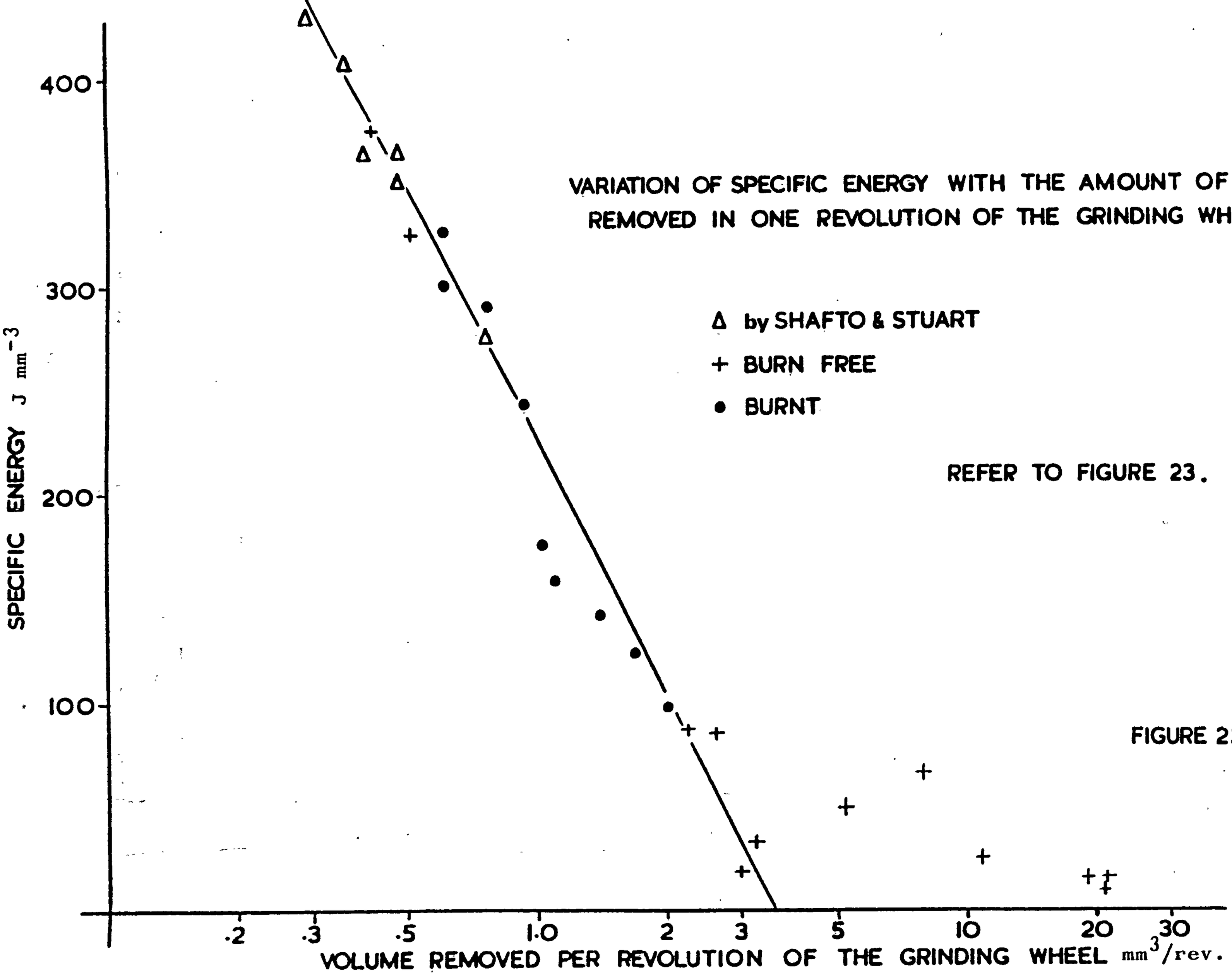

FIGURE 22.

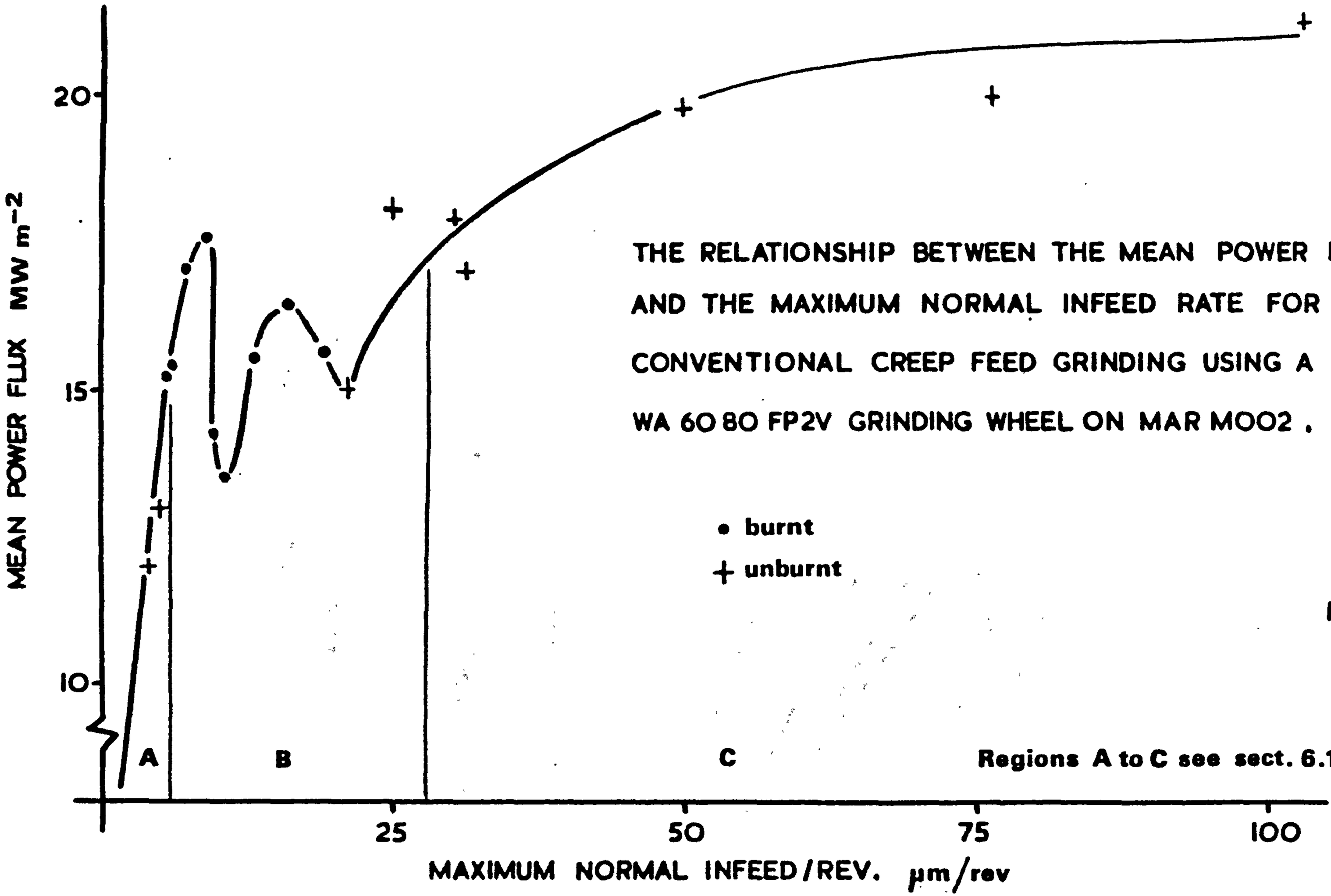

THE RELATIONSHIP BETWEEN THE MEAN POWER FLUX AND THE MAXIMUM NORMAL INFEED RATE FOR CONVENTIONAL CREEP FEED GRINDING USING A WA 60 80 FP2V GRINDING WHEEL ON MAR M002 .

FIGURE 23.

THE VARIATION OF SPECIFIC ENERGY WITH GRINDING WHEEL SPEED.

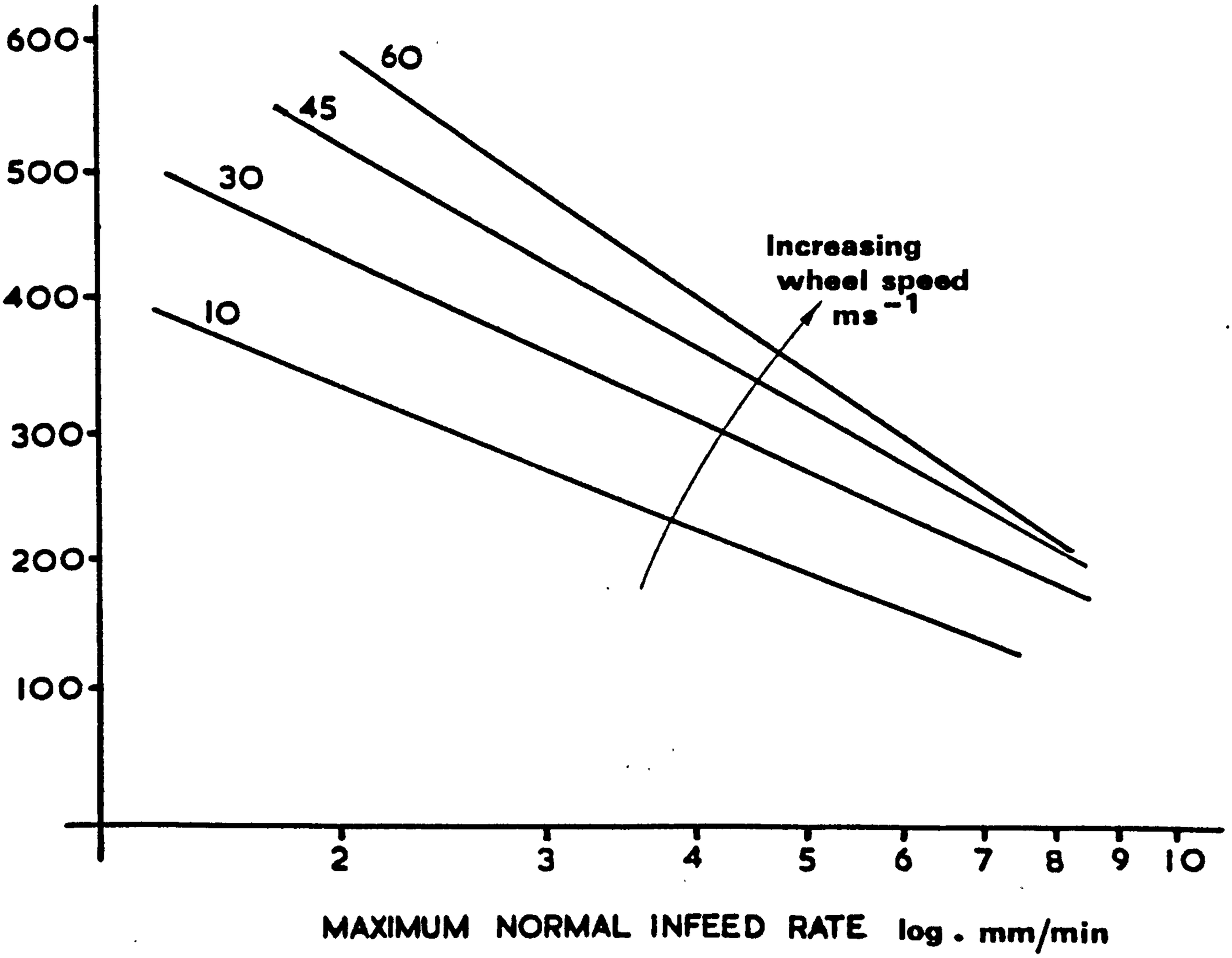

Wheel Grade - WA 60 80 FP 2V

Material - C 1023

FIGURE 24

THE RELATIONSHIP BETWEEN THE SPECIFIC ENERGY AND THE PERCENTAGE WEAR FLAT AREA

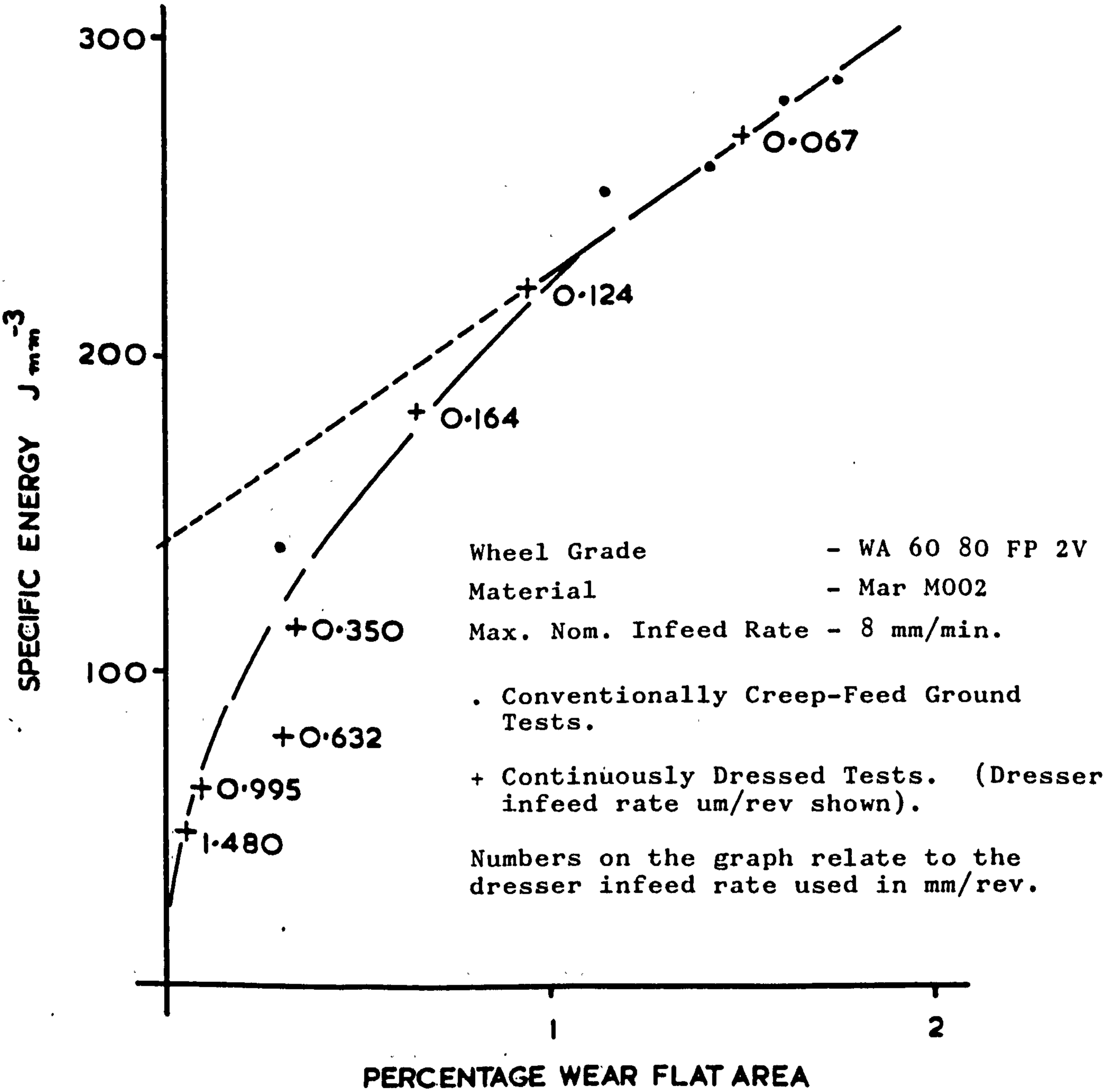

FIGURE 25

THE RELATIONSHIP BETWEEN THE SPECIFIC ENERGY AND THE PERCENTAGE WEAR FLAT AREA

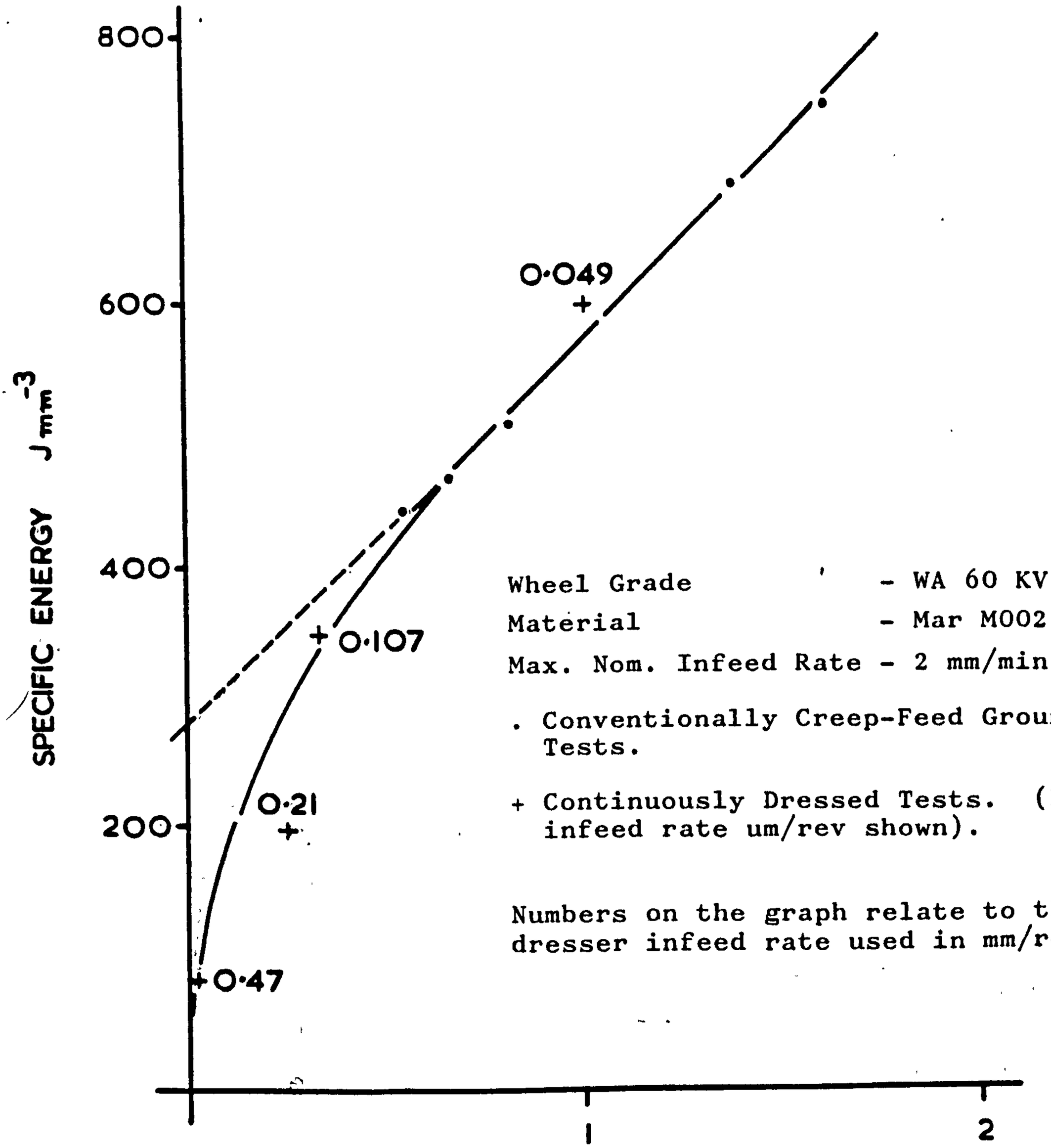

FIGURE 26

VARIATION OF MAXIMUM NORMAL INFEED RATE AT BURN WITH DEPTH OF CUT

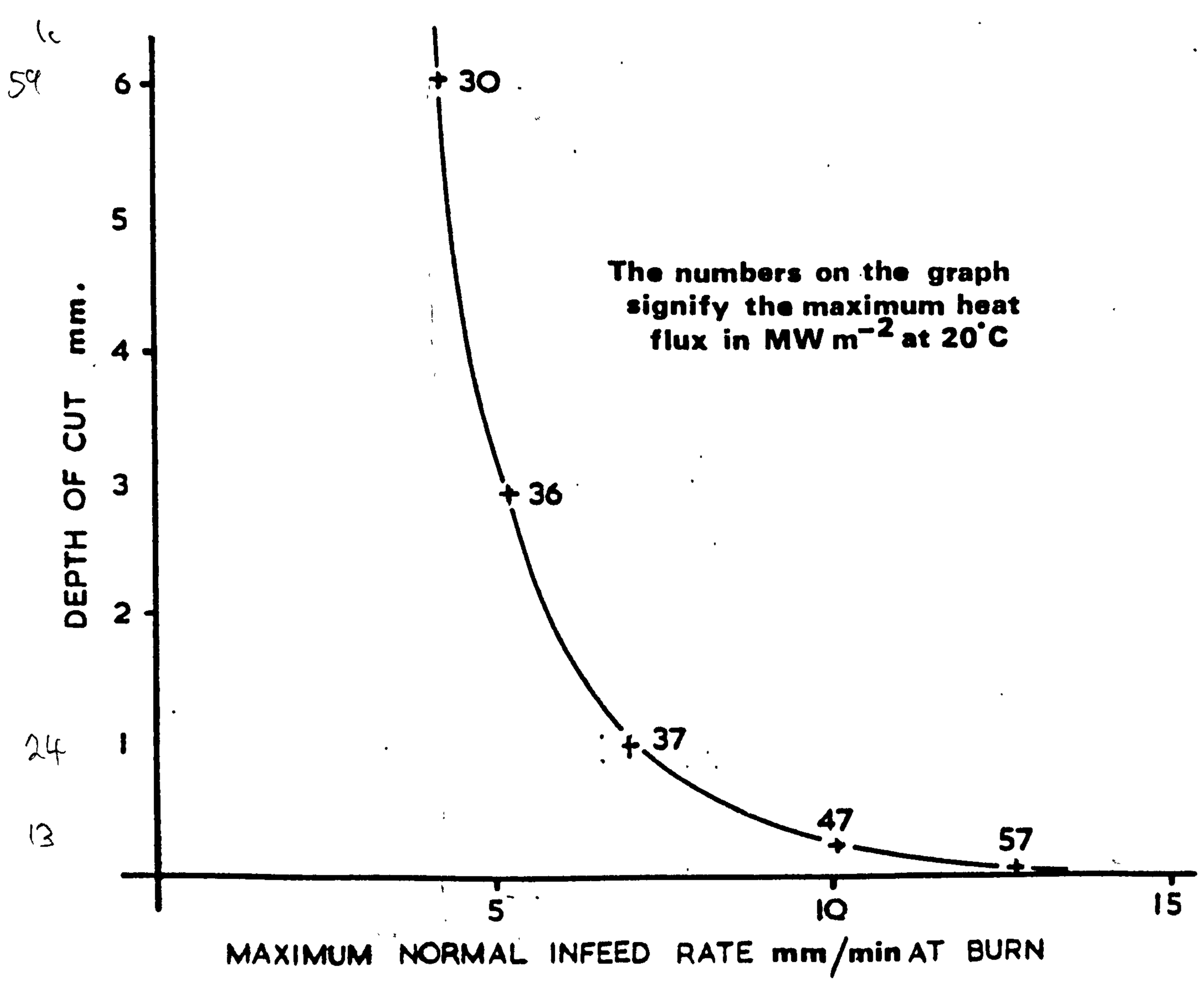

FIGURE 27

VARIATION OF MEAN POWER FLUX WITH ARC LENGTH FOR THREE CUTTING FLUID TEMPERATURES

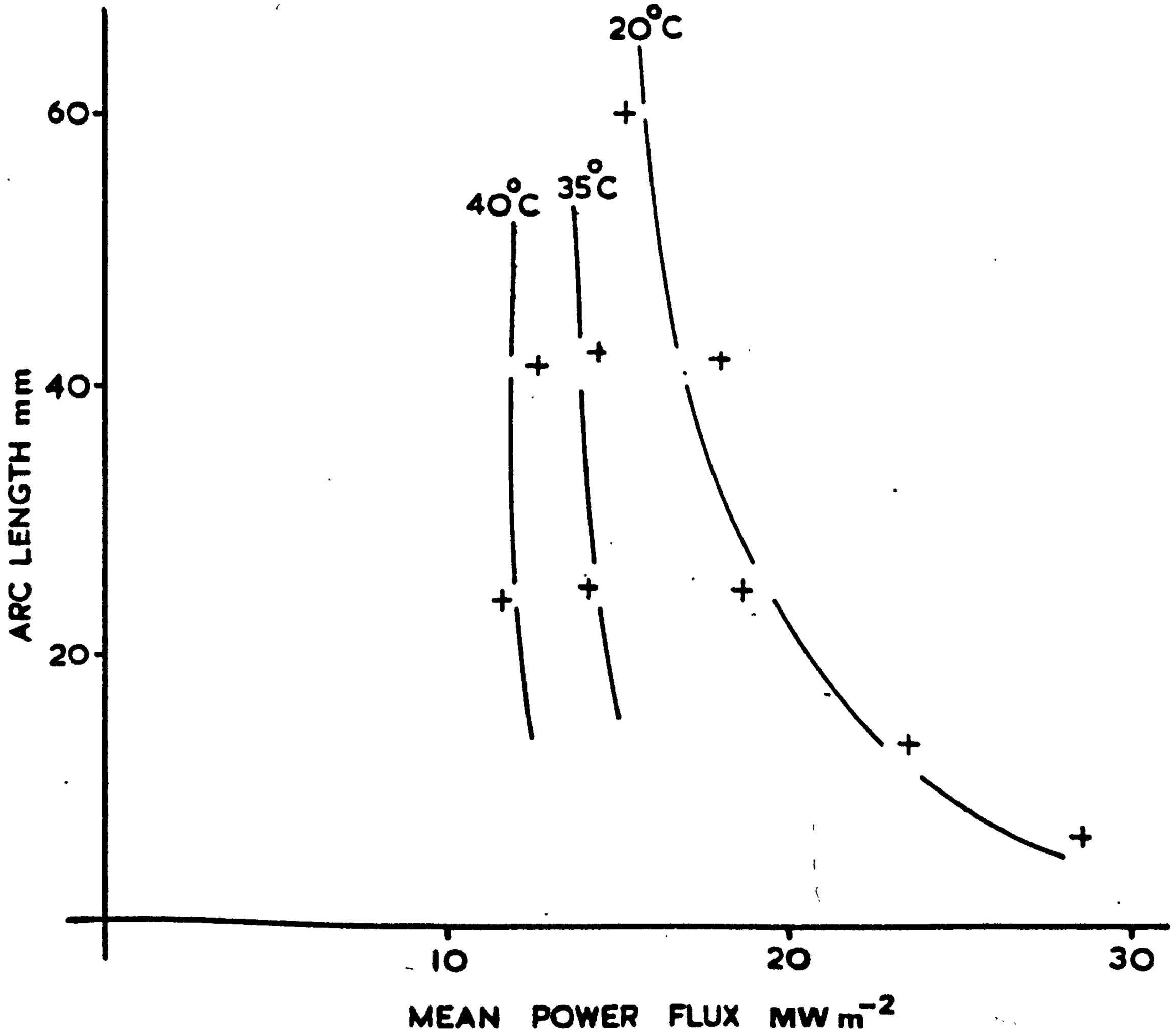

FIGURE 28

THE EFFECT OF THE CUTTING FLUID TEMPERATURE ON THE STOCK REMOVAL RATE .

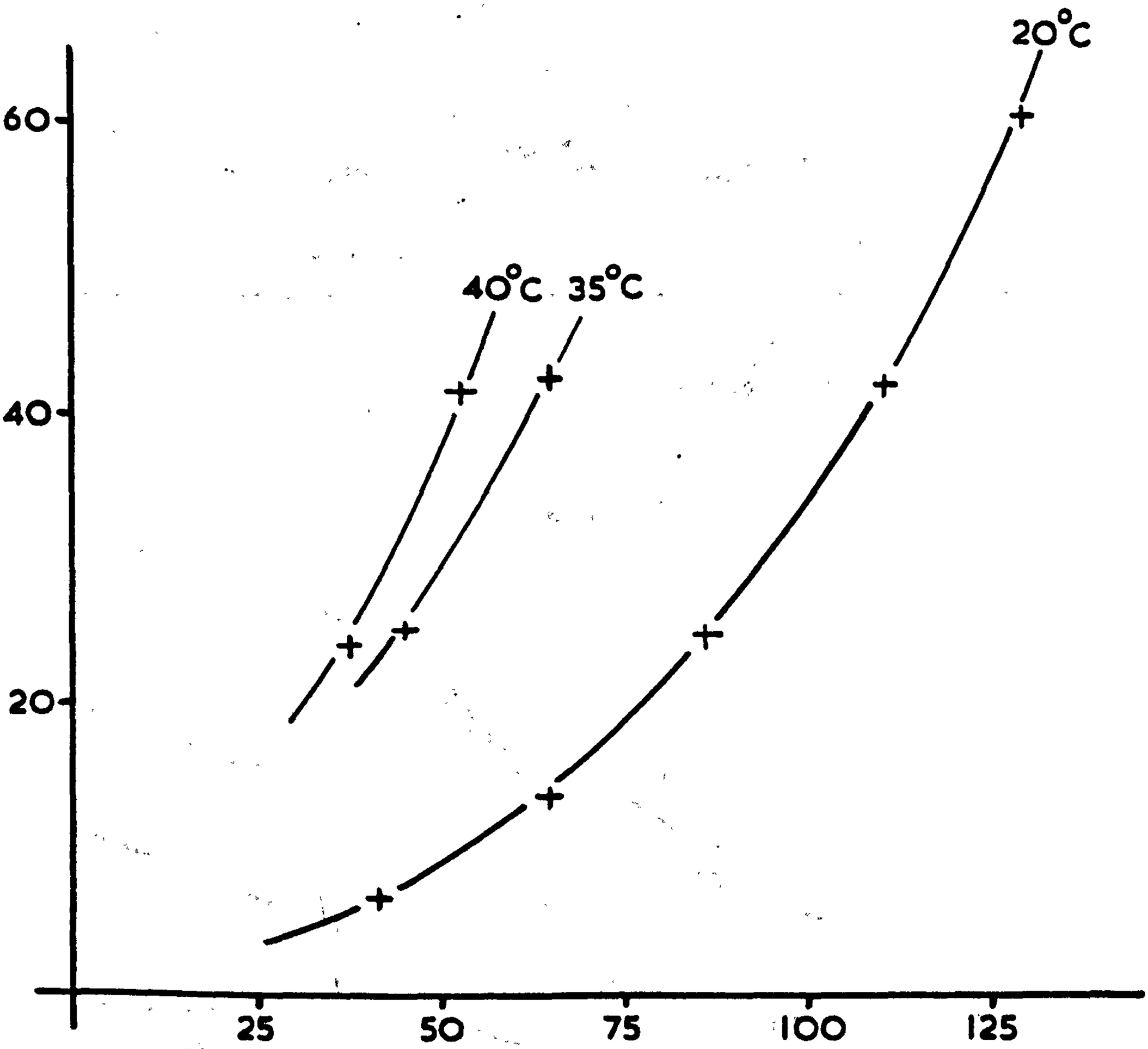

FIGURE 29

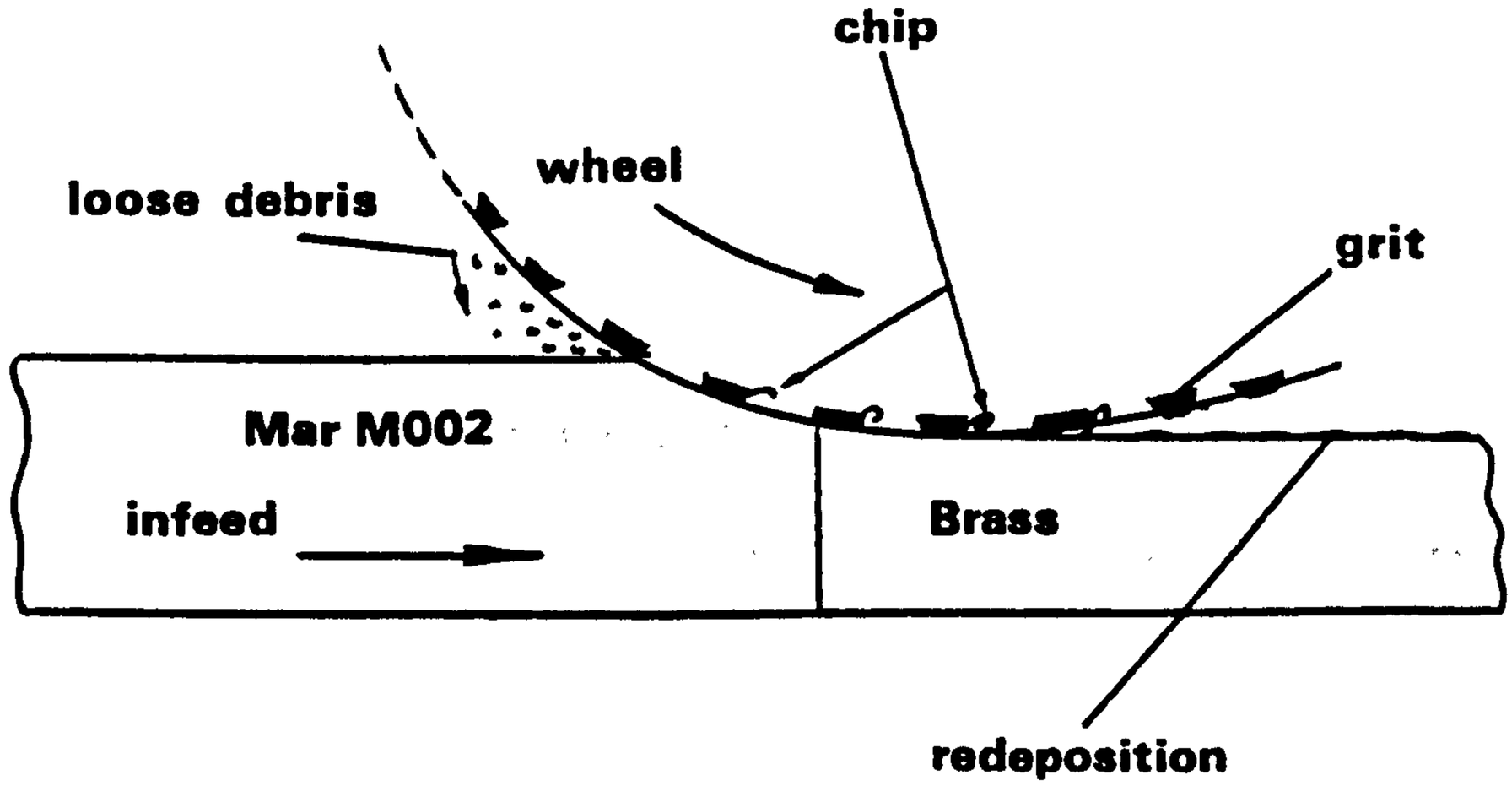

COMPOSITE BRASS AND MAR M002 SPECIMEN.

FIGURE 30.

POSSIBLE MODIFICATION TO MALKINS PARTITION OF ENERGY FOR CUTTING AND PLOUGHING

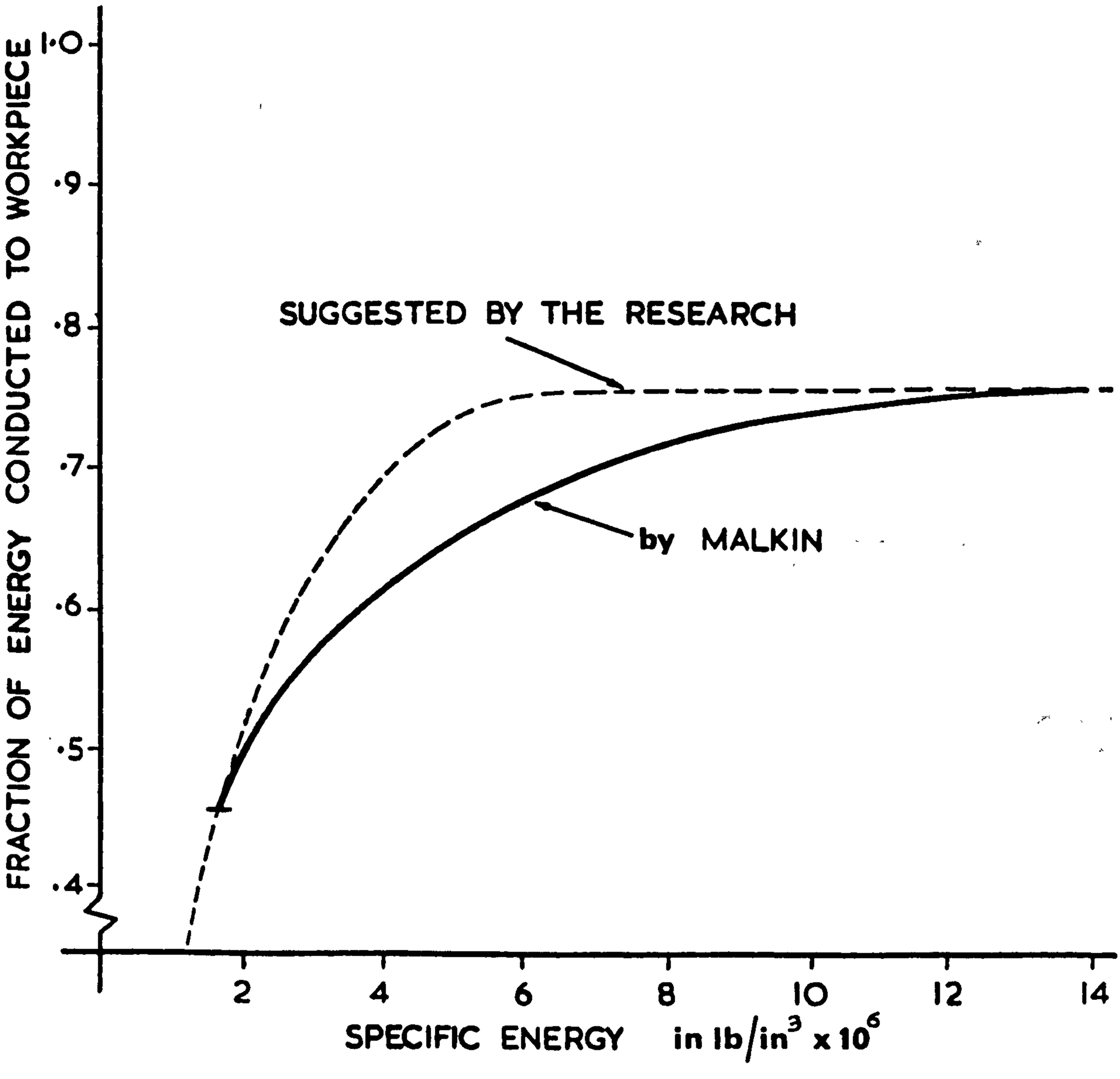

The graph shows a possible modification to Malkins cutting and ploughing partition of energy. The research showed that the total cutting and ploughing energy was a great deal less than Malkin assumed. The percentage of the cutting energy conducted to the workpiece is expected to be less than 45% and the fraction of energy conducted to the workpiece is expected to rise sharply as the specific energy increases due to the characteristic shape of the Specific Energy v Wear Flat Area graph (see figs. 25 and 26). The speed of the moving heat source in creep-feed grinding is slower than conventional reciprocating grinding, hence it is expected that the percentage of the ploughing energy conducted to the workpiece might be greater than 75%. An assessment of these modifications to Malkins partition of energy is recommended for further work.

FIGURE 31.

HEATING ELEMENT SIMULATION TEST RESULTS BY POWELL

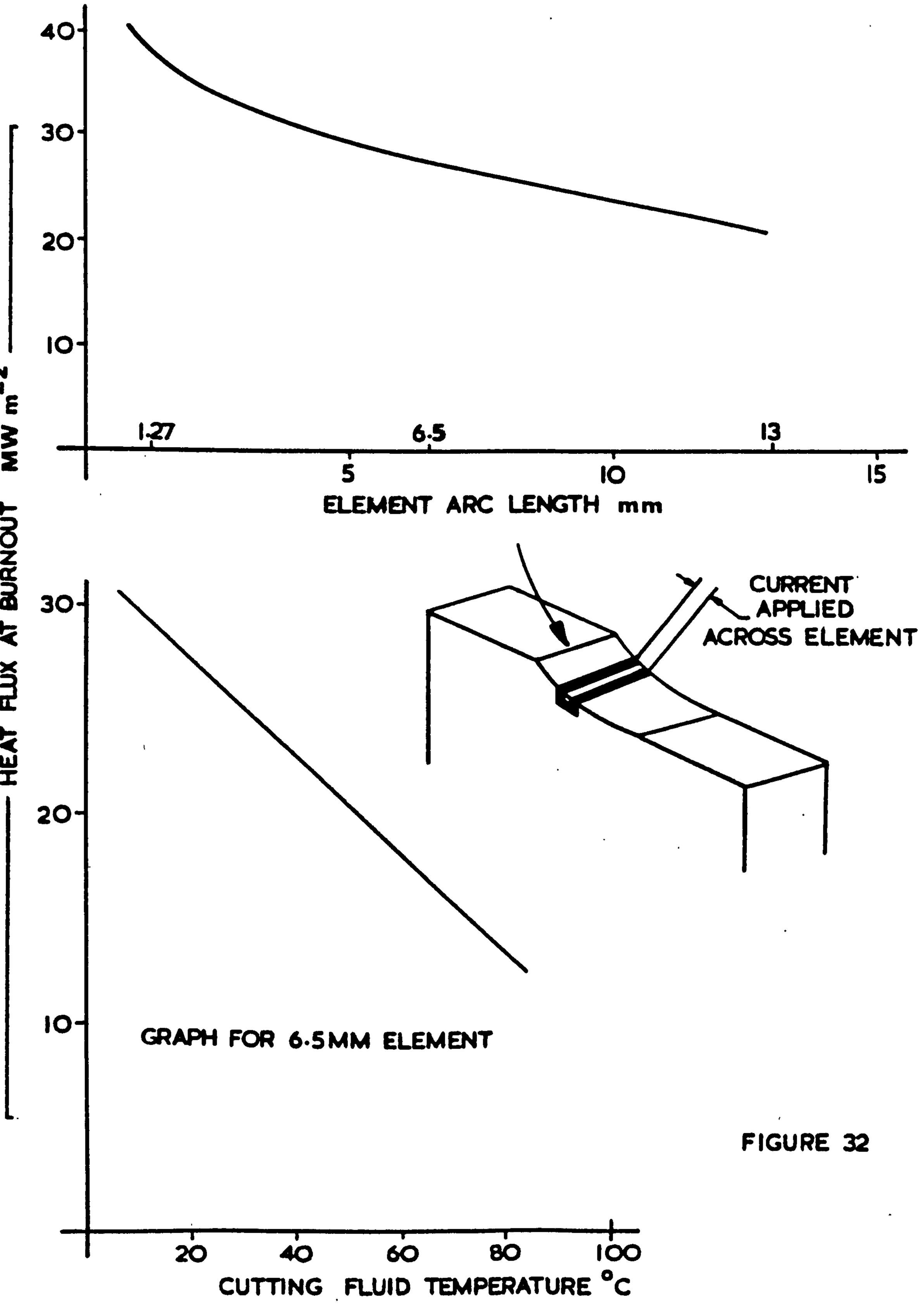

FIGURE 32

PLATES

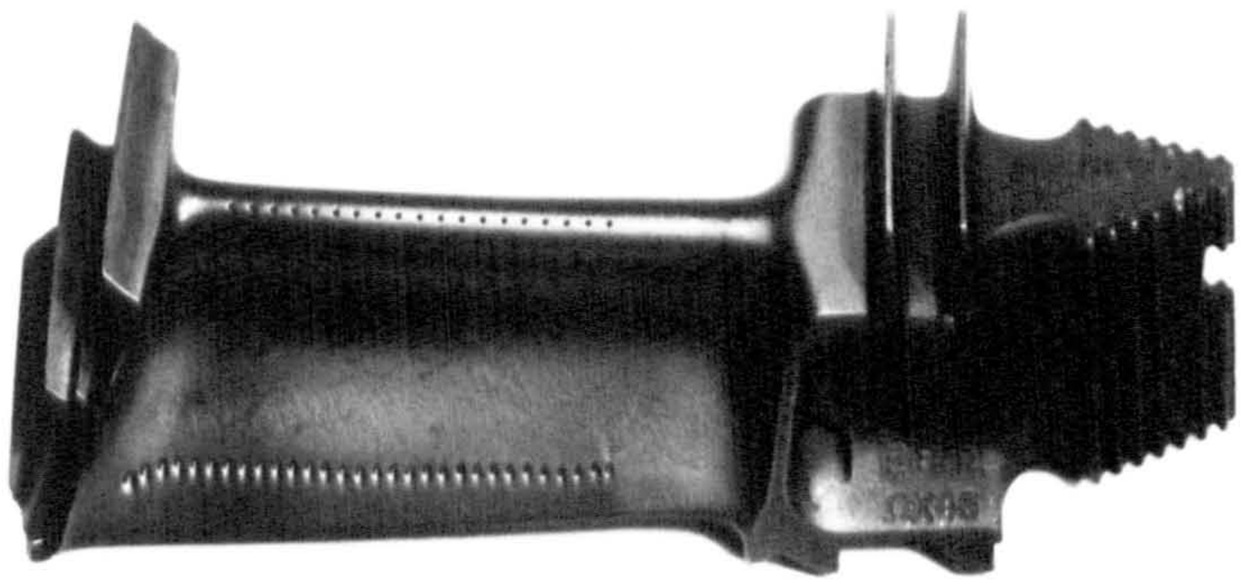

PLATE 1. This photograph shows a typical cast aero engine turbine blade. The aerofoil remains in the as cast condition apart from polishing and the machining of the cooling holes. The shroud and the root of the blade are creep-feed ground. It is the manufacture of this blade which has been studied as part of the economic assessment of the creep-feed grinding process in Appendix 6.

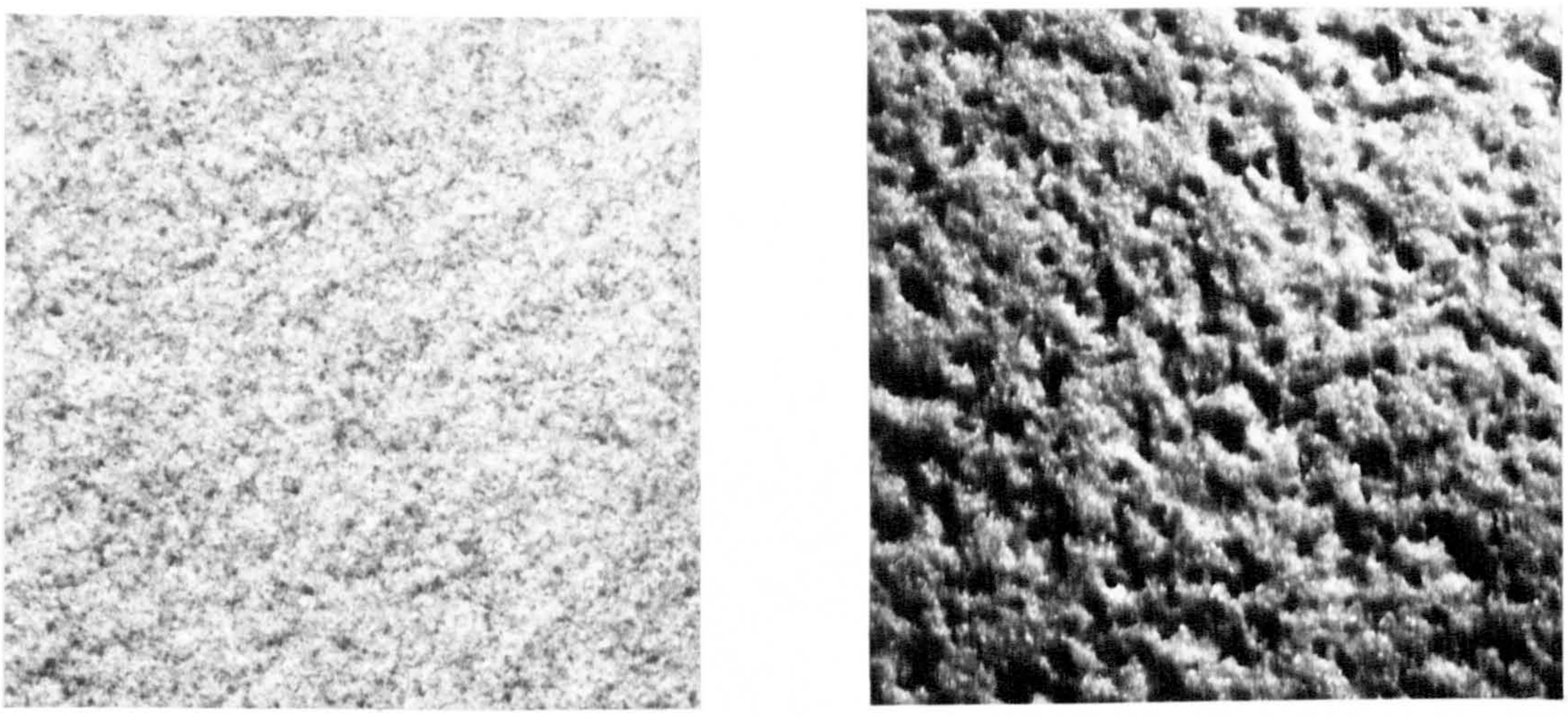

PLATE 2. The photographs above (x4 magnification) show the surfaces of the two grades of grinding wheel used in the research work reported in this thesis. On the left is the WA 60 KV grade and on the right is the WA 60 80 FP 2V grade, notice the induced porosity of the WA 60 80 FP 2V grade. The specification for each grinding wheel is listed in Appendix 1.

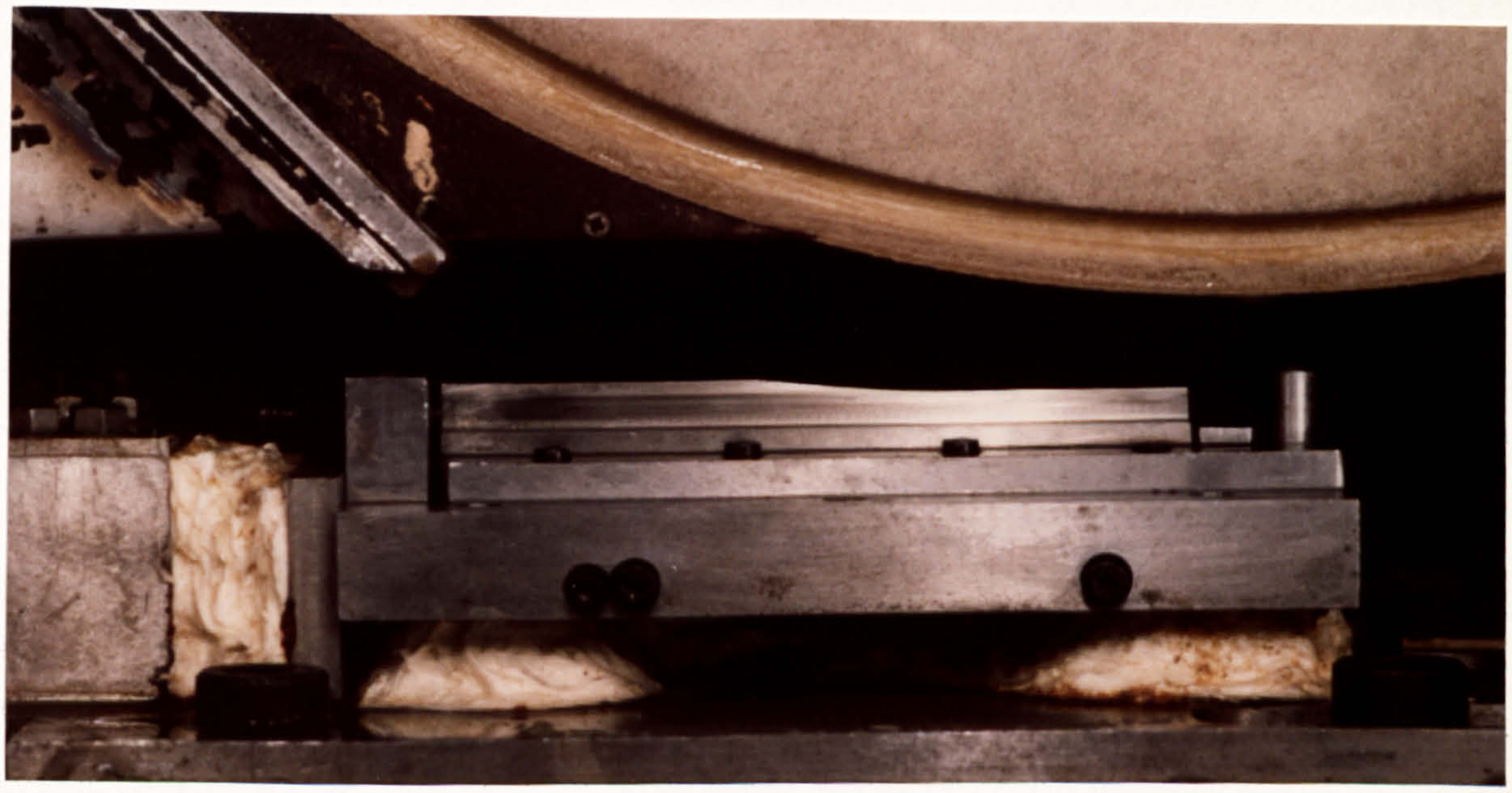

PLATE 3. This is a close-up view of the working zone. A machined specimen has been loaded into the dynamometer without packing for clarity. The dynamometer is fixed to the machine slideway and moves from left to right, the grinding wheel remains stationary. Notice the position of the cutting fluid shoe in intimate contact with the grinding wheel, the anti-clockwise rotation of the grinding wheel 'drags' the cutting fluid into the arc of cut.

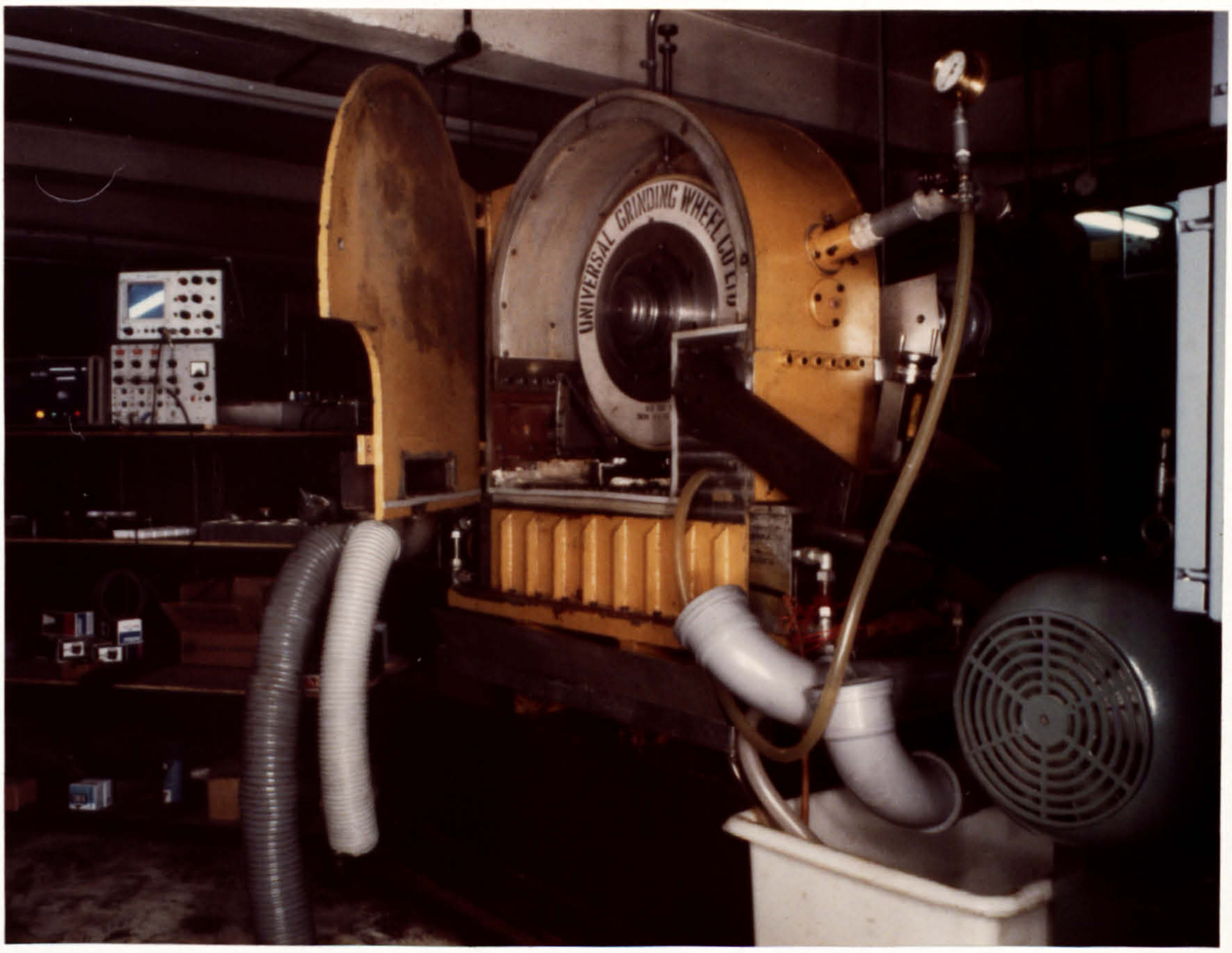

PLATE 4. This photograph shows a general view of the High-Speed Creep-Feed Grinding Research Rig. Particular points to note are the diamond roller dresser in-feed mechanism to the right of the rig, the cutting fluid shoe on the left of the grinding wheel and the attention to safety shown by the steel plating and energy absorbent layer surrounding the grinding wheel in order to contain a wheel burst. The instrumentation and data recording system is situated on the trolley to the left of the rig.

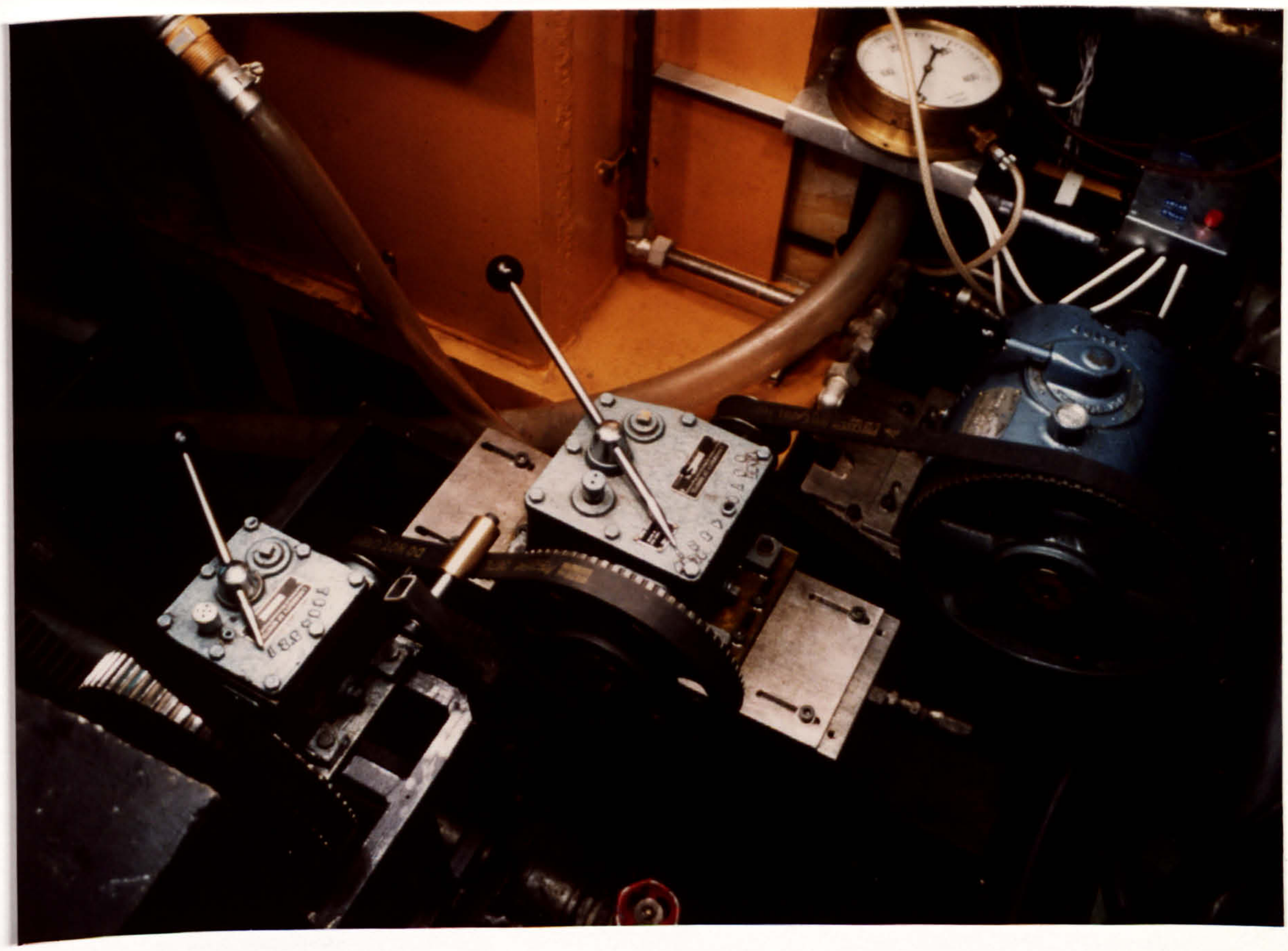

PLATE 5. The photograph shows the train of three gearboxes which transmit the drive from the main splindle motor to the ball-screw nut on the machine slideway. A wide range of slideway traverse speeds can be achieved by the selection of pulley wheel combinations and the gearbox ratios. The final drive to the ball-screw nut is transmitted via an automatic elctromagnetic clutch shown in the top right of the picture.

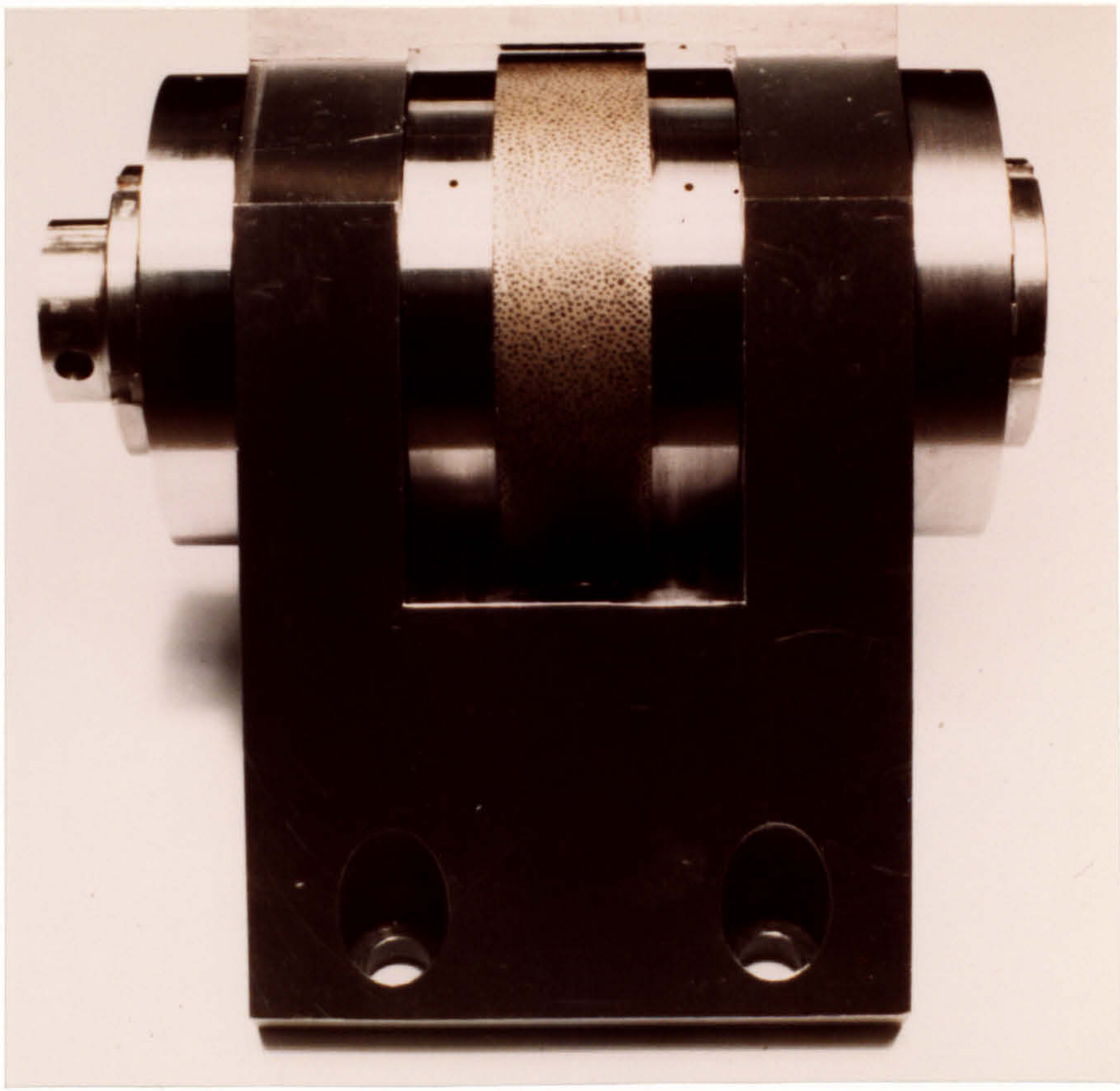

PLATE 6. The photograph shows the external appearance of the diamond roller dresser unit prior to its installation in the rig. Below is illustrated the internal details of the angular contact bearings and the V-ring seal arrangement.

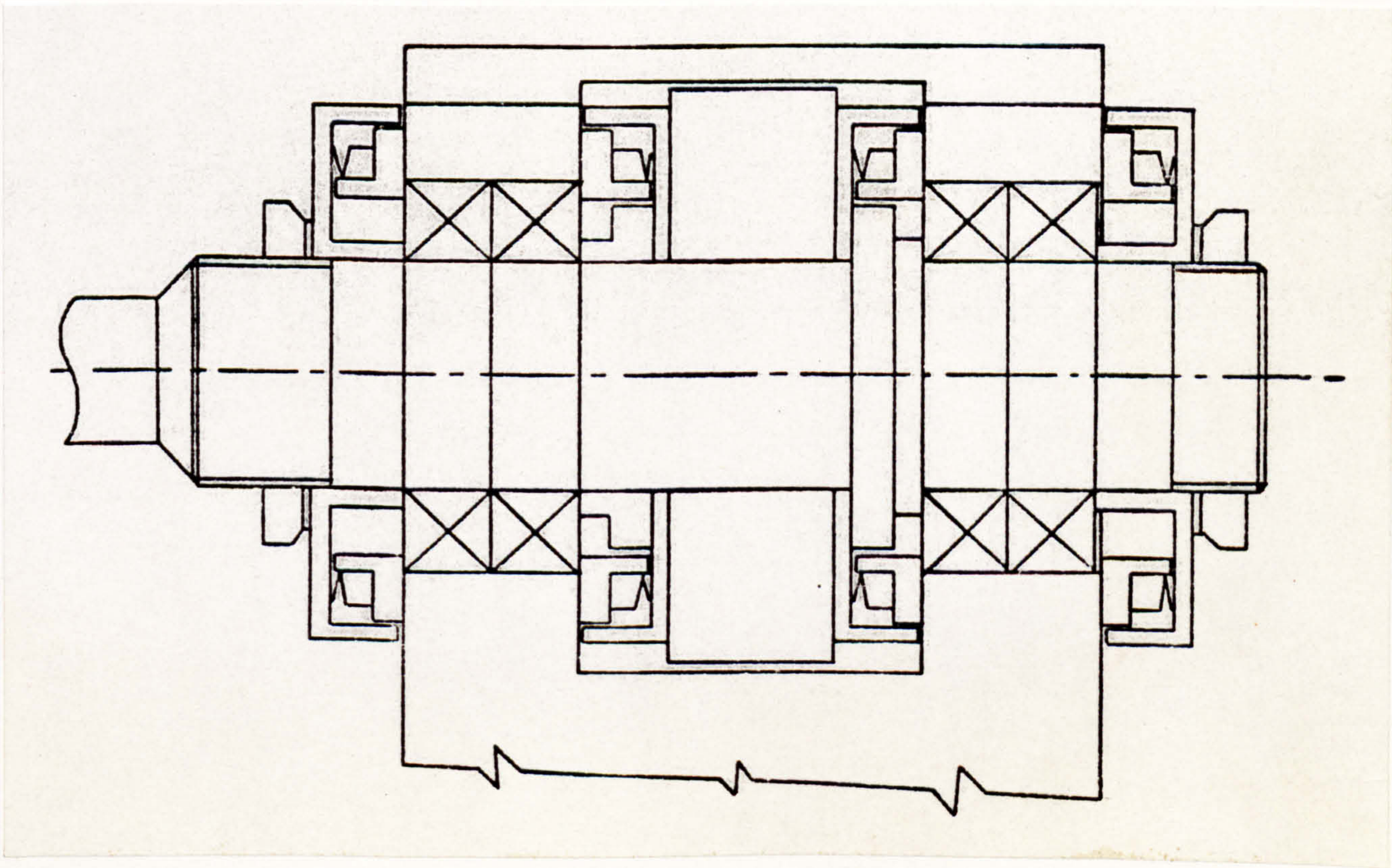

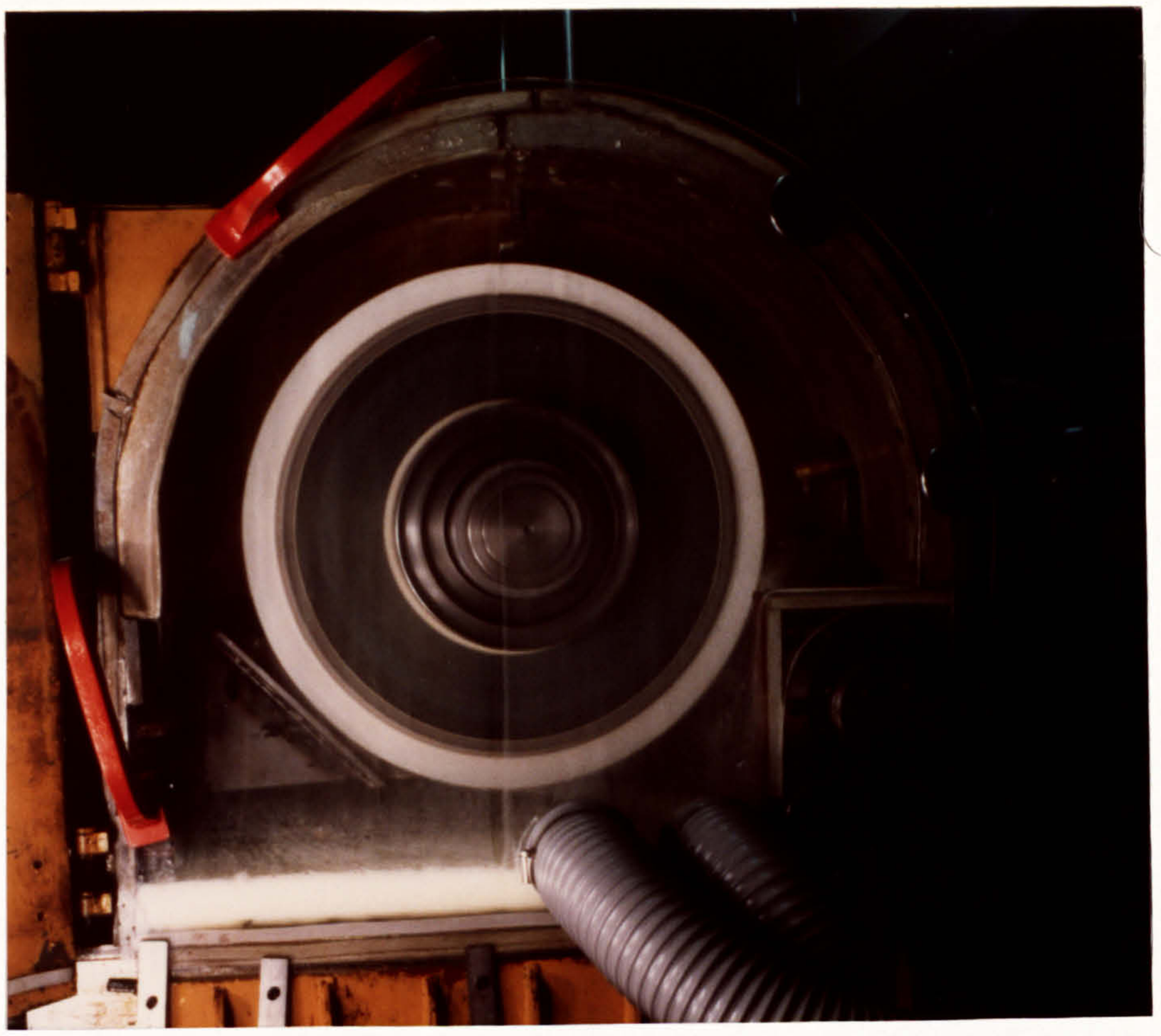

PLATE 7. A perspex window was made to assist the filming of the process for the BBC TV programme 'Tomorrows World'.

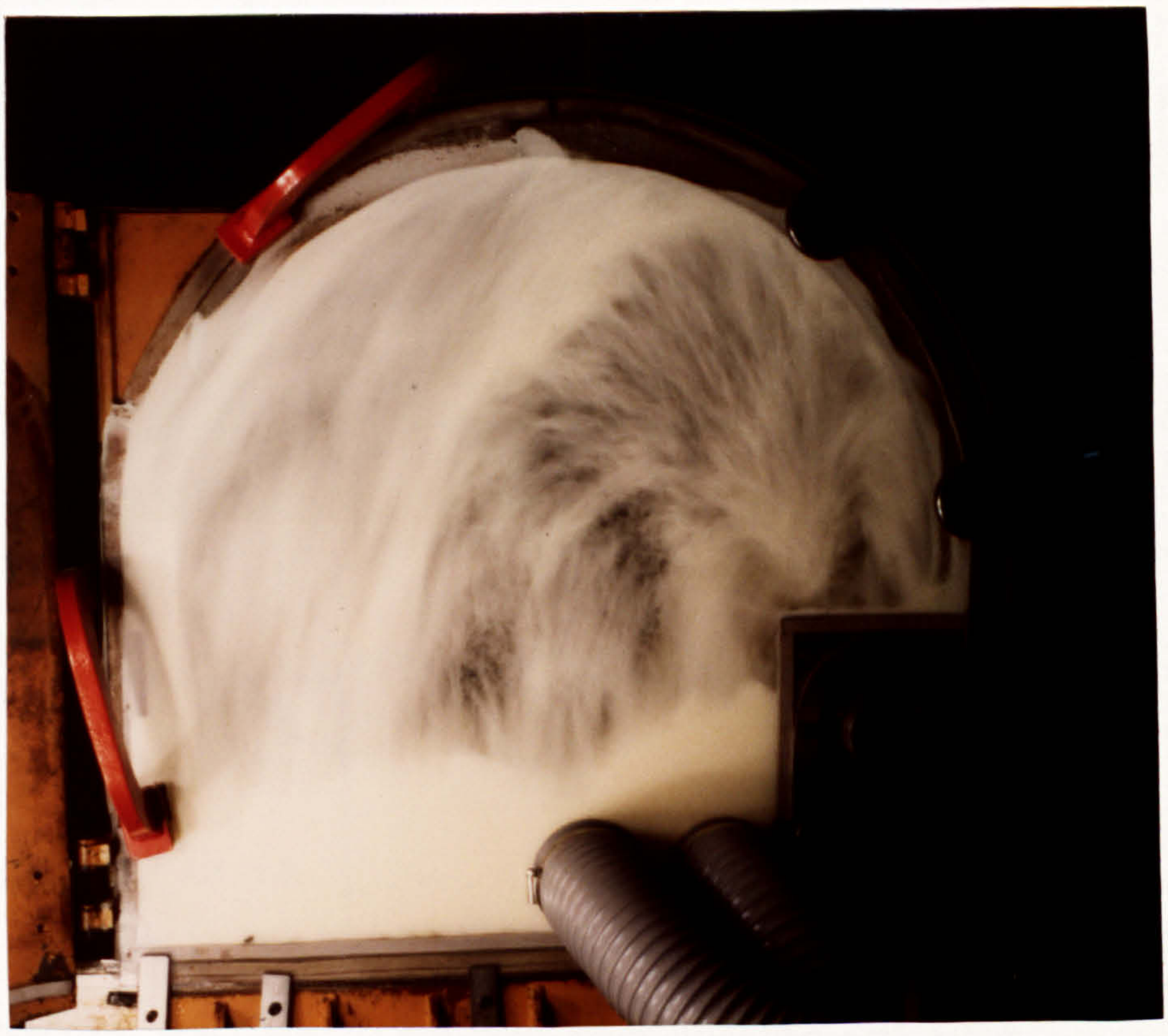

The photograph at the top shows the rig running before the cutting fluid is turned on, notice the position of the shoe (left). The photograph below shows the extent of the cutting fluid flow in the rig at 6 litres per second.

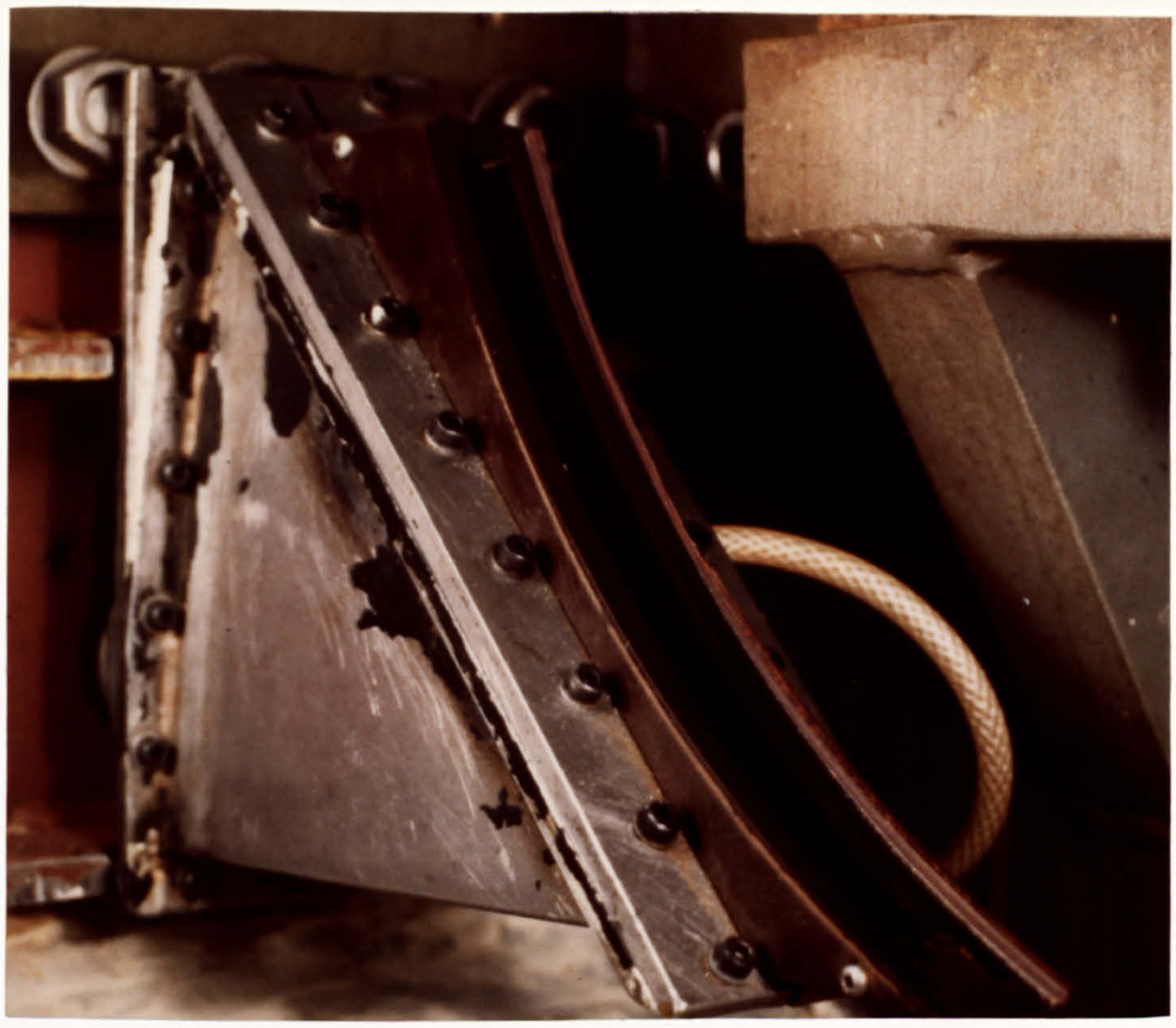

PLATE 8. The photograph above, shows the cutting fluid shoe which is kept in intimate contact with the grinding wheel by the adjuster mechanism shown below. The shoe is made from 'Tufnol' and is consumable. The arrangement is such that a worn shoe can be replaced without removing the grinding wheel from the main spindle.

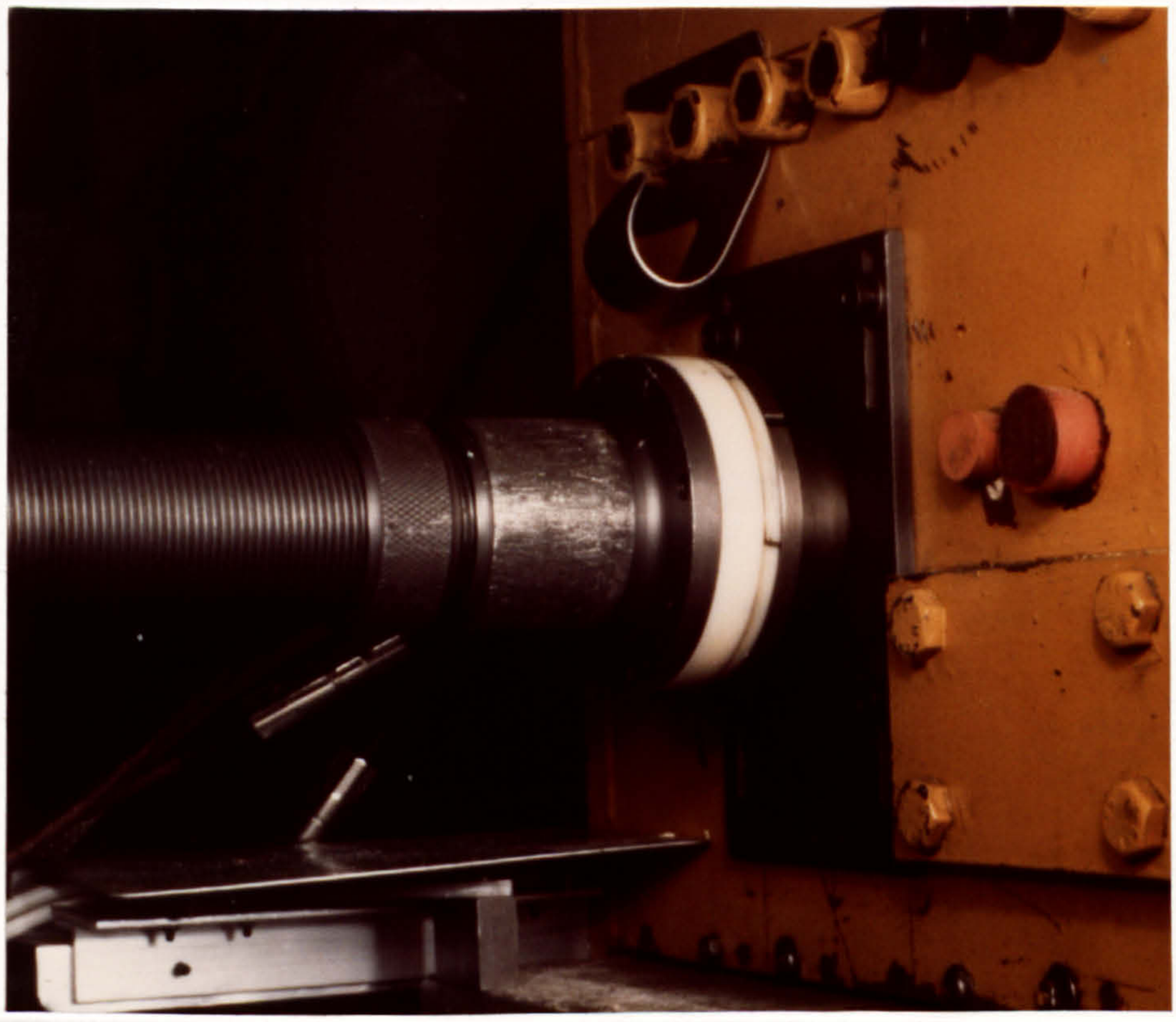

The adjuster mechanism is a very tight plain nylon bearing both sides of a steel flange, the bearing housing is a nut which screws onto the threaded pipe which is attached to the shoe in the rig. This allows the shoe to be adjusted from outside the rig whilst continuously dressing the grinding wheel, in order to maintain the pressure of the cutting fluid in the shoe.

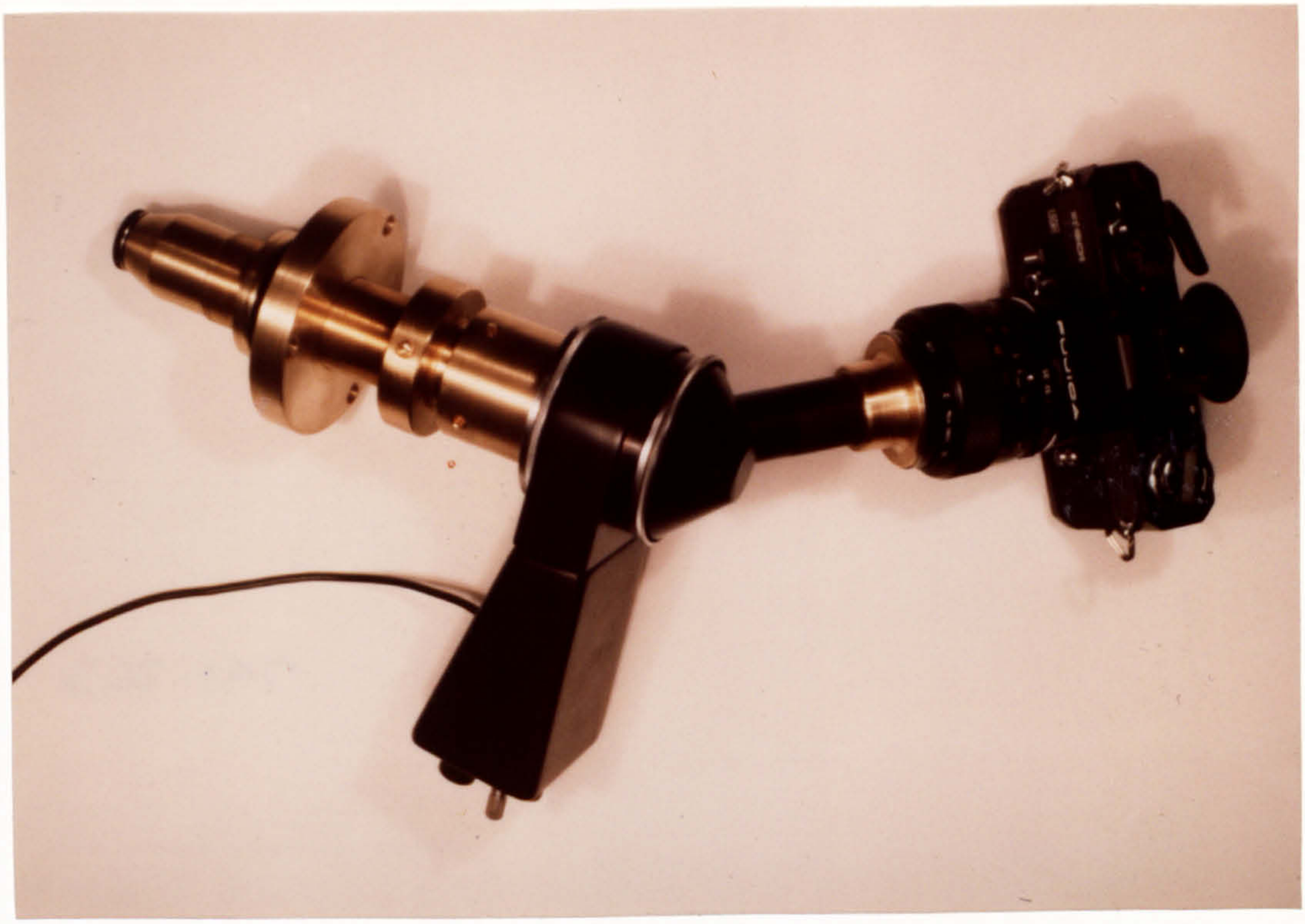

PLATE 9. The photograph shows the microscope-camera unit. Below is a schematic layout of the lens system.

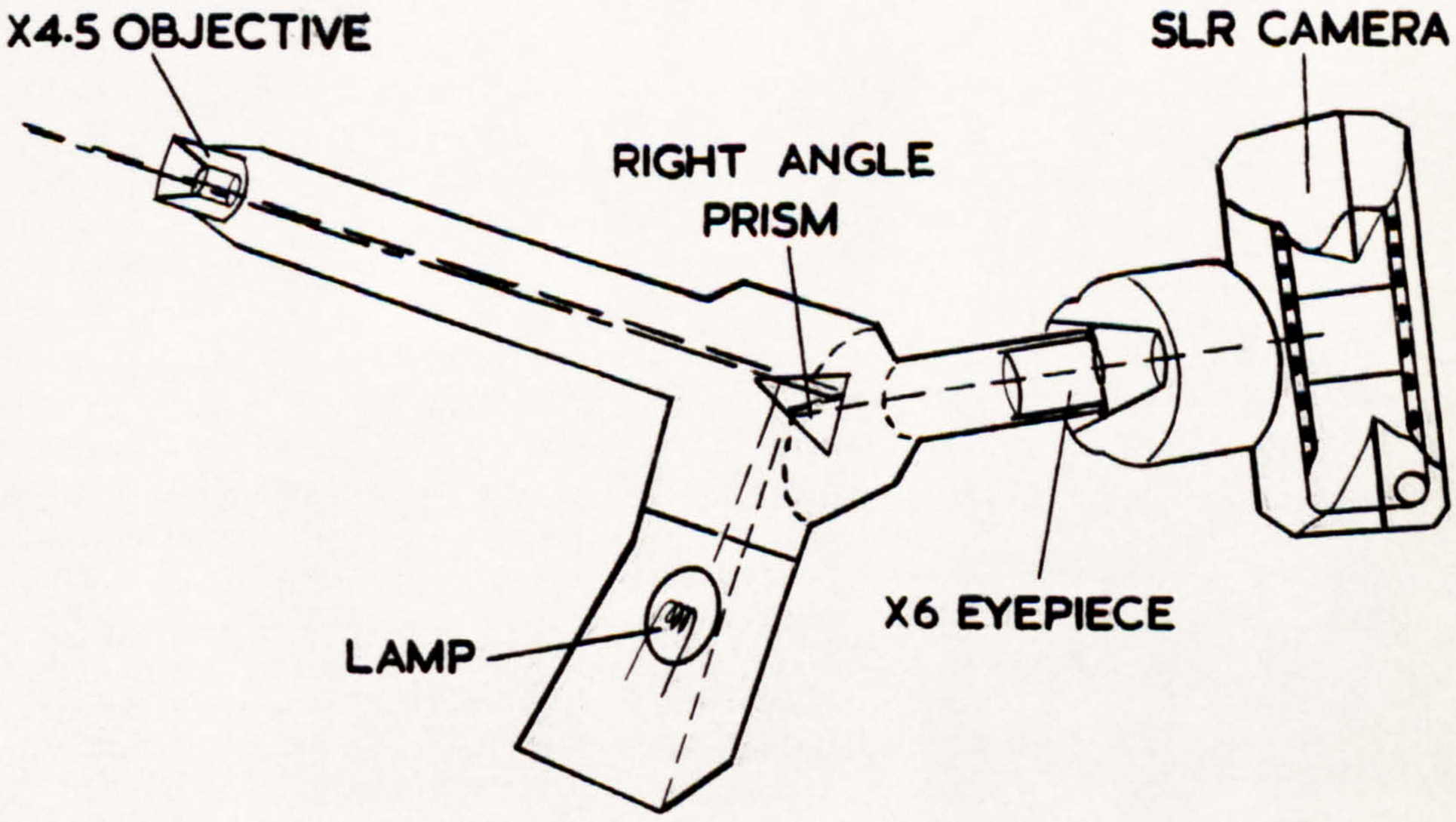

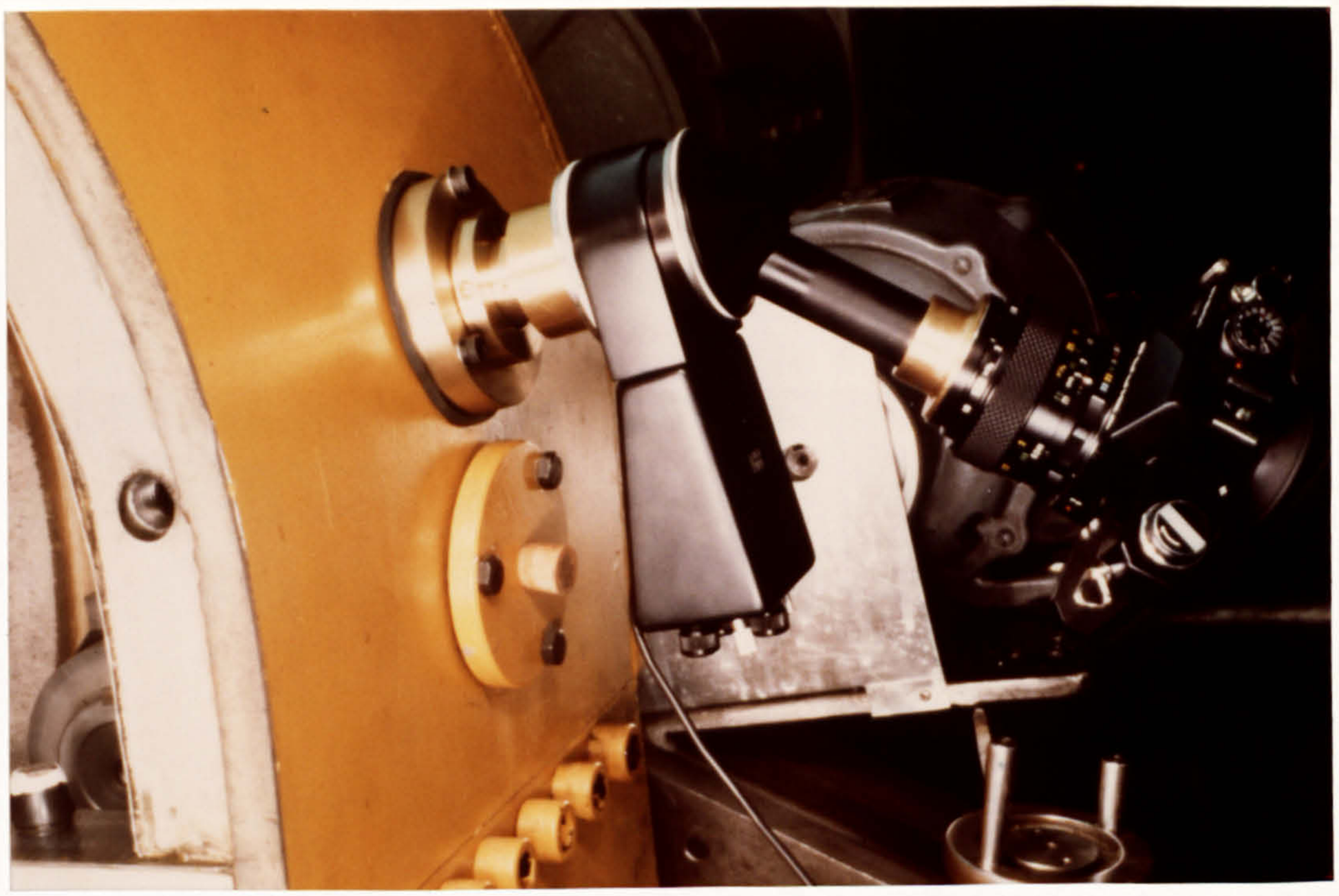

PLATE 10. The photographs show how the microscope-camera is fitted to the rig. The unit is fixed on a three point mounting which allows the microscope to be positioned normal to the surface of the grinding wheel.

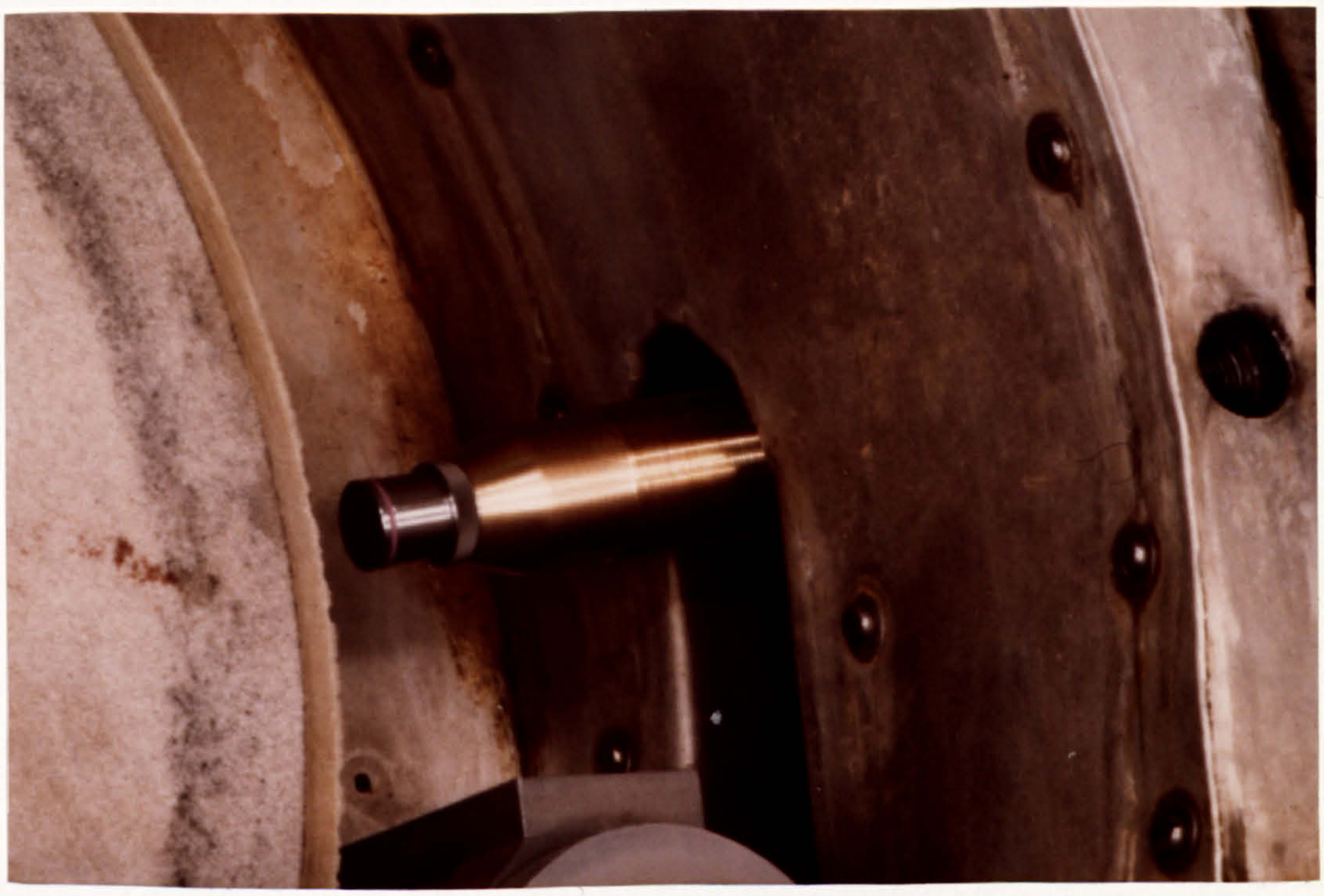

The microscope is left in position on the rig during testing, however the objective lens is removed and replaced by a plug which protects the tube from contamination by cutting fluid and grinding debris.

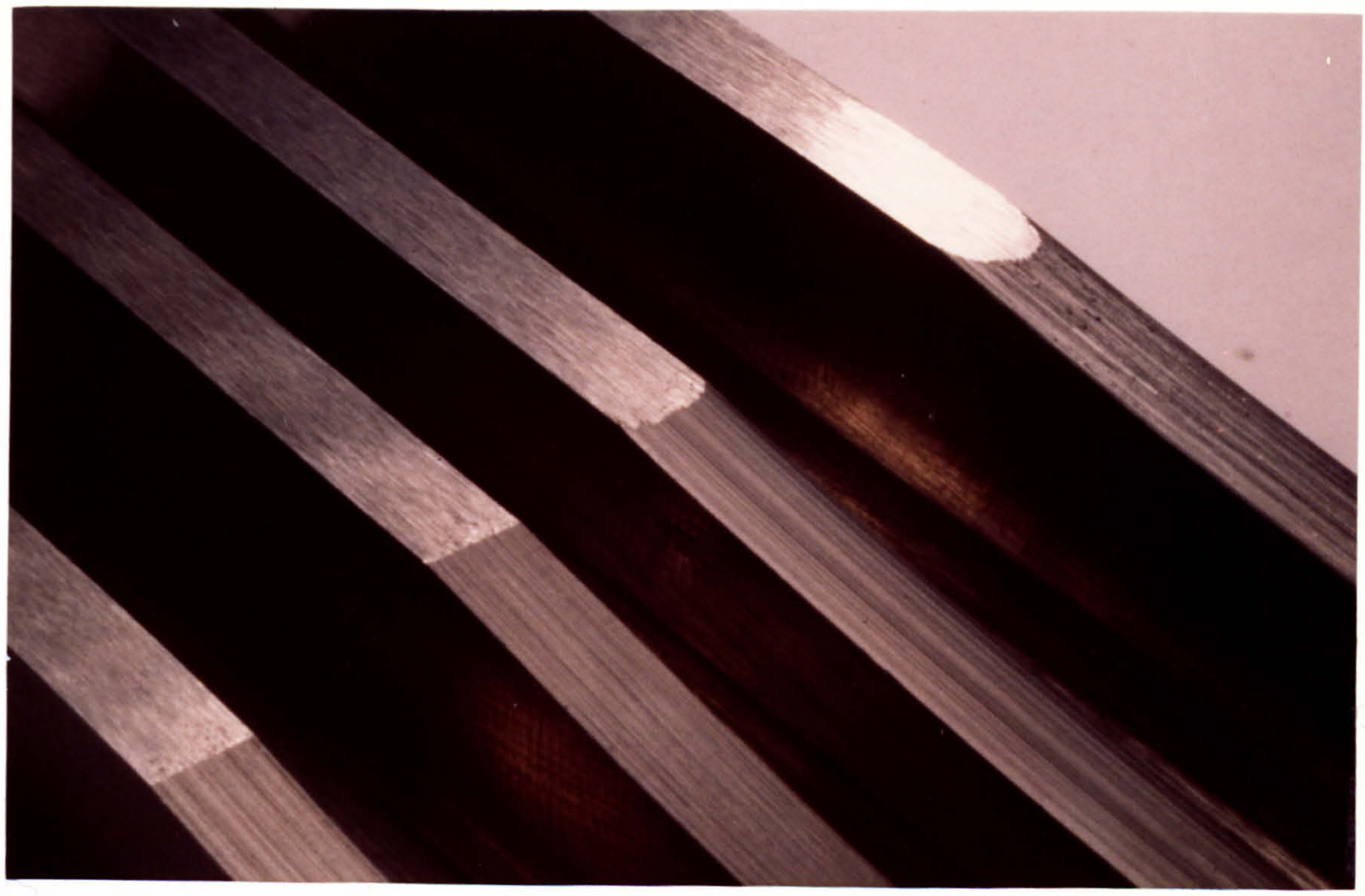

PLATE 11. The photograph shows the top of the arc of cut of four workpieces, i.e., the point of maximum normal infeed rate. Each specimen has been ground by the continuously dressed creep feed grinding process using a WA 60 80 FP 2V grade grinding wheel.

The specimen in the bottom left corner of the photograph was ground with a maximum normal infeed rate of 150 mm/min. and a dresser infeed rate of approx. 3 μm/rev. Moving to the right, the next specimen was ground with a maximum normal infeed rate of 170 mm/min. and a similar dresser infeed rate. Notice the pitted surface on the face of the unmachined surface believed to be caused by loose grits and debris from the grinding wheel.

The specimen in the top right corner of the photograph was ground with a maximum normal infeed rate of about 200 mm/min. and a dresser infeed rate of 2.8 μm/rev. Here, catastrophic breakdown of the workpiece profile took place. Moving to the left, the next specimen just begins to show signs of the edge of the form breaking away at 190 mm/min. maximum normal infeed rate and a similar dresser infeed rate. Burn did not occur on any of the specimens shown.

TYPICAL WEAR FLAT AREA PHOTOGRAPHS. PLATE 12

Wheel Grade: WA 60 KV Workpiece: Mar M002 Depth of Cut: 3mm
Width of Cut 5mm Workpiece Feed Rate 14 mm/min.
Amount of stock removed by each test 900 mm^3.

CONTINUOUSLY DRESSED

Dresser Infeed Rate: 0.47 μm/rev.
Wear Flat Area: 0.02%

CONTINUOUSLY DRESSED

Dresser Infeed Rate: 0.107 μm/min.
Wear Flat Area: 0.32%

CONVENTIONALLY CREEP-FEED GROUND

Dressed Prior to Grinding
Wear Flat Area: 1.85%

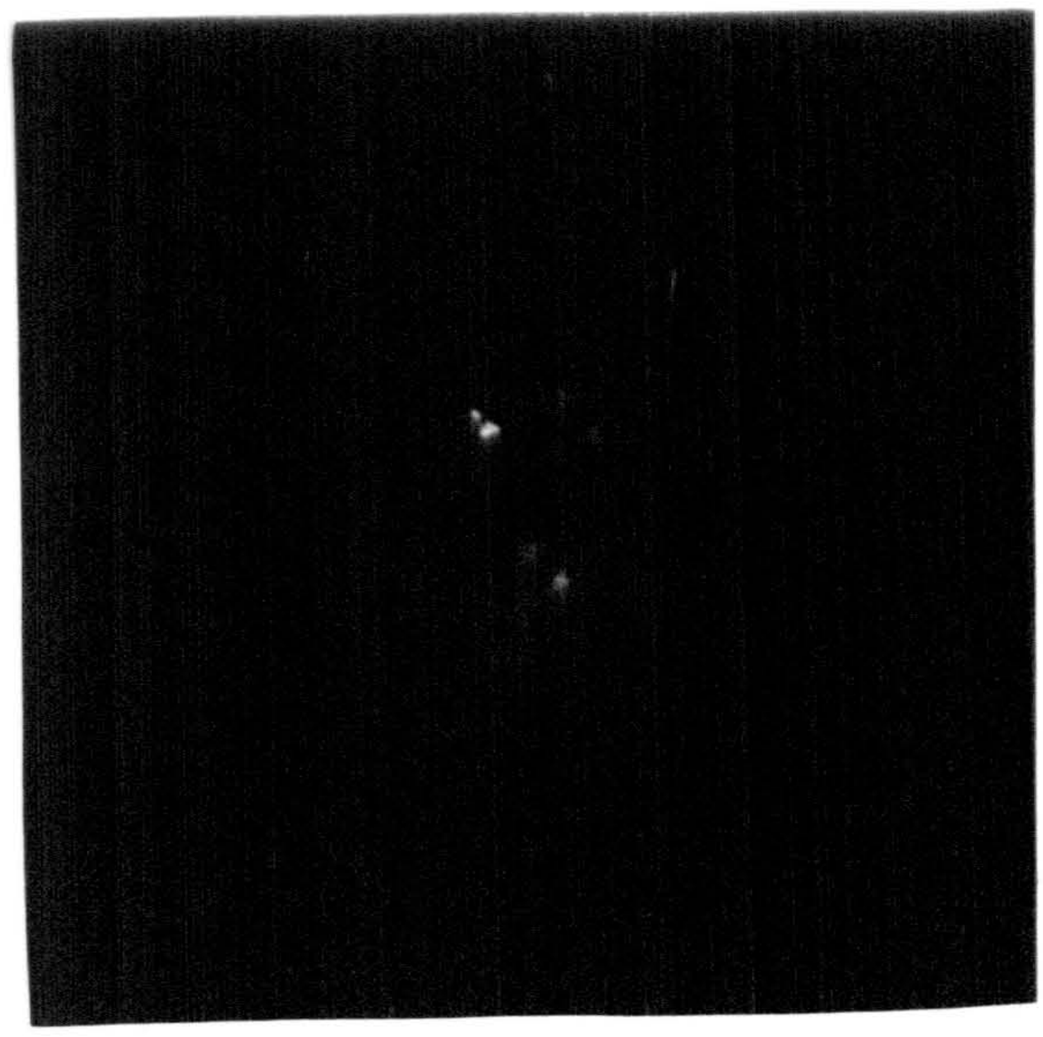

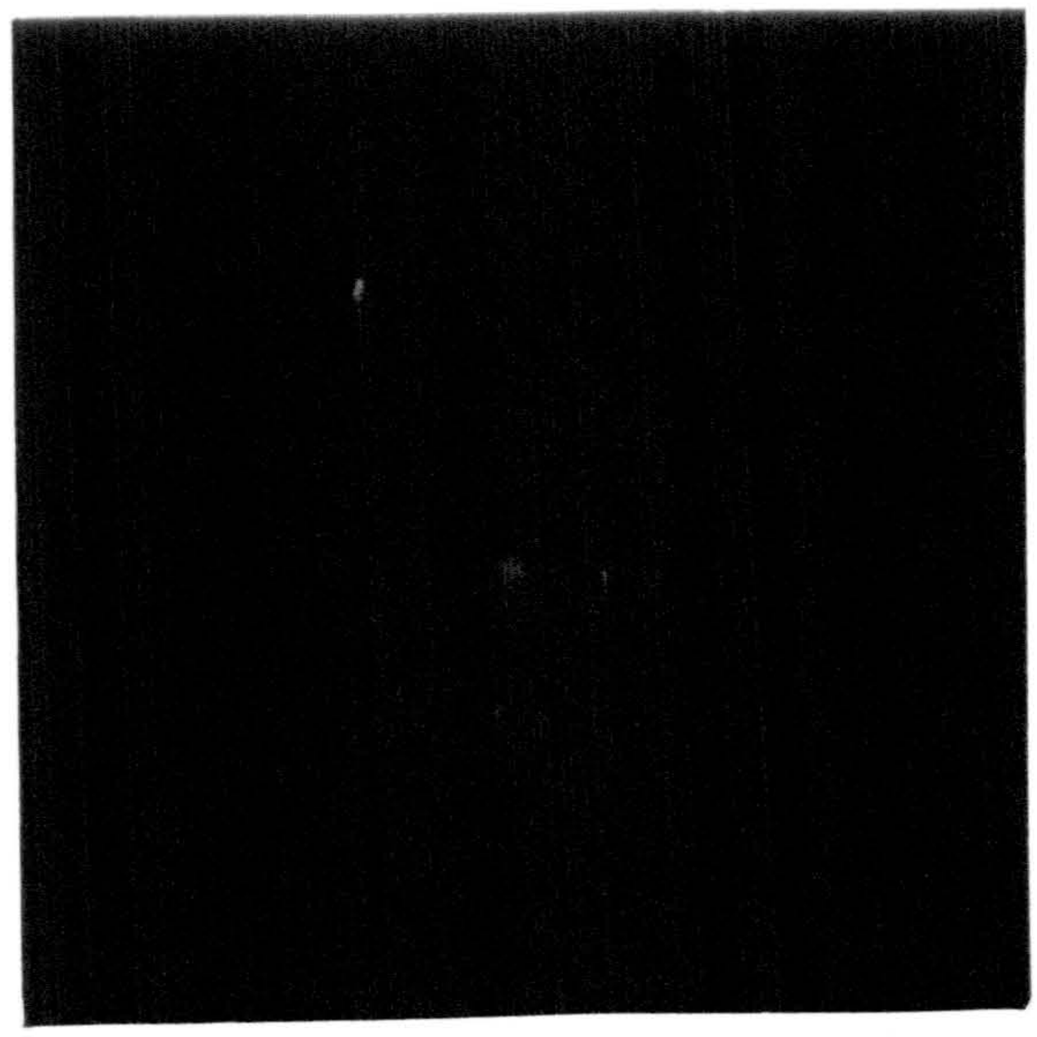

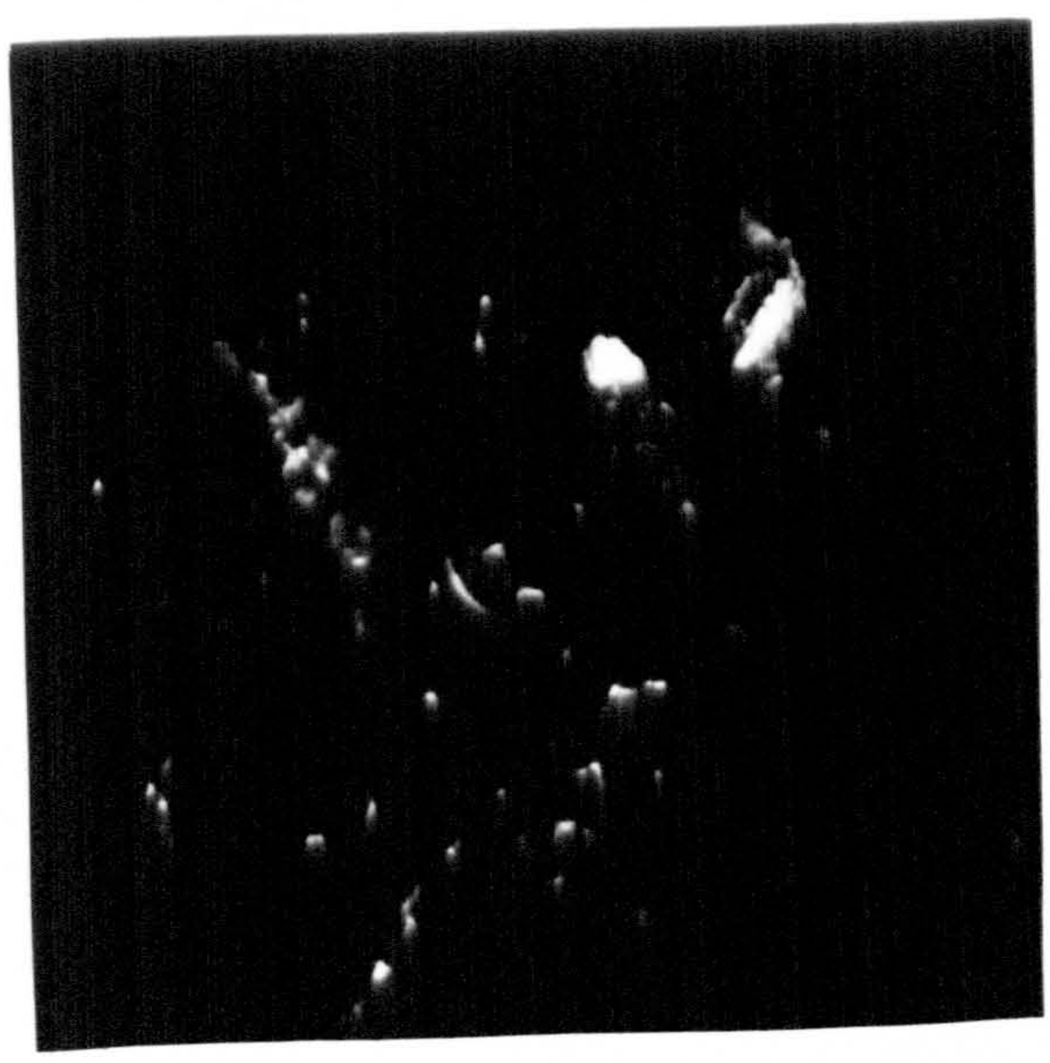

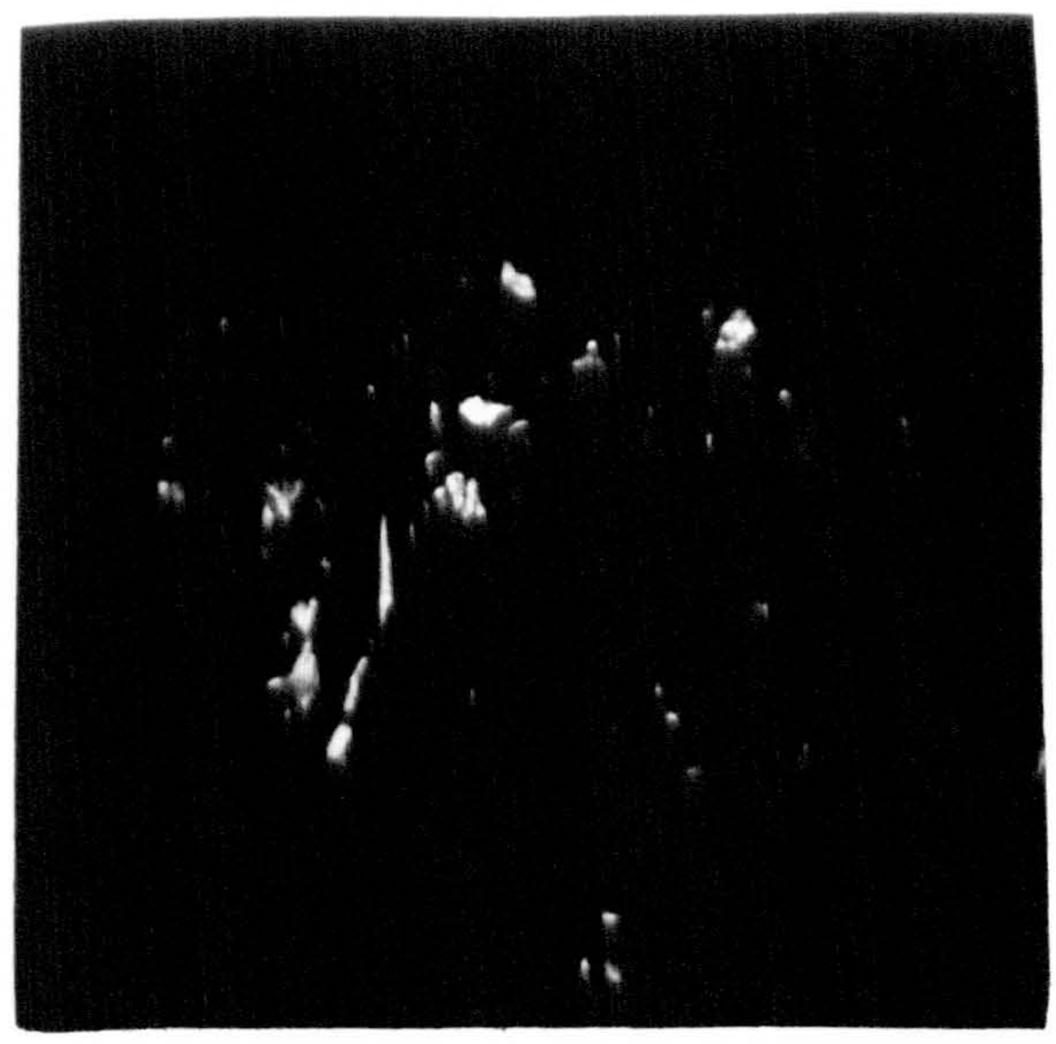

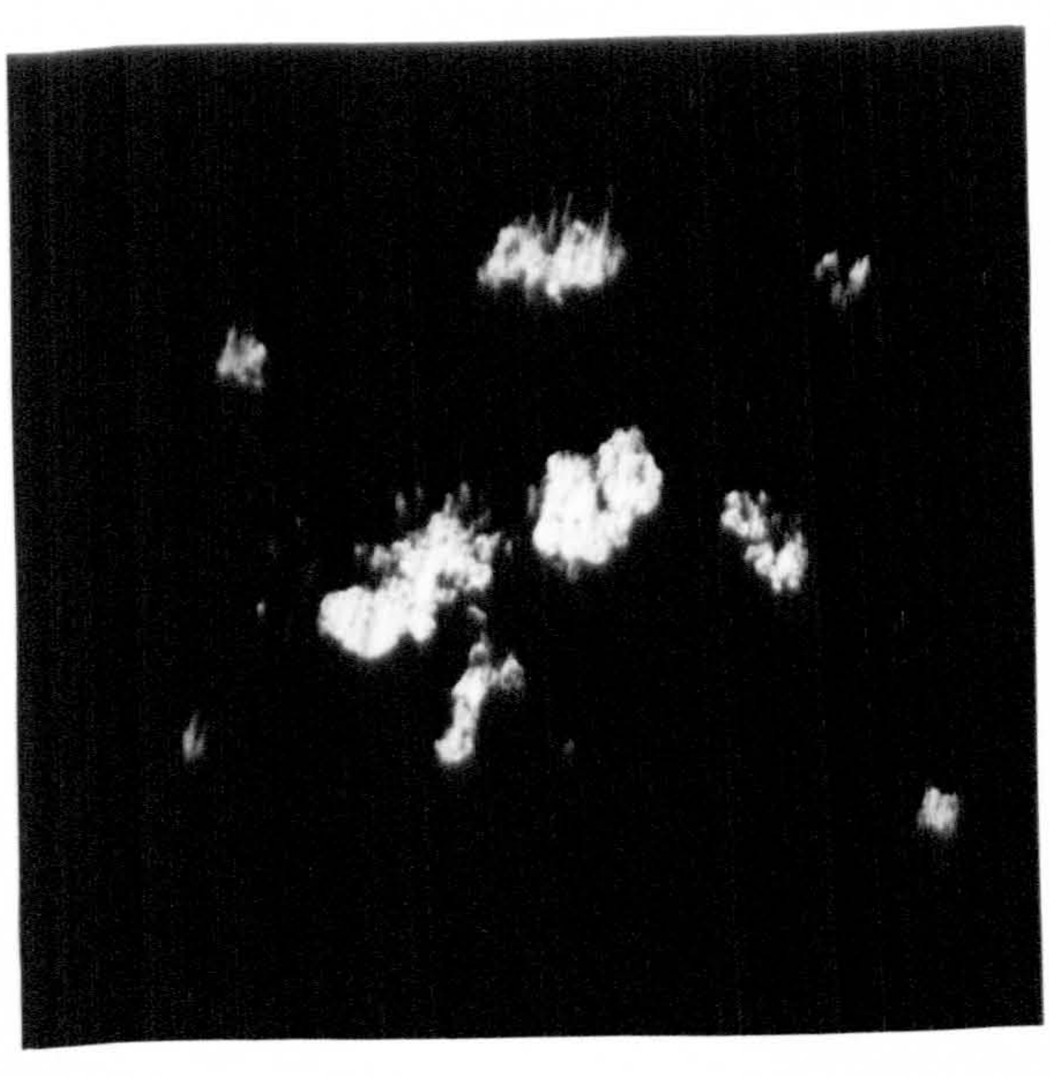

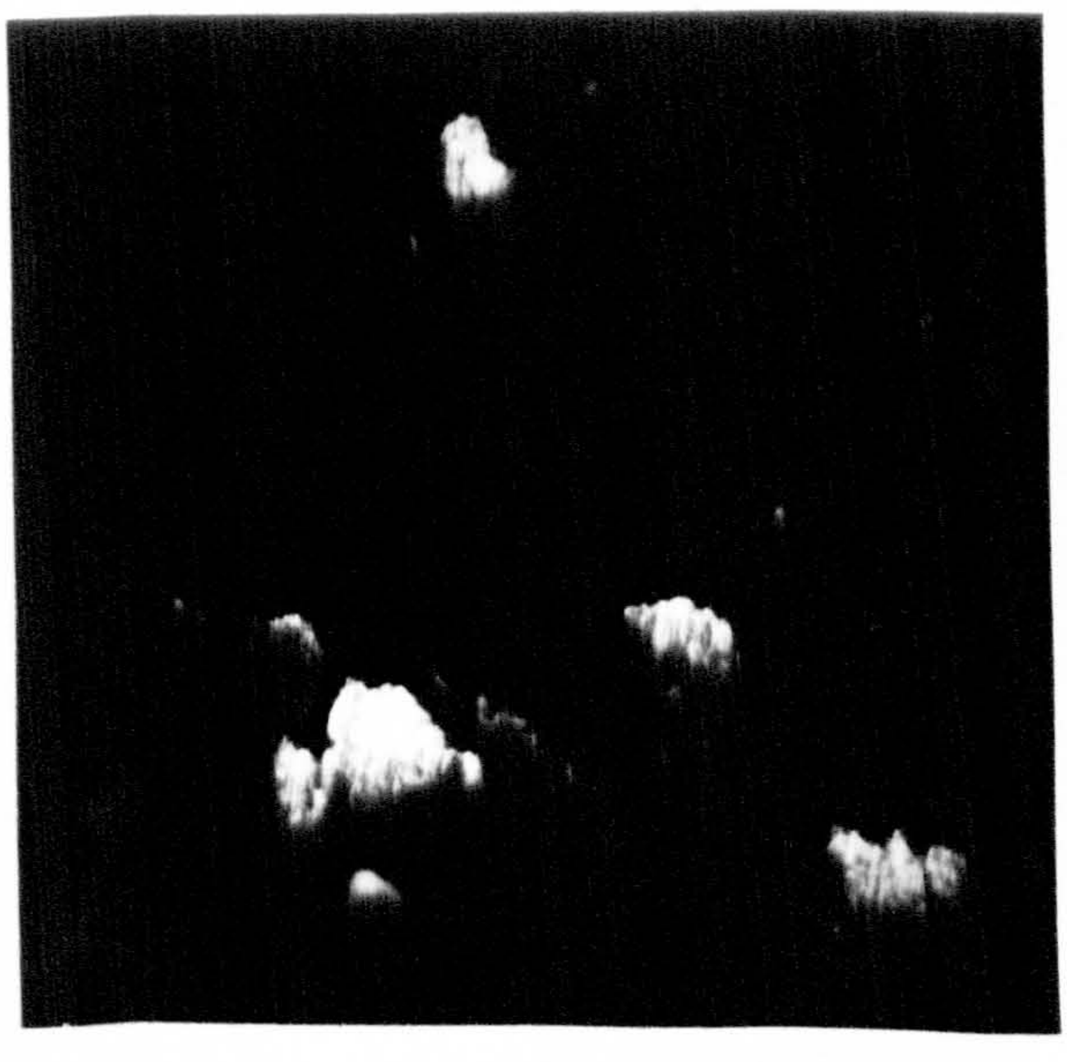

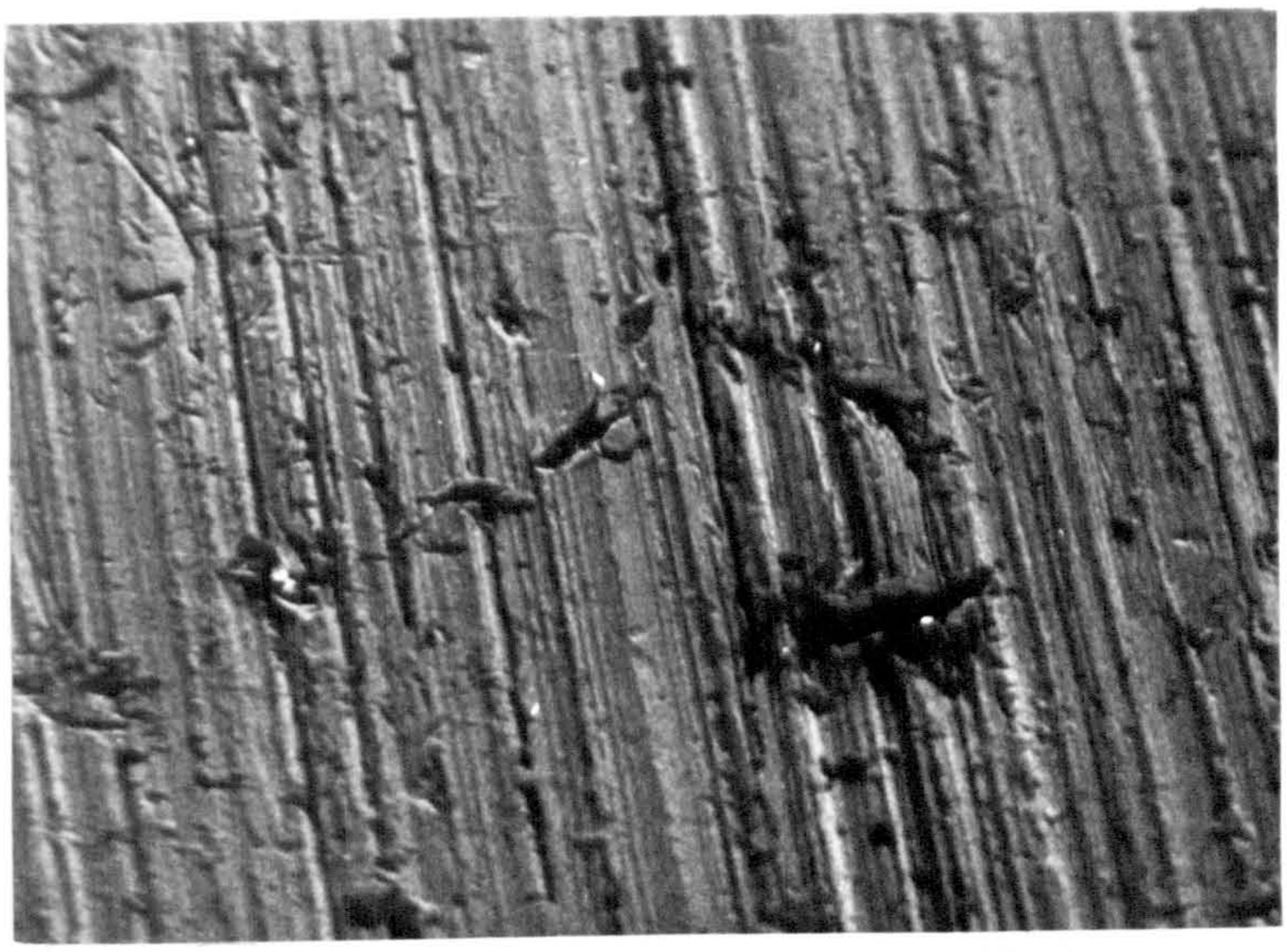

PLATE 13. The micrograph above (X 100 mag.) shows the characteristic pitted surface of a Mar M002 specimen which has been creep-feed ground with continuous dressing.

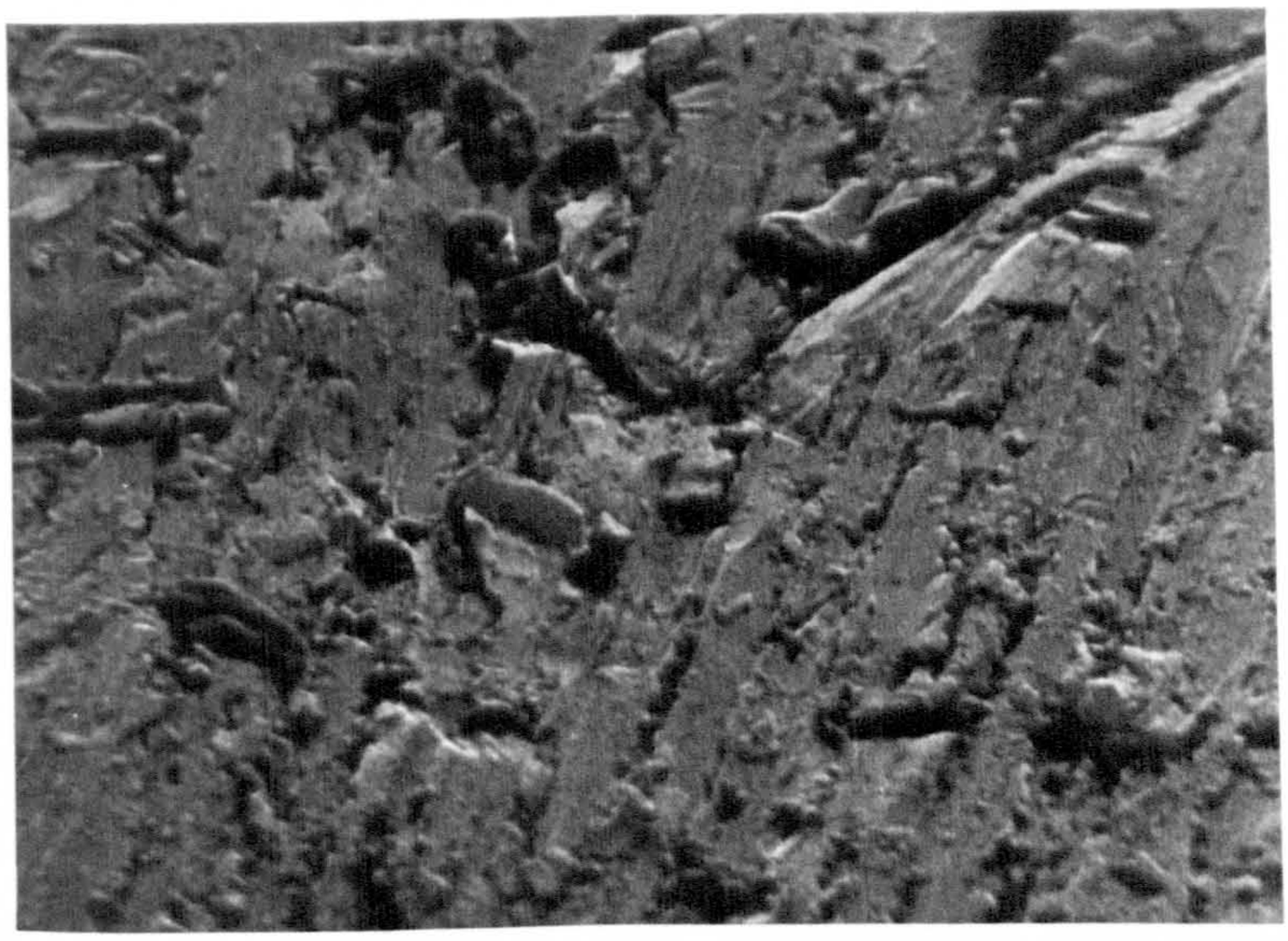

Above (X 400 mag.) shows the abused surface of a continuously dressed Mar M002 specimen, notice the smearing of material and the detritus adhered to the surface.

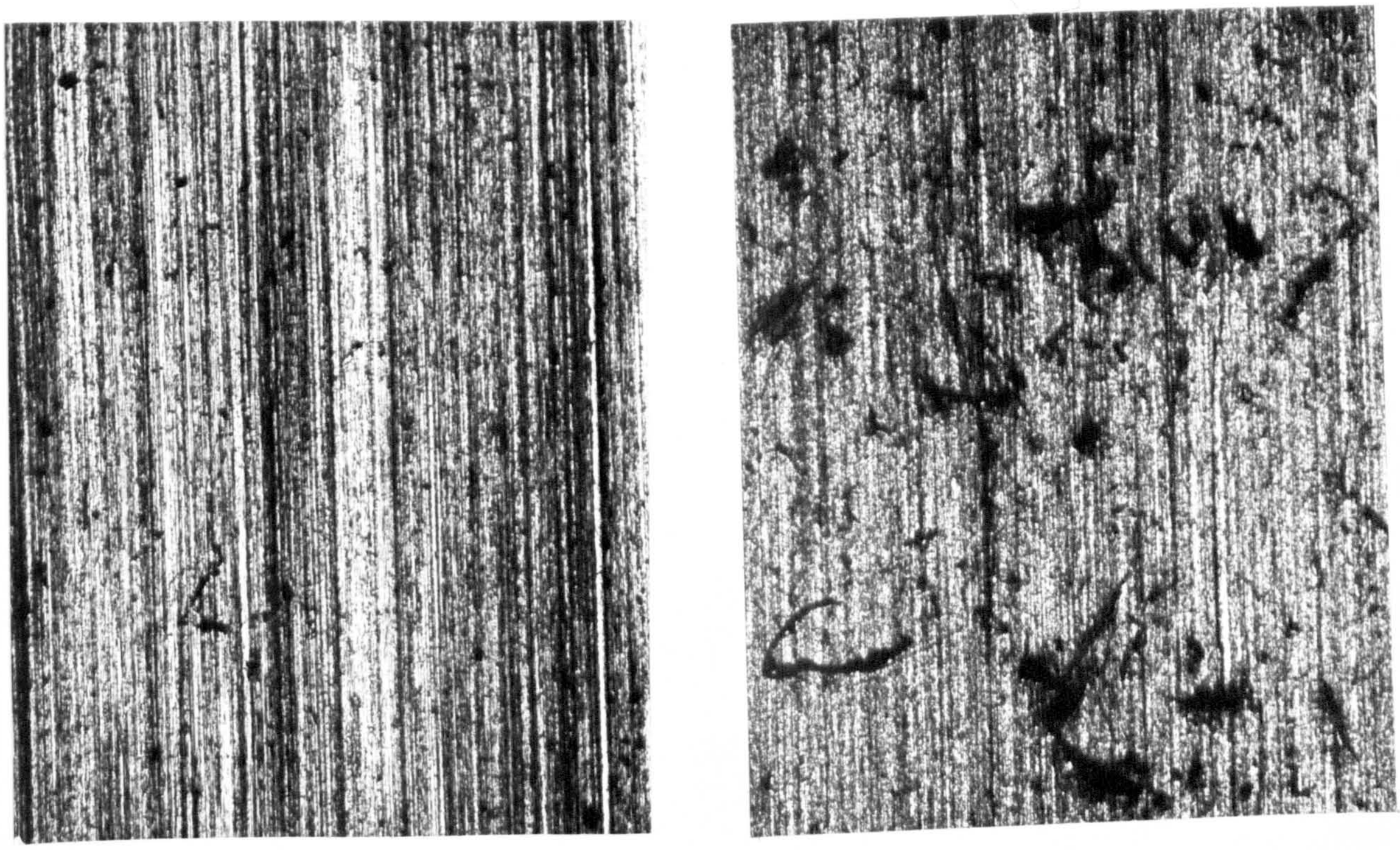

PLATE 14. Refer to fig. 30. On the left is shown the surface of the brass outside the path of the Mar M002. On the right is shown the surface of the brass inside the path of the Mar M002. The direction of grinding is down the page. Micro-probe analysis showed no evidence of nickel on the brass in either case.

APPENDICES

APPENDIX 1

SPECIFICATIONS

1. The High Speed Creep Feed Grinding Research Rig

Grinding Wheel Dimensions - 600mm diameter, 50mm width and 200 or 250mm bore

Range of Grinding Wheel Wear - 25mm radial wear

Grinding Wheel Drive - 35kW Thyristor Controlled DC Drive

Grinding Wheel Speeds - Constantly variable up to 100ms dependent on wheel diameter

Slideway Speeds - The available speeds depend on the selection of suitable gear boxes and pulleys. The maximum speed run on the rig was 1500mm/minute.

Traverse Movement of Slideway - 90mm

There is no vertical adjustment on the rig, the depth of cut is set by packing. The maximum distance between the dynamometer platform and the grinding wheel at minimum diameter is 55mm.

Bearing Stiffness:

The grinding wheel spindle bearing and the slideway bearings are Hydrostatic. They operate from a power pack supplying Castrol AWS 10 at a minimum pressure of 60b.

Vertical Static Stiffness of Spindle Bearing - $0.3GNm^{-1}$

Vertical Static Stiffness of Slideway Bearing - $1.1GNm^{-1}$

The dynamic stiffness of the spindle/grinding wheel/slideway system, measured by the deflection at spark-out from a known grinding force. - $0.11GNm^{-1}$

Cutting Fluid Delivery and Filtration Equipment:

The cutting fluid is delivered from a "Darenth" filtration system at a maximum flow rate of $6ls^{-1}$ and a

1. Continued

maximum pressure of 10b. The cutting fluid used for the research was Edgar Vaughans 'Houghtogrind 55' diluted with tap water 60:1.

2. Grinding Wheel Specifications

WA 60 80 FP2V - Creep Feed Grinding Wheel

The composition of the grinding wheel is 37% grit and 7.5% bond. The porosity of the wheel is induced by particles of naphthalene mixed into the grit and bond, the wheel is pressed and the naphthalene removed prior to firing. The size of the naphthalene particles is between 550-800μm.

WA 60 KV - Conventional Grinding Wheel

The composition of the grinding wheel is 50% grit and 7.5% bond. There is no induced porosity.

3. Diamond Roller Dresser

The Diamond Roller Dresser is 100mm in diameter and 28.47mm wide. The dresser was manufactured by Van Moppes and coded: DIAMESH 82971 IPE DD150. The surface area coverage of diamonds is 15.2% with 150 stones/carat. There is a plain form on the dresser parallel to the axis of the dresser.

4. Specimen Material Compositions

Both materials are 'superalloys' used in the manufacture of aero engine turbine blades. Their nominal compositions are as follows:-

	MARM 002	C1023
Aluminium	5.5%	4.0%
Cobalt	10.0%	10.0%
Chromium	9.0%	15.0%

4. Continued

	MARM 002	C1023
Hafnium	1.5%	-
Tantalum	2.5%	-
Molybdenum	-	8.0%
Titanium	1.5%	3.5%
Tungsten	10.0%	-
Other Elements	1.0%	0.5%

Remainder Nickel.

APPENDIX 2

DYNAMOMETER DESIGN AND INSTRUMENTATION

A most important part of the dynamometer design was the load sensing machanism. In this case foil type strain gauges of the type EA-06-125TG-350 were bonded to a short necked beam and connected in a 4-way temperature compensating bridge network, the active gauges monitoring the tensile and compressive strain in the beams. The beams were necked in order to prevent bending, simulating a pinned joint, a step to encourage pure compression or tension in the beam. The beams were designed short because the distance between the grinding wheel and the machine slideway needed to be as large as possible in order to make economic use of the specimen and packing material. The tests carried out by Stuart (4) provided valuable data for the expected grinding forces. The beams were designed to give maximum stiffness yet be sufficiently sensitive to detect the grinding forces and provide a high degree of accuracy.

The beam was designed as follows:

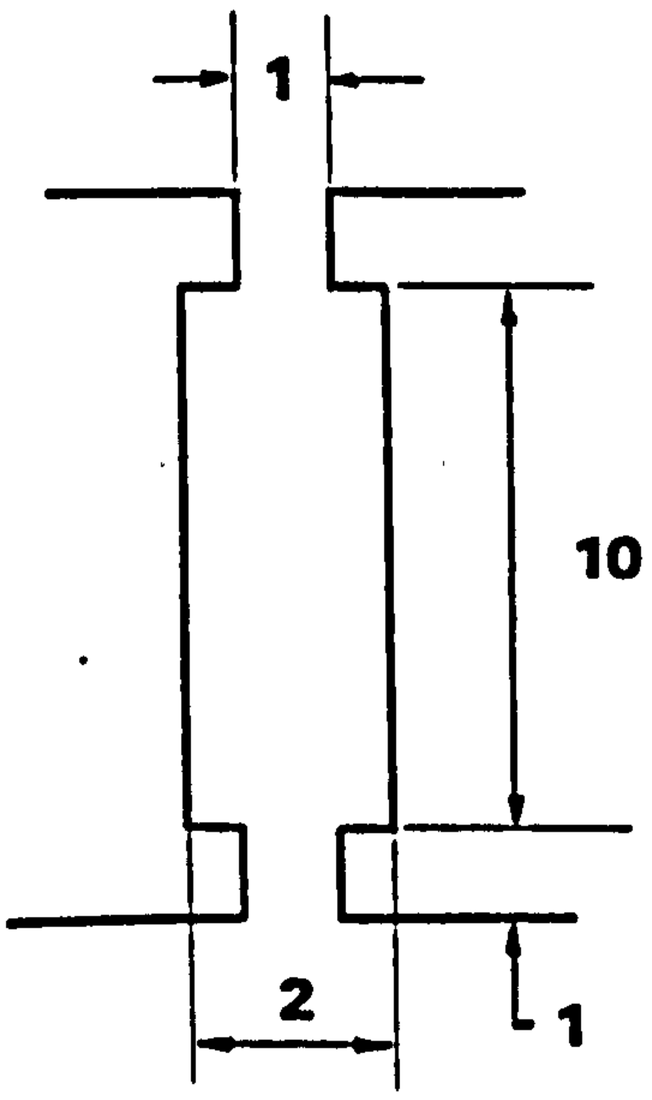

The beams were manufactured from EN 25 steel which has a Youngs Modulus of 210 GNm^{-2}. The cross-section of the beam is shown on the left and is 36mm. long. From the stress-strain relationship and stiffness of the system is 1.512 GNm^{-1}. The output sensitivity was 1.32 μ V/N for the 4-way bridge system shown in Appendix Fig 2.1.

The overall stiffness of the dynamometer assembly was calculated in both the vertical and horizontal planes in order to establish the lowest natural frequency of vibration. The system was also analysed for the 'rocking' mode about the centre of gravity of the dynamometer platform, however the lowest natural frequency was found to be in the horizontal plane; a frequency of 3.755 kHz. The calculations assumed a rigid system and neglected joint stiffnesses, it was therefore expected that the theoretical frequency would be higher than the actual frequency. A 'tap test' was performed in the horizontal plane by giving the dynamometer a sharp tap (step input) and monitoring the decay frequency, this frequency was in the order of 1.1 kHz. and assumed to be representative of the actual natural frequency.

To surpress any interference on the strain gauge signal, in particular wheel frequency vibration (16.6 Hz at 30 ms^{-1}) which might occur due to out of balance of the grinding wheel, three 10 Hz low pass active filters were designed and made, one for each of the beams in the dynamometer. The circuit and frequency response of the filters is shown in Appendix fig 2.2. The complete data recording circuit is shown in Appendix fig 2.3 with reference to the problem of earth loops. The galvonometers used in the U-V recorder were 1 KΩ, fluid damped, compatible with the strain gauge system which was amplified 1000 times to give a full scale deflection across the 150mm wide U-V paper for 1kN load.

Appendix Fig. 2.1

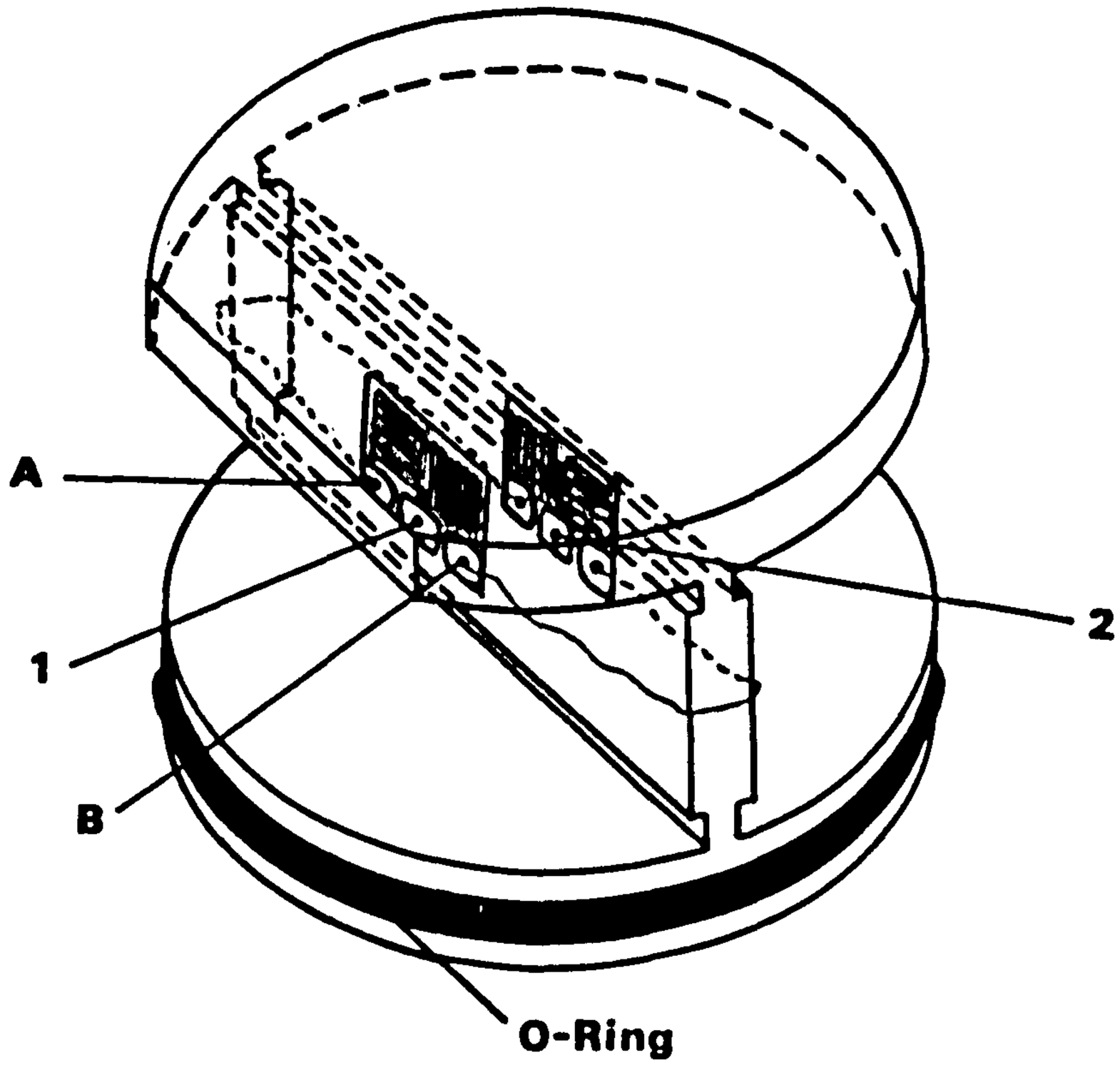

Micro-Measurement type EA-06-125 TG-350 strain gauges were used in the configuration shown above. Cu-Ag Kapton covered and screened leads were attached to the strain gauge bridge, A and B carried the bridge supply voltage 10 V, and 1 and 2 the signal output to the amplifier.

CIRCUIT AND FREQUENCY RESPONSE FOR 10Hz CUT-OFF FILTER

UNITY GAIN -40 db/decade

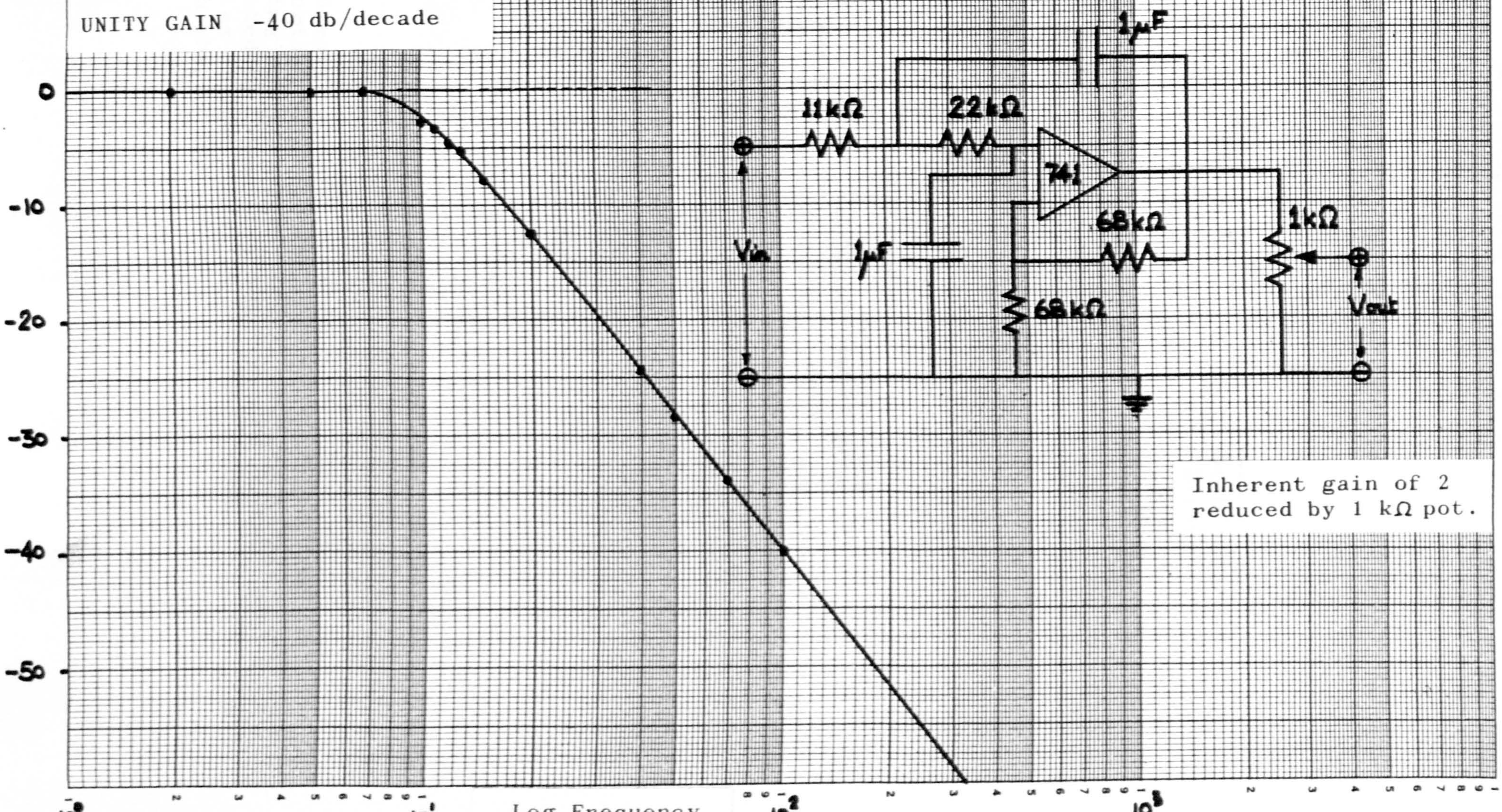

Appendix Fig. 2.2

Appendix Fig. 2.3

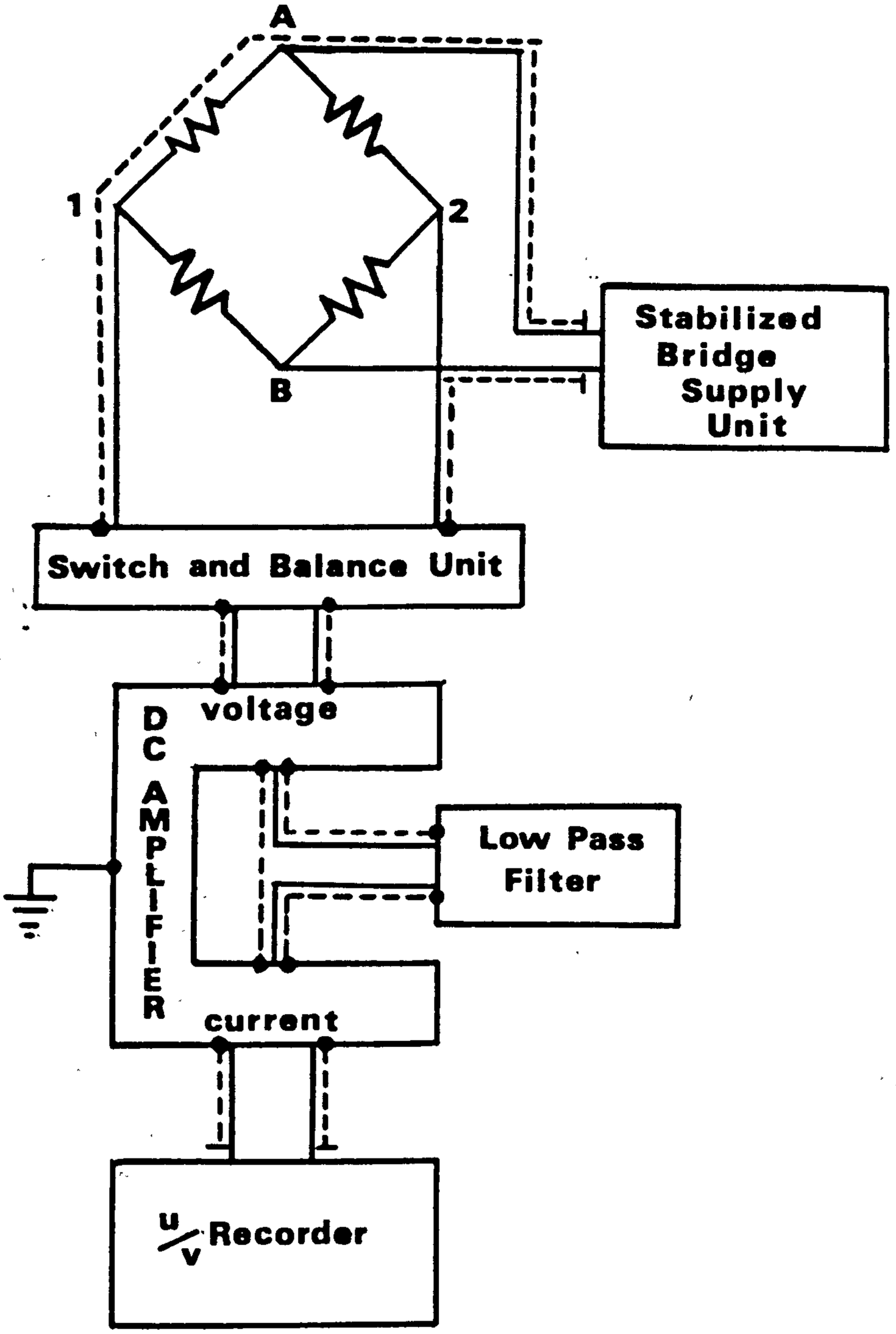

The schematic circuit diagram shows the strain gauge bridge with its amplification, filter and recording ancilliaries. Earth loops were eliminated by connecting the screened cables (shown as dashed lines) to a common earth through the DC amplifier.

APPENDIX 3

GRINDING THEORY

Nomenclature.

D = Grinding wheel diameter

V = Peripheral speed of the grinding wheel.

N = Angular speed of the grinding wheel.

V = Workpiece infeed rate.

K = Number of grits along a peripheral line of the grinding wheel, assuming that the number of grits per row are equal and regularly spaced.

C = Number of active grits per unit area of the wheel.

t = Grit depth of cut.

l = Length of the arc of cut.

d = Grinding wheel depth of cut.

b'= Mean width of grit.

b = Grinding wheel width of cut.

Refer to Appendix Fig.3.1.

d is greatly exaggerated (yet perhaps not for the creep feed grinding process), the length of cut (l) may be found to a good approximation:

$$l^2 = \frac{D^2}{4} - \left(\frac{D}{2} - d\right)^2 + d^2$$

$$= Dd$$

$$l = \sqrt{Dd} \qquad - 1$$

Refer to Appendix Fig. 3.2

$$AB = \sqrt{\left(\frac{D}{2}\right)^2 - \left(\frac{D}{2} - d\right)^2}$$

$$= \sqrt{(D - d)\, d}$$

Assuming that the arc of cut is a straight line.

$$t = f.\sin\theta$$

$$= F(AB) \,/\, (D/2)$$

$$= \frac{2f\sqrt{(D - d)d}}{D}$$

because d is much less than D then:

$$t = 2f\sqrt{(d/D)}$$

f is the distance that the workpiece advances in $\frac{1}{K}$ revolutions of a grinding wheel having K grits around a peripheral line.

Thus $f = v/(KN)$

$$t = \frac{2v}{KN}\sqrt{\frac{d}{D}} \qquad - 2$$

C the number of grits per unit area has to be determined by a suitable method, then the surface area of grinding wheel of grits b' wide is $\pi Db'$

$$K = \pi Db'C \qquad - 3$$

Looking at the frontal area of an idealised grit:

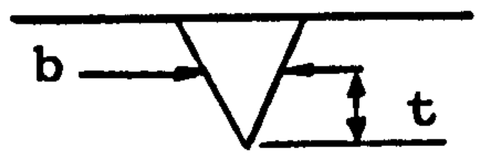

The ratio of width to depth for plunge grinding $r = \frac{b'}{t}$

For surface and cylindrical grinding the mean grit depth of cut is used $\frac{t}{2}$. Hence $r = \frac{2b'}{t}$

Equation 3 becomes $K = \pi \frac{DrtC}{2}$

Substituting into equation 2 :

$$t = \frac{4v}{DNCrt}\sqrt{\frac{d}{D}}$$

$V = \pi DN$

$$t = \sqrt{\frac{4vd}{VCrl}} \qquad - 4$$

Micro-milling Analogy. (Ref. 67)

Taking single point cutting

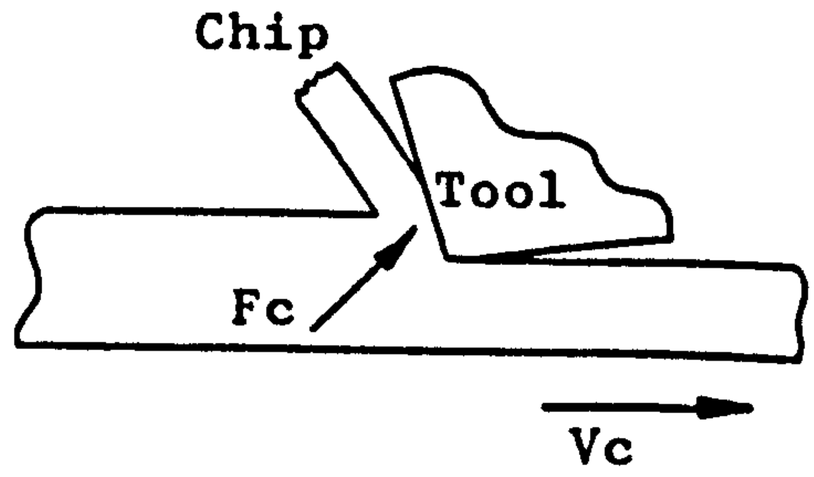

where b = width of cut

t = underformed chip thickness

u = specific energy

for single point cutting $u = \frac{FcVc}{btVc}$

(cutting force) $Fc = ubt$

The cutting force in grinding is attributed to the tangential force, so for grinding:

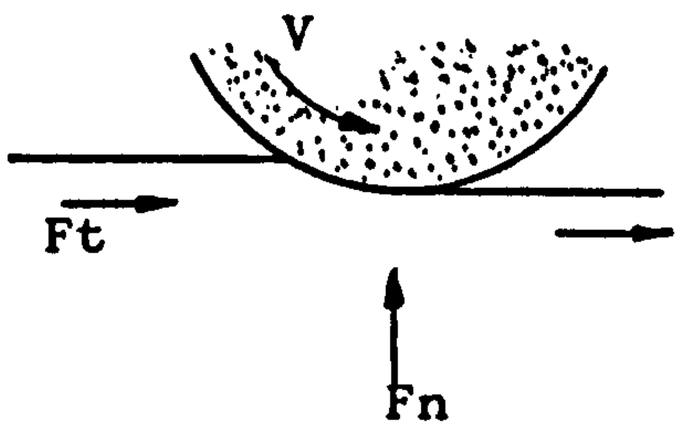

$$u' = \frac{FrV}{vbd}$$

(cutting force) $Fc = u'\frac{bdv}{V}$

The knowledge of the mean force acting on a single grit is necessary when considering how the effective hardness of a grinding wheel is altered by the grinding conditions.

Work done / unit time = $u'vbd$

Number of grits / unit time = VCb

Work done / grit = $\frac{u'vd}{VC}$

The mean force F" acting on a single grit may be obtained by dividing the work done / grit by the length of the arc of cut:

$$F'' = \frac{u'vd}{VCl} \qquad - 5$$

from eqn.4. $t^2 = \frac{4vd}{VCrl}$

$$1 = \frac{4vd}{VCrt^2}$$

substitute for 1 in 5

$$F'' = \frac{u't^2r}{4} \qquad - 6$$

The principal ways of decreasing the effective hardness of a grinding wheel are with reference to equations 4 and 5.

1. To increase the workpiece infeed rate v.

2. Decrease grinding wheel speed V.

3. Increase the grinding wheel depth of cut d.

4. Decrease the number of active grits C.

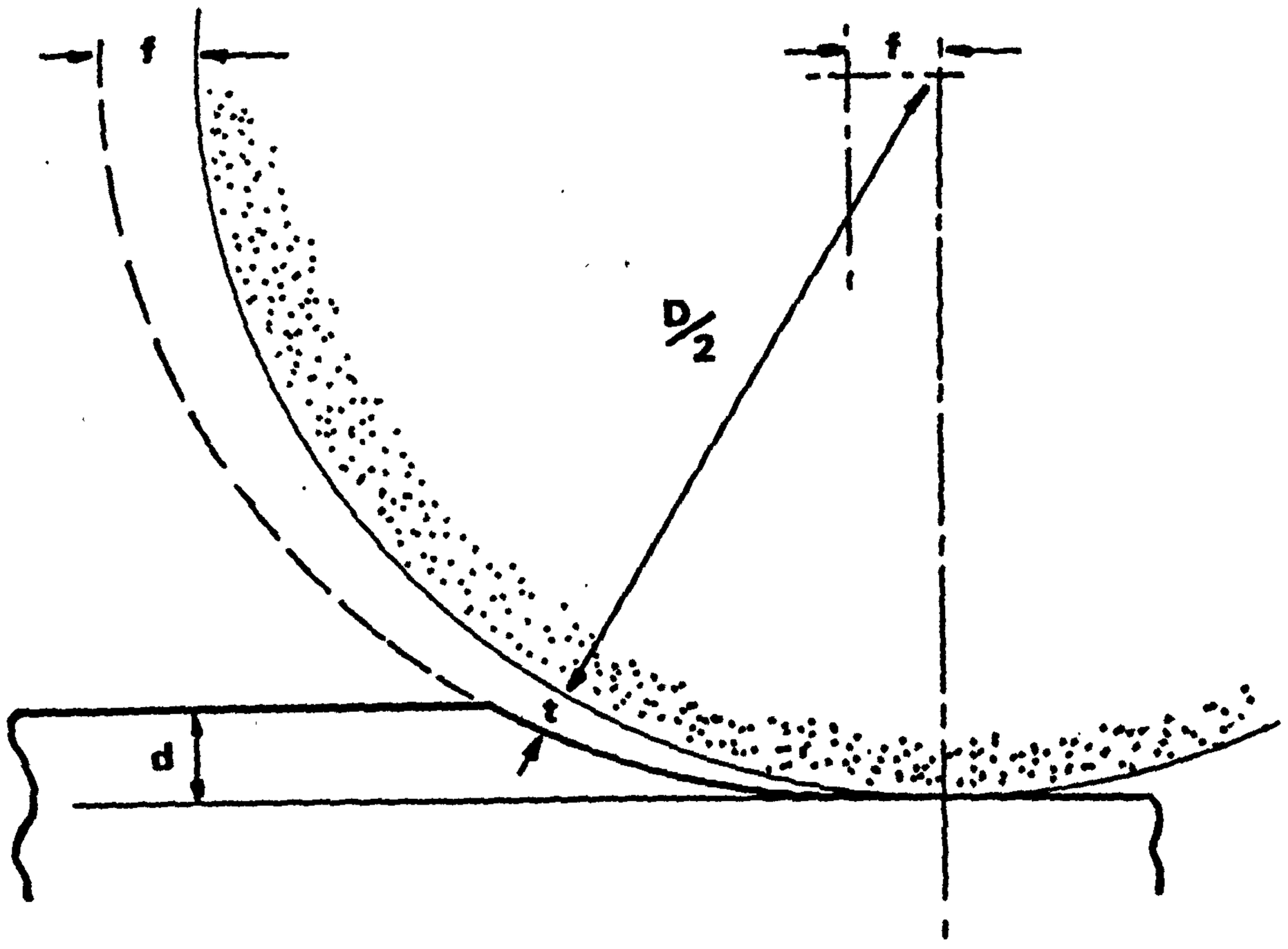

MICRO-MILLING ANALOGY

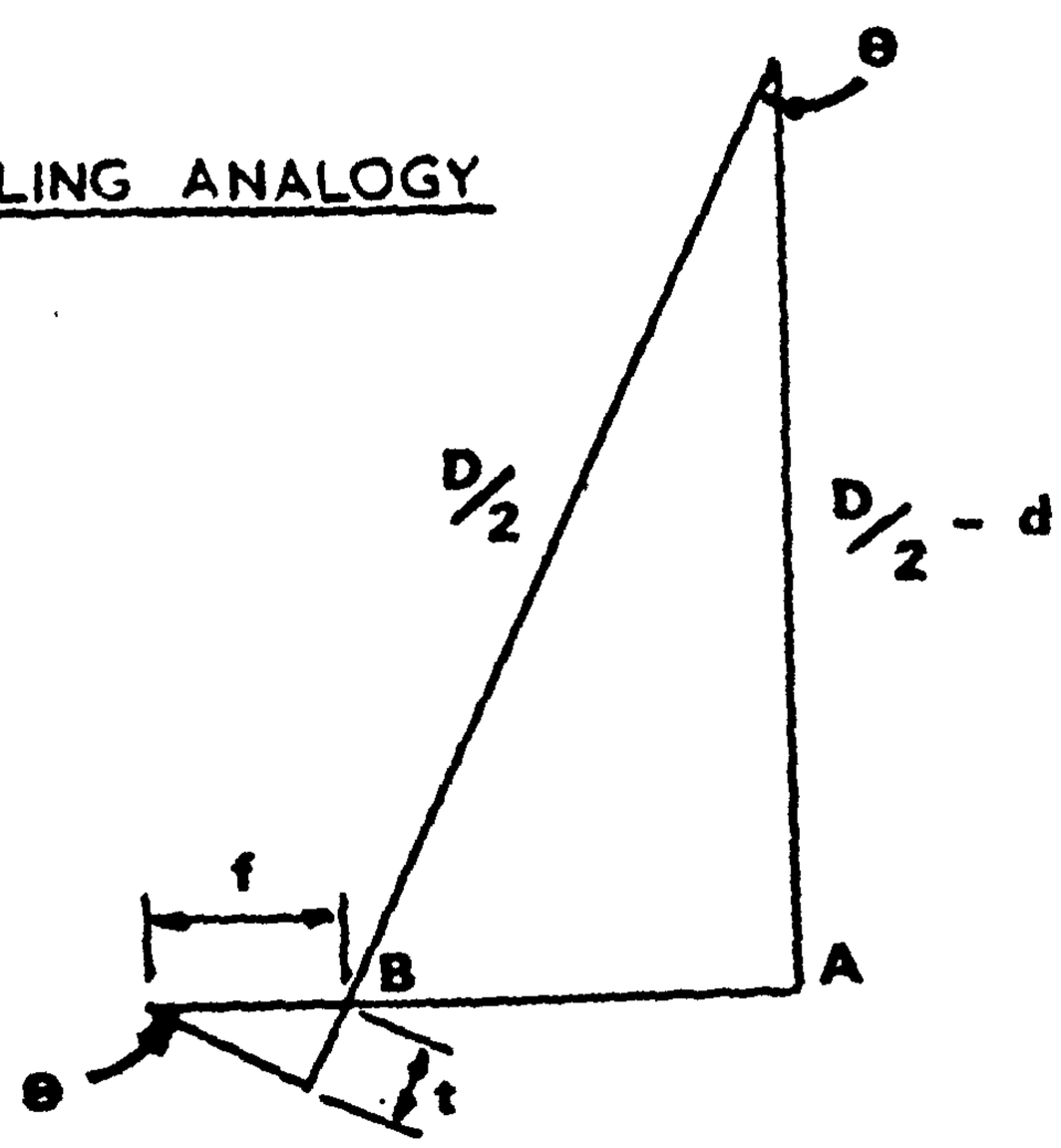

Appendix Fig. 3.1

APPENDIX 4

ANALYSIS FOR WEAR FLAT AREA MEASUREMENT

The 'wear flat area' on the surface of the grinding wheel was measured by a random sampling method. Photographs were taken at a number of random stations on the surface of the grinding wheel using the microscope-camera (see section 4.4.7). The magnification of the system was low, X 4.7 objective and X 6 eyepiece. The observed area was enclosed by a circle 1.5 mm in diameter. The 'wear flat area' was measured using a Quantimet Image Analyser which scans the photograph, discriminating between pre-set levels of lightness and darkness, after having been calibrated to a standard level of light. The number of scanning points on the Quantimet is 500,000 which provides for a high degree of accuracy.

The photographic reproduction was closely controlled so that the level of contrast was consistant for each print. The photographs were taken with maximum microscope illumination on Ilford FP4 film exposed for $\frac{1}{2}$ second at f 2.8. The film was developed for 4 minutes in Ilford Contrast FF diluted 7:1 with tap water and fixed for 10 minutes in Kodak Solution diluted 3:1 with tap water. The photographs were printed on Kodak grade 4 paper, half plate size. The paper was exposed to the negative for 15 secs. using a 50 mm lens at f 11. The paper was developed in a 7:1 Contrast FF developer for $1\frac{1}{2}$ minutes and fixed in Kodak solution for 5 minutes, then washed and dried.

In order to estimate the sample size necessary for the degree of accuracy required a large sample of data was plotted (140 photographs) and found to be normally distributed.

This made valid the following statistical formula for an estimate of the sample size:

$$z = \frac{e\sqrt{N}}{\sigma}$$

where z = Normal deviate.

e = Number of error points.

N = Sample size.

σ = Standard deviation.

The error margins were set as follows:

Risk of error - 5% (95% Confidence Limit).

This sets z at 1.96 from the normal distribution table.

The accuracy in percentage wear flat area was set at 0.05% which makes e = 250 (0.05% of 500,000).

The standard deviation of the sample was 1078.

$$1.96 = \frac{250\sqrt{N}}{1078}$$

$$N = 71.43$$

The standard deviation of every sample was tested to ensure that it was less than 1078 and the sample size was fixed to be greater than 80. This means that the 'wear flat area' was measured within the statistical limit to an accuracy of better than 0.05%.

APPENDIX 5

MATHEMATICAL MODEL OF THE WARMING UP EFFECT OF THE CUTTING FLUID

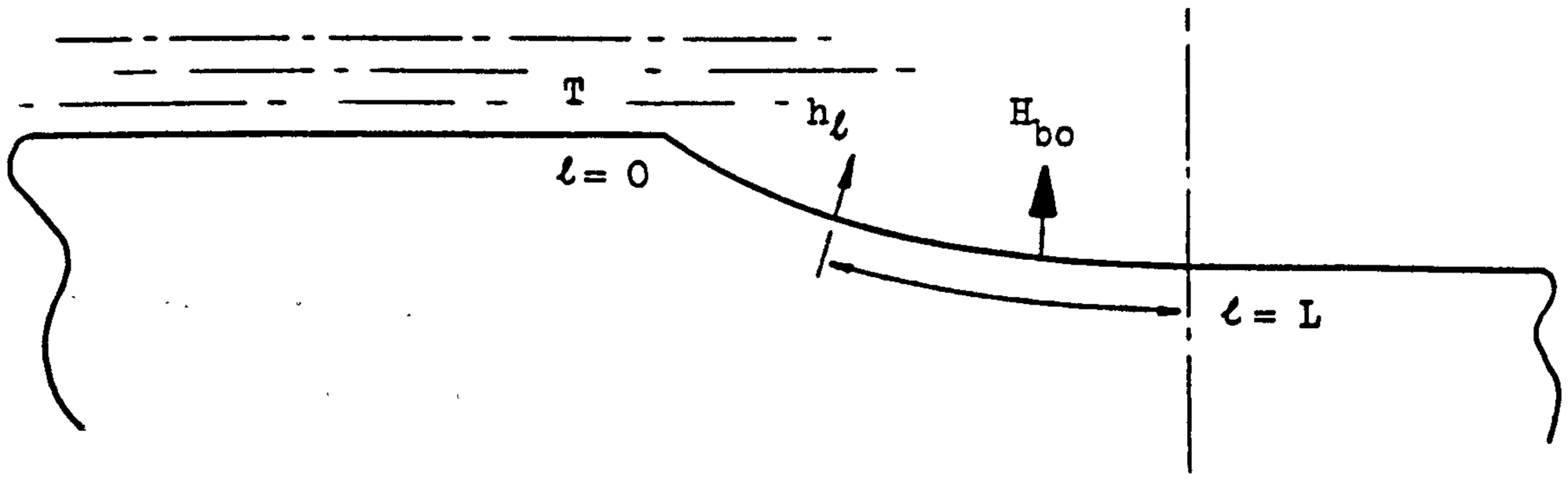

T = The bulk temperature of the cutting fluid.

ℓ = An increment of arc length.

OL = The total arc length.

H_{bo} = Heat flux at burn-out.

h_ℓ = Heat flux at ℓ.

Two relationships were shown by Powell (6), see Fig. 32.

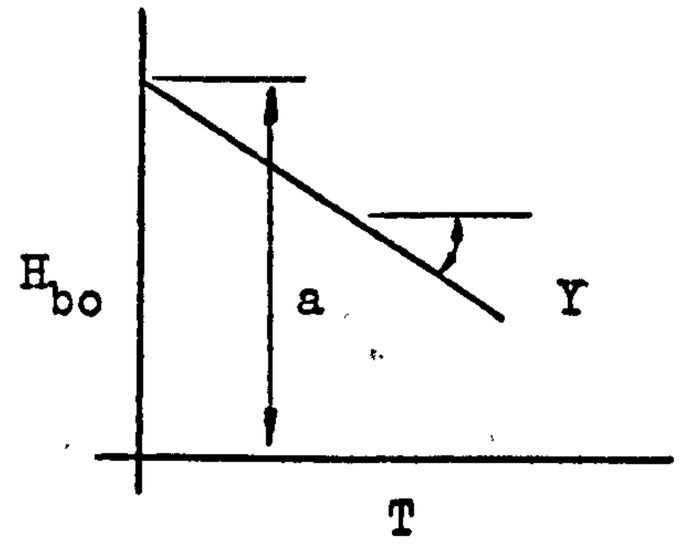

(i) Only true for a known arc length. (6.5 mm)

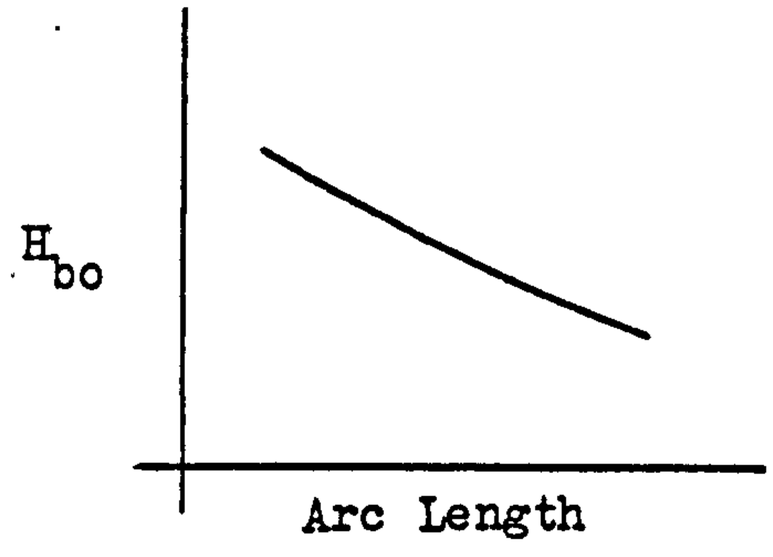

(ii) Only small arc lengths up to 13 mm tested.

From (i) $H_{bo} = a - YT$

The bulk temperature varies in the arc of cut due to warming-up, hence the temperature might be expressed as follows:

$$T = \int_0^L (qh_\ell - c)d\ell$$

where q is a thermal conductivity constant
and c is a constant for cooling by convention and conduction in the cutting fluid.

Hence $$H_{bo} = a - Y\int_0^L (qh_\ell - c)d\ell \qquad (1)$$

For a block heat input profile - $h_\ell = H_{bo}$

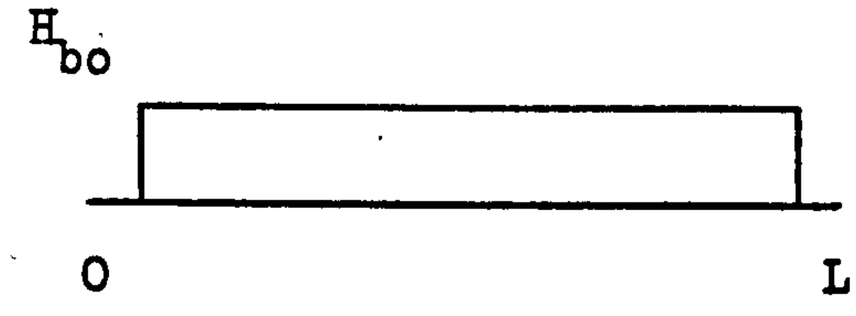

Integrating - ℓ.

$$H_{bo} = a - Y(qh_\ell L - cL)$$

$$H_{bo} = a - YL(qH_{bo} - c) \qquad (2)$$

Powell's heat input profile was a block profile dictated by the design of the heating element; unfortunately, the power flux profile for the real grinding situation is unknown. However, Shafto (20) has postulated that the profile is triangular or trapezoidal.

let $R = H_{bo}_{max} - H_{bo}_{min}$

$$h = H_{bo}_{max} - \frac{(R\ell)}{L}$$

Substitute for h in equation (1).

$$H_{bo} = a - Y\int_0^L \left[q\left(H_{bo}_{max} - \frac{(R\ell)}{L}\right) - c\right] d\ell$$

Integrating and substituting back for R:

$$H_{bo} = a - \frac{YqL}{2}\left(H_{bo}_{max} + H_{bo}_{min} - \frac{2c}{q}\right) \qquad (3)$$

The model might be refined from equation (1) where c, the cooling term, is likely to be a function of the bulk temperature T.

Equation (1) becomes:

$$H_{bo} = a - Y\int_0^L (qh_\ell - cT)d\ell \qquad (4)$$

where $\frac{dT}{d\ell} = qh_{\ell} - cT$ (5)

For a block heat input profile $h = H_{bo}$, hence equation (5) becomes a differential equation:

$$\frac{qH_{bo}}{c} = T + \frac{dT}{cd\ell}$$

Complimentary function of the form: $T = Ae^{-G\ell}$

$$\frac{dT}{d\ell} = -AGe^{-G\ell}$$

substituting back into the differential equation:

$$Ae^{-G\ell} - \frac{AGe^{-G\ell}}{c} = 0$$

therefore $G = c$ and $T = Ae^{-c\ell}$

rewriting the differential equation:

$$T = \frac{qH_{bo}}{c} + Ae^{-c\ell}$$

in the limit

T=0 when L=0

Complimentary function is $-\frac{qH_{bo}}{c} e^{-c\ell}$

for the zero order polynomial the Particular integral is:

$$\frac{qH_{bo}}{c}$$

Hence $T = qH_{bo}(1 - e^{-c\ell})$

Substituting back into equation (4):

$$H_{bo} = a - Y\int_0^L \left[qH_{bo} - c\left[\frac{qH_{bo}}{c}(1 - e^{-c\ell})\right]\right]$$

$$= a - YqH_{bo}\int_0^L e^{-c\ell}\, d\ell$$

$$= a - Y\frac{qH_{bo}}{c}(1 - e^{-c\ell})$$

The heat input profile can be modified from a block profile to a triangular or trapezoidal. Equation (5) becomes:

$$\frac{dT}{d\ell} = q\left(H_{\substack{bo \\ max}} - \frac{(R\ell)}{L}\right) - cT \qquad (6)$$

as before the complementary function is of the form: $T = Ae^{-G\ell}$

Rearranging equation (6) and substituting as follows:

$$M = qH_{\substack{bo \\ max}} \qquad \text{and} \qquad N = \frac{qR}{L}$$

$$T = \frac{1}{c}(M - N\ell + Ace^{-c\ell})$$

In the limit T=0 when L=0 therefore $A = -\frac{M}{c}$

The complementary function is $-\frac{M}{c}e^{-c\ell}$

$\frac{dT}{d\ell} + cT = (M - N\ell)$ is in the form of a 1^{st} order polynomial

$$\text{say} \quad T = x + y\ell \qquad \frac{dT}{d\ell} = y \qquad (7)$$

and substituting back:

$$y + cx + cy\ell = M - N\ell$$

equating coefficients:

$$cy = -N \qquad \text{so} \quad y = \frac{-N}{c}$$

$$y + cx = M \qquad x = \frac{1}{c}\left(M + \frac{N}{c}\right)$$

substituting back into equation (7)

$$T = \frac{1}{c}\left(M + N\left(\frac{1}{c} - \ell\right)\right)$$

Replacing M and N the particular integral is:

$$\frac{1}{c}\left(qH_{\substack{bo \\ max}} + \frac{qR}{L}\left(\frac{1}{c} - \ell\right)\right)$$

$$T = \frac{1}{c}\left(qH_{\substack{bo \\ max}} + \frac{qR}{L}\left(\frac{1}{c} - \ell\right)\right) - \left(\frac{qH_{\substack{bo \\ max}}}{c}e^{-c\ell}\right)$$

h_ℓ and T are substituted back into equation (4) and solved for H_{bo}.

Equation (4) becomes:

$$H_{bo} = a - qY\int_0^L \left(H_{\substack{bo \\ max}} e^{-c\ell} - \frac{R}{Lc} \right) d\ell$$

Integrating and substituting for R

$$H_{bo} = a - \frac{qY}{c}\left(H_{\substack{bo \\ min}} - H_{\substack{bo \\ max}} e^{-c\ell} \right)$$

The mathematical model of the warming-up effect of the cutting fluid around the arc of cut is a representation of the real situation based on data derived from simulation tests carried out by Powell (6). The shape of the power flux profile is a most important part of the modelling. It is thought that a change in the profile is brought about by the transition from cutting to rubbing (see Section 6.2). It is hoped that the model will provide a basis for further work to evaluate the power flux profile and so predict the burn-out heat flux for a set of known grinding conditions.

APPENDIX 6

THE ECONOMICS OF THE CREEP FEED GRINDING PROCESS - A CASE STUDY

The results of the high stock removal tests (see sect. 5.2) showed that the stock removal capability of the creep feed grinding process, when continuously dressing the grinding wheel, can be increased by a factor of 25 times with an apparent wheel wear of twice that of conventional creep feed grinding.

With the conventional creep feed grinding process, the limitation to the stock removal rate has been shown to be the onset of thermal damage, whereas the limitation to the continuously dressed creep feed grinding process is grinding wheel breakdown. Both limitations were established at a depth of cut of 3mm, (3mm being a typical depth of cut value, industrially), the maximum normal infeed rates being 8 and 200mm/minute respectively. In terms of stock removal rate per unit width of the workpiece, the results indicate that at a depth of cut of 3mm the conventional creep feed grinding process has a maximum stock removal rate of $160mm^3/min/mm$ width and the continuously dressed process has a limiting stock removal rate of $4100mm^3/min/mm$ width.

It must be appreciated that the conventional grinding process is not 'ever stable' as the grinding wheel surface will degrade as the abrasive wears (see sect. 2.3), whereas the continuously dressed grinding wheel is in a constant state of sharpness.

The 25 times increase in stock removal rate does not read directly across to the shop floor. Intermittent cutting, when more than one component is machined in any one pass of the machine bed, affects the actual stock removal rate. At the

beginning of a cut the grinding wheel has to progress into a full depth of cut situation which means that the stock removal rate is not constant until full depth of cut is achieved.

A suitable component was chosen from the shop floor for comparison between the existing production process and a proposed continuously dressed creep feed grinding process. The component is an aero engine turbine blade manufactured in MAR M002 (see plate 1). A particular operation in the manufacture of the blade was chosen because it was a plain form similar to that machined on the test pieces. The operation is shown in plate A of this appendix. The object is to remove a portion of the workpiece 8mm deep and 17mm in length.

<u>The Present Production Method</u>

The blades are machined in batches of two. They are set in a fixture which locates the blades 25mm apart. An Elb W06 creep feed grinding machine is used with the following settings:

Grinding Wheel Speed	- 15 ms^{-1}
Grinding Wheel Diameter	- 400mm
Workpiece Infeed Rate	- 70mm/minute
Radial Infeed of the Dresser per Batch of 2 Blades	- 0.15mm

The machining time per blade is = 49.29 secs.

The amount of wheel used is = 94.21 mm^3/mm width/blade.

The G ratio (work/wheel) is = 1.44

<u>The Present Production Method Adapted for Continuous Dressing</u>

Supposing the existing Elb grinding machine was capable of both continuous dressing and a maximum normal infeed rate of 190 mm/min (190mm/minute has been chosen to be just below

the onset of grinding wheel breakdown). With the same fixture, machining two blades in one pass, the machine settings would be as follows:-

Grinding Wheel Speed - 30 ms^{-1}

Grinding Wheel Diameter - 400mm

Workpiece Infeed Rate - 678.57mm/min

Continuous Dresser Infeed - 2.5µm/rev of the wheel

The machining time per blade would be = 5.08 secs

The amount of wheel used would be = 380.18 mm^3/mm width/blade

The G ratio (work/wheel) would be = 0.36

By continuously dressing the grinding wheel, the machining time per blade would appear to have decreased by 9.7 times against the conventional creep feed grinding process, however the grinding wheel usage would increase by 4.03 times.

As shown in this work, continuous dressing maintains the grinding wheel in a constant state of sharpness. This has the advantage that large batch quantities can be accommodated. By increasing the batch size the time taken for the grinding wheel to progress into the full depth of cut at the start of a cut becomes an insignificant part of the total machining time. Further to this, an increase in grinding wheel diameter means that the arc length of cut becomes an increasingly smaller proportion of the grinding wheel circumference. The angle subtended by the arc of cut from the centre of the wheel is small, allowing proportionally faster work speeds for equivalent maximum normal infeed rate. The continuous dressing action is a function of infeed/rev. of the grinding wheel, the larger the grinding wheel diameter the higher the G ratio for the proportionally higher work speed.

A new concept in creep feed grinding can be postulated, however it must be pointed out that the arguments relating to the change in grinding wheel diameter are based on the assumption that the effects of arc length established in this work are valid for all grinding wheel diameters.

The setting of a revolutionary grinding machine might be as follows:-

Grinding Wheel Speed - $30ms^{-1}$

Grinding Wheel Diameter - 4 metres

Workpiece infeed rate - 2126.39mm/minute

Continuous dresser infeed rate - 2.5 μm/rev.

Batch size - 45

The machining time per blade would be = 1.28 secs.

The amount of wheel used would be = $96mm^3$/mm width/blade

The G ratio would be = 1.42

The machining time is 38.5 times faster than the present method in production for almost the same G ratio. The large wheel diameter has further economic advantage in that a number of work stations can be situated around the wheel periphery providing increased machine tool utilisation. There is still a potential growth for the process because High Speed Creep Feed grinding becomes viable as the rubbing energy component has been dramatically reduced by the action of continuous dressing. However the combination of high grinding wheel speeds and continuous dressing will have to form part of a process evaluation in a programme of further work.

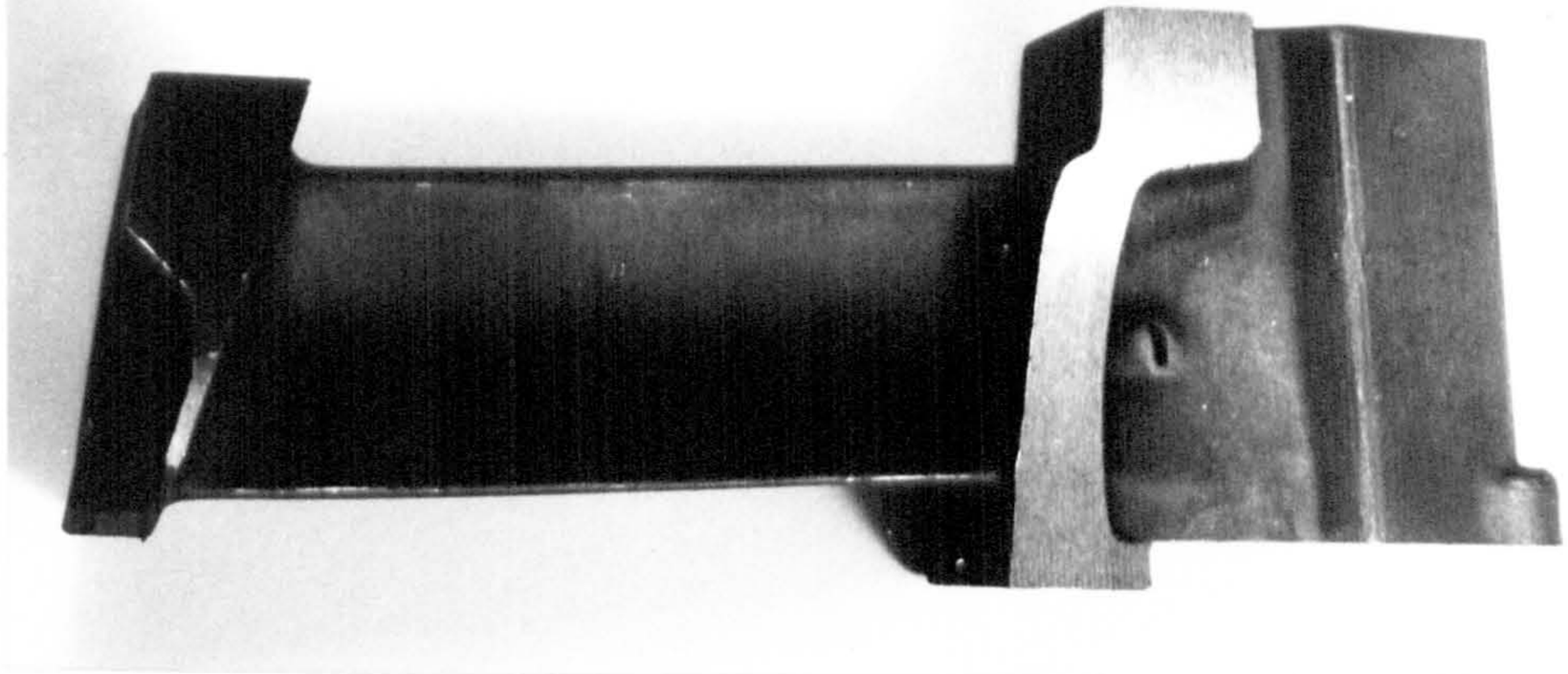

APPENDIX 6. PLATE A.
The operation shown in the photographs illustrates the removal of stock from the root end of a turbine blade. The pre-machined condition is depicted above and the post-machined condition to the right.

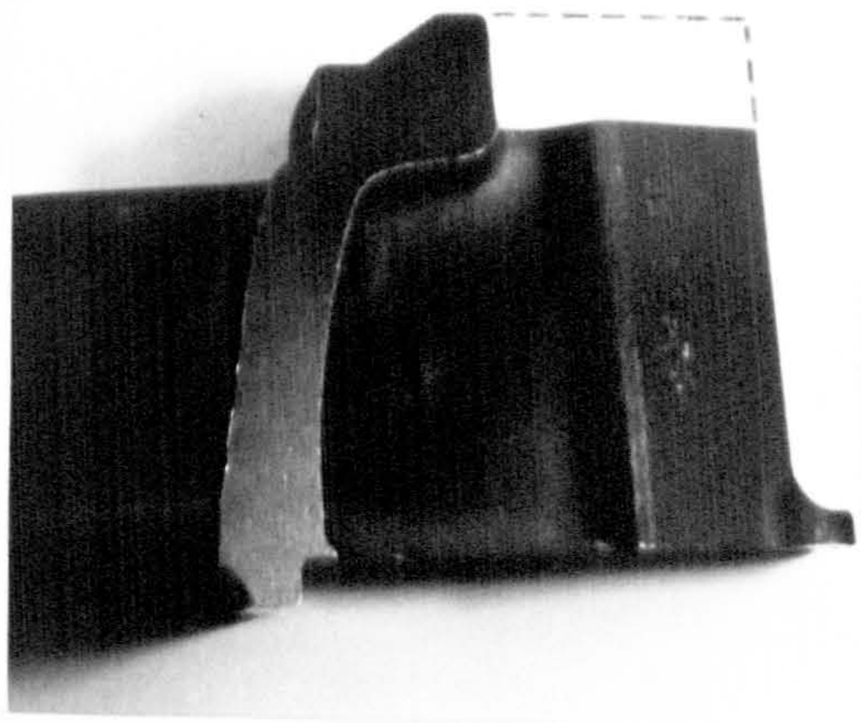

APPENDIX 7

A COMPUTER PROGRAM FOR EVALUATING TEST DATA

A computer program was designed to calculate the rig settings and analyse the data recorded from each grinding test. The test data, grinding forces, torque, power, resultant, normal and tangential forces and their ratio, stress distribution and specific energy are presented in tabular form. The results are summed and the mean values summarised. The grinding wheel diameter changes signifcantly when continuously dressing and the point of action of the resultant grinding force also changes in relation to the strain gauged dynamometer beams over the duration of a test. The program is designed to take into account the geometric changes by an iterative process. The program steps are explained in detail below with reference to Appendix Fig. 7.1.

The alpha-numerics used in the program are given in brackets.

Line Number.

10 - 240 Program introduction and titles.

250 - 370 Entry of test requirements - (A) Test number, (W1) Wheel speed, (D) Wheel diameter, (01) Maximum normal infeed rate, (02) Workpiece feed rate, Dresser speed ratio.

380 - 390 Fixed dresser diameter of 100mm.

400 - 430 Entry of specimen size - Width (W) and Length (V0).

440 - 650 Calculations for Wheel RPM (V2), Expected depth of cut (D1), Actual workpiece feed rate (V1), Dresser speed (H) and print out.

660 - 850 This section calculates the continuous dressing settings from the entry of geometric coefficients (Y1,Y2,Y3) from scale drawings of the dresser infeed mechanism (see fig. 12). Settings calculated are the Dresser infeed rate (V3), Slope of the workpiece (B4), Packing height for preparing the specimen (Y0), the set depth of cut (D9), Arc length (A1) and printed out.

860 - 920 Provision is made here for the entry of conventional wheel wear data for the calculation of the G ratio.

930 - 970 The time for a grit to traverse the arc of cut is calculated along with the volume of material removed in one sweep of the arc of cut (T1 and M1).

980 - 1070 The analytical part of the program begins here with titles and an option to exit the program if analysis is not required.

1080 - 1140 The number of data points are entered to set the array size (Z), the time interval between each data point (I1) and the actual depth of cut achieved in the test (D2).

1150 (D1) is calculated which is the distance that the workpiece has to travel prior to full arc of cut. Refer to Appendix Fig. 7.2.

1160 - 1230 Array declarations.

1240 - 1390 The data is read in and the zero drift calculated and offset across the data.

1400 - 1470 This is the dynamometer calibration matrix for the calculation of the grinding forces from the test data.

1480 - 1580 The grinding forces are calculated and tabulated.

1590 The workpiece feed rate is changed from mm/min to mm/sec as the time interval between data points is measured in seconds.

1600 - 1620 The total vertical force and horizontal force is calculated along with the vertical/horizontal ratio.

1630 - 1660 The point of intersection of the line of action of the resultant force and the horizontal plane is calculated with reference to the right hand beam of the dynamometer for every data point.

1670 - 1730 Print out of forces, titles for torque, power and the position of the resultant force line of action on the arc of cut.

1740 - 2030 Refer to Appendix Fig. 7.2. A series of equations are solved to calculate the torque, power and the position of the resultant force on the arc of cut. There is a geometric pattern which is solved iteratively in order to establish the position of the resultant force on the arc of cut for each data point. The common solution to the equations of the straight line of the action of the resultant force and the circle described by the circumference of the grinding wheel gives the root of the point of intersection of the resultant force on the arc of cut for each data point. The results are separated into those which are in full depth of cut and those which are not.

2040 - 2070 Print out of the titles for tangential and normal forces and the tangential/normal force ratio.

2080 - 2130 From the solution of the resultant force and its position the tangential and normal forces can be resolved and are printed out.

2140 - 2340 The tabulated forces which occurred at full depth of cut are summed and the mean value printed out.

2350 The stock removal rate is calculated (V4).

2360 - 2420 Titles for the stress distribution, normal, tangential, maximum normal infeed rate and position on the arc.

2430 - 2780 A series of calculations allow an estimate of the stress distribution to be made. The results are no more than an estimate as they are not calculated from direct measurements, however they can provide a factor for comparison.

2790 - 2910 The mean power flux (P2) is calculated.

2920 - 2950 Print out of titles for specific energy.

2960 - 3050 The specific energy is calculated for every data point and tabulated.

3060 - 3150 Results for presentation in a summary are calculated.

3160 Provision for conventional tests - exclusion of the calculation for the dresser infeed/rev.

3170 - 3430 Summary of results.

3440 - 3460 Titles for a theoretical stress distribution assuming linearity. (after the work of Shafto).

3470 - 3950 Using the method of Shafto (Ref. 20) the maxima and minima of an assumed linear stress distribution are calculated.

3960 - 4040 Print out of the theoretical max and min tangential and normal stresses and a theoretical position for the position of the resultant force on the arc of cut.

4050 - 4200 Data storage space.

4210 END.

Appendix Fig. 7.1

```
0010  REM    SCRAP is an interactive program which calculates the
0020  REM    rig settings required for your test conditions. There
0030  REM    is a second part to the program which is analytical.
0040  REM    Data from the data recording system on the Creep-Feed
0050  REM    Surface Grinding Rig is input between lines 4050-4200
0060  REM    The forces,power,specific energy and stock removal
0070  REM    rates are calculated from this data in conjunction
0080  REM    with the rig settings.
0090  REM
0100  PRINT '       *****   *****   *****      *      *****'
0110  PRINT '       *       *       *   *     * *     *    *'
0120  PRINT '       *       *       *   *    *   *    *    *'
0130  PRINT '        ***    *       *****    *****    *****'
0140  PRINT '           *   *       * *      *   *    *'
0150  PRINT '           *   *       *  *     *   *    *'
0160  PRINT '       *****   *****   *   *    *   *    *'
0170  PRINT
0180  PRINT 'RIG SETTINGS CALCULATOR & RESULTS ANALYSIS PROGRAM.'
0190  PRINT
0200  PRINT
0210  PRINT '                    RIG SETTINGS.'
0220  PRINT '                    ************'
0230  PRINT
0240  PRINT
0250  PRINT 'ENTER TEST NUMBER.'
0260  INPUT A
0270  IF A=0 GOTO 4210
0280  PRINT 'ENTER WHEEL SPEED IN M/S'
0290  INPUT W1
0300  PRINT 'ENTER REQUIRED MAXIMUM NORMAL INFEED RATE IN MM/MIN.'
0310  INPUT O1
0320  PRINT 'ENTER WHEEL DIAMETER IN MM.'
0330  INPUT D
0340  PRINT 'ENTER WORKPIECE FEED RATE AT 1000 R.P.M. IN MM/MIN.'
0350  INPUT O2
0360  PRINT 'ENTER DRESSING RATIO.'
0370  INPUT R8
0380  REM  -------- D5 IS THE DIAMETER OF THE DRESSER IN MM. -------
0390  D5=100
0400  PRINT 'ENTER WIDTH OF CUT IN MM.'
0410  INPUT W
0420  PRINT 'ENTER LENGTH OF SPECIMEN IN MM.'
0430  INPUT VO
0440  R=D/2
0450  V2=((W1*60000)/(3.14159*D))
0460  V1=(O2*V2)/1000
0470  O3=O1*(R/V1)
0480  D1=(D-SQR((D*D)-(4*O3*O3)))/2
0490  C1=ATN(O3/(R-D1))
0500  A1=R*C1
0510  T1=A1/(1000*W1)
0520  M1=(D1*V1*T1)/60
0530  PRINT
0540  PRINT
0550  PRINT
0560  PRINT 'WHEEL R.P.M. IS ';V2
0570  PRINT
0580  PRINT 'EXPECTED DEPTH OF CUT IS ';D1;'MM.'
```

```
0590  PRINT
0600  PRINT 'ACTUAL WORKPIECE FEED RATE IS ';V1;'MM/MIN.'
0610  PRINT
0620  H=(D/D5)*R8*V2
0630  PRINT 'FOR A DRESSING RATIO OF ';R8;'THE DRESSER'
0640  PRINT 'MUST BE RUN AT ';H;'R.P.M.'
0650  PRINT
0660  PRINT 'IF YOU HAVE CW,TAN & WEDGE ANGLE TYPE 1 IF NOT TYPE 0.'
0670  INPUT 07
0680  IF 07=0 GOTO 860
0690  PRINT 'ENTER CW,TAN AND WEDGE ANGLE IN DEGREES.'
0700  INPUT Y1,Y2,Y3
0710  Y4=TAN(2*3.14159*(Y3/360))
0720  V3=((Y1*V1*Y4)/(1+(Y4/Y2)))
0730  PRINT
0740  PRINT 'DRESSER INFEED RATE IS ';V3;'MM/MIN.'
0750  PRINT
0760  B4=ATN(V3/V1)
0770  PRINT 'SLOPE OF WORK IS ';B4;'RADIANS.'
0780  PRINT
0790  Y0=V0*B4
0800  PRINT 'PACKING HEIGHT FOR PREPARATION IS ';Y0;'MM.'
0810  PRINT
0820  D9=(((03/V1)*V3)+D1)
0830  PRINT 'SET DEPTH OF CUT IS ';D9;'MM.'
0840  PRINT '                          **********'
0850  PRINT
0860  PRINT 'ARC LENGTH IS';A1;'MM.'
0870  REM
0880  REM -- FOR CONVENTIONAL GRINDING LINE 910 MUST READ V3=(FEED) -
0890  REM -- WHERE (FEED) IS EQUAL TO A CALCULATED DRESSER INFEED ---
0900  REM ------- RATE TO CAUSE THE MEASURED WHEEL WEAR. ------------
0910
0920  PRINT
0930  PRINT 'TIME FOR GRIT TO TRAVERSE THE FULL ARC IS ';T1;'SECS.'
0940  PRINT
0950  PRINT 'AMOUNT OF MATERIAL REMOVED PER UNIT WIDTH IN'
0960  PRINT 'ONE SWEEP OF THE ARC OF CUT IS ';M1;'MM3.'
0970  PRINT
0980  PRINT 'DO YOU REQUIRE ANY RESULTS ANALYSIS.'
0990  PRINT 'IF SO TYPE 1 IF NOT TYPE 0.'
1000  INPUT K9
1010  IF K9=0 GOTO 4210
1020  PRINT
1030  PRINT
1040  PRINT '                          ANALYSIS.'
1050  PRINT '                          ********'
1060  PRINT
1070  PRINT
1080  PRINT 'ENTER THE NUMBER OF READINGS.'
1090  INPUT Z
1100  PRINT 'ENTER TIME INTERVAL BETWEEN READINGS IN SECS.'
1110  INPUT I1
1120  PRINT 'ENTER ACTUAL DEPTH OF CUT IN MM.'
1130  INPUT D2
1140  PRINT
1150  D1=SQR((R*R)-((R-D2)*(R-D2)))
1160  DIM F(50,3),N(50,3),L(50,3)
1170  DIM Q(50),T(50),A(50),B(50)
1180  DIM M(50),G(50),P(50),S(50)
```

```
1190  DIM J(50),H(50),R(50)
1200  DIM D(50),E(50)
1210  DIM W(50),U(50)
1220  DIM X(50),Z(50),O(50)
1230  DIM C(50),Y(50)
1240  FOR J=1 TO 3
1250  FOR K=1 TO Z
1260  READ N(K,J)
1270  NEXT K
1280  NEXT J
1290  FOR I=1 TO Z
1300  PRINT N(I,1),N(I,2),N(I,3)
1310  NEXT I
1320  FOR J=1 TO 3
1330  E=(N(1,J)-N(Z,J))/(Z-1)
1340  FOR K=2 TO Z-1
1350  N(K,J)=N(K,J)+(E*(K-1))
1360  N(K,J)=N(K,J)-N(1,J)
1370  NEXT K
1380  NEXT J
1390  FOR I=1 TO Z
1400  REM -------- THIS IS THE DYNAMOMETER CALIBRATION MATRIX. -------
1410  N(I,1)=N(I,1)*5.835
1420  N(I,2)=N(I,2)*5.375
1430  N(I,3)=N(I,3)*(-5.666)
1440  L(I,1)=(N(I,2)*(.007))+(N(I,3)*(-.011))
1450  L(I,2)=(N(I,1)*(-.048))+(N(I,3)*(.004))
1460  L(I,3)=(N(I,1)*(-.071))+(N(I,2)*(.007))
1470  REM ------------------------------------------------------------
1480  F(I,1)=N(I,1)+L(I,1)
1490  F(I,2)=N(I,2)+L(I,2)
1500  F(I,3)=N(I,3)+L(I,3)
1510  NEXT I
1520  PRINT
1530  PRINT
1540  PRINT '                                FORCES IN NEWTONS.'
1550  PRINT '                               **********************'
1560  PRINT
1570  % '     LHV                RHV                HRZ                H/V'
1580  % '    *****              *****              *****              *****'
1590  V1=V1/60
1600  FOR I=2 TO Z-1
1610  T(I)=F(I,1)+F(I,2)
1620  Q(I)=F(I,3)/T(I)
1630  A(I)=((F(I,1)*133)/T(I))-2
1640  B(I)=(V1*(I-1)*I1)-D1
1650  M(I)=A(I)-B(I)
1660  NEXT I
1670  FOR I=2 TO Z-1
1680  PRINT F(I,1),F(I,2),F(I,3),Q(I)
1690  NEXT I
1700  PRINT
1710  PRINT
1720  PRINT ' TORQUE NM.      POWER WATTS.      POS. OF RESULTANT.'
1730  PRINT '************    **************    **********************'
1740  R1=D/2
1750  FOR I=2 TO Z-1
1760  R=R1-((V3/60)*(I1*(I-1)))
1770  P4=ATN(Q(I))
1780  P5=M(I)/Q(I)
```

```
1790  P6=343.62+P5
1800  P7=Q(I)*P6
1810  T5=1+(Q(I)*Q(I))
1820  T6=(2*P7*Q(I))
1830  T7=((P7*P7)-(R*R))
1840  E4=4*T5*T7
1850  E5=SQR((T6*T6)-E4)
1860  T8=(-T6-E5)/(-2*T5)
1870  T9=SQR(ABS((R*R)-(T8*T8)))
1880  F4=ATN(T9/T8)
1890  A3=SQR((R*R)-((R-D2)*(R-D2)))
1900  A4=ATN(A3/(R-D2))
1910  E(I)=F4/A4
1920  F5=SQR(ABS((T(I)*T(I))+(F(I,3)*F(I,3))))
1930  P9=P6*F5*(SIN(P4))
1940  G(I)=P9*.001
1950  P(I)=G(I)*V2*2*3.14159/60
1960  J(I)=P9/R
1970  H(I)=SQR((F5*F5)-(J(I)*J(I)))
1980  R(I)=J(I)/H(I)
1990  IF B(I)>=0 GOTO 2020
2000  PRINT G(I);'*',P(I);'*',E(I);'*'
2010  GOTO 2030
2020  PRINT G(I);' ',P(I);' ',E(I)
2030  NEXT I
2040  PRINT
2050  PRINT
2060  PRINT ' TAN. FORCE      NORM. FORCE        RATIO'
2070  PRINT '************   **************      *******'
2080  FOR I=2 TO Z-1
2090  IF B(I)>=0 GOTO 2120
2100  PRINT J(I);'*',H(I);'*',R(I);'*'
2110  GOTO 2130
2120  PRINT J(I);' ',H(I);' ',R(I)
2130  NEXT I
2140  C=0
2150  H9=0
2160  H3=0
2170  FOR I=2 TO Z-1
2180  IF B(I)<0 GOTO 2220
2190  C=C+1
2200  H9=H9+J(I)
2210  H3=H3+H(I)
2220  NEXT I
2230  H9=H9/C
2240  H3=H3/C
2250  N5=H9/H3
2260  PRINT
2270  PRINT
2280  PRINT 'MEAN TANGENTIAL FORCE IS ';H9;'NEWTONS.'
2290  PRINT
2300  PRINT 'MEAN NORMAL FORCE IS ';H3;'NEWTONS.'
2310  PRINT
2320  PRINT 'RATIO OF FORCES IS ';N5
2330  PRINT
2340  PRINT
2350  V4=V1*W*D2*60
2360  PRINT
2370  PRINT
2380  PRINT '                    STRESS DISTRIBUTION N/MM2.'
```

```
2390  PRINT '                    ********************************'
2400  PRINT
2410  % '  NORMAL       TANGENTIAL          MNIFR          POS.ON ARC'
2420  % ' ********    ************       *******       ************'
2430  X9=ATN(D1/(R1-D2))
2440  FOR I=2 TO Z-1
2450  IF B(I)>0 GOTO 2560
2460  R=R1-((V3/60)*(I1*(I-1)))
2470  C9=SQR((R*R)-(B(I)*B(I)))
2480  A8=R*ATN(-B(I)/C9)
2490  X8=A8/R
2500  X(I)=X9-X8
2510  Z(I)=X(I)*R*W
2520  O(I)=(X(I)/2)+X8
2530  W(I)=SIN(O(I))*V1*60
2540  X9=X8
2550  NEXT I
2560  C(2)=F(2,3)
2570  Y(2)=T(2)
2580  FOR I=3 TO Z-1
2590  IF B(I)>0 GOTO 2630
2600  Y(I)=T(I)-T(I-1)
2610  C(I)=F(I,3)-F(I-1,3)
2620  NEXT I
2630  FOR I=2 TO Z-1
2640  IF B(I)>0 GOTO 2790
2650  D7=ATN(Y(I)/C(I))
2660  D8=D7-O(I)
2670  D6=SIN(D8)
2680  D4=COS(D8)
2690  UO=Y(I)*Y(I)
2700  TO=C(I)*C(I)
2710  RO=SQR(ABS(UO-TO))
2720  S7=(RO*D6)/Z(I)
2730  S6=(RO*D4)/Z(I)
2740  FO=R*O(I)
2750  PRINT S7,S6,W(I),FO
2760  NEXT I
2770  PRINT
2780  PRINT
2790  C=0
2800  P1=0
2810  M7=0
2820  FOR I=2 TO Z-1
2830  IF B(I)<0 GOTO 2870
2840  C=C+1
2850  P1=P1+P(I)
2860  M7=M7+E(I)
2870  NEXT I
2880  P1=P1/C
2890  M7=M7/C
2900  R1=R1-((V3/60)*(I1)*(Z-2))/2
2910  P2=P1/(W*R1*(ATN((SQR((R1*R1)-((R1-D2)*(R1-D2))))/(R1-D2))))
2920  PRINT
2930  PRINT
2940  PRINT 'SPECIFIC ENERGY J/MM3.'
2950  PRINT '**********************'
2960  FOR I=2 TO Z-1
2970  S(I)=60*P(I)/V4
2980  IF B(I)>=0 GOTO 3010
```

```
2990  PRINT S(I);'*'
3000  GOTO 3020
3010  PRINT S(I)
3020  NEXT I
3030  S=60*P1/V4
3040  PRINT
3050  PRINT
3060  T4=V4/W
3070  Z6=(D-(2*V3))
3080  M6=(3.14159/4)*((D*D)-(Z6*Z6))
3090  G=T4/M6
3100  D3=D-(2*(Z-2)*(V3/60)*I1)
3110  U=V4/(3.14159*((D+D3)/2)*W)
3120  Z8=2*V1*D1*60/D
3130  S8=V3/V2
3140  S0=Z8/V2
3150  B0=V4/V2
3160  IF 07=0 GOTO 3190
3170  PRINT
3180  PRINT 'DRESSER INFEED/REV. IS ';S0;'MM.'
3190  PRINT
3200  PRINT 'MAXIMUM NORMAL INFEED/REV. IS ';S0;'MM.'
3210  PRINT
3220  PRINT 'VOLUME OF MATERIAL REMOVED /REV. IS';B0;'MM3.'
3230  PRINT
3240  PRINT 'VOLUMETRIC REMOVAL RATE IS ';V4;'MM3/MIN.'
3250  PRINT
3260  PRINT 'VOLUMETRIC REMOVAL RATE/UNIT WIDTH IS ';T4;'MM3/MIN/MM.'
3270  PRINT
3280  PRINT 'MEAN POWER IS ';P1;'WATTS.'
3290  PRINT
3300  PRINT 'MEAN POWER FLUX IS ';P2;'MW/M2.'
3310  PRINT
3320  PRINT 'MEAN SPECIFIC ENERGY IS ';S;'J/MM3.'
3330  PRINT
3340  PRINT 'MEAN WHEEL FACTOR IS ';U;'VOLUME OF WORK REMOVED'
3350  PRINT '                                  /MIN/MM2 OF WHEEL'
3360  PRINT
3370  PRINT 'MAXIMUM NORMAL INFEED RATE IS ';Z8;'MM/MIN.'
3380  PRINT
3390  PRINT 'MEAN POSITION OF THE RESULTANT ON THE ARC IS ';M7
3400  PRINT
3410  PRINT 'G RATIO IS ';G
3420  PRINT
3430  PRINT
3440  PRINT '    THE FOLLOWING STRESS CALCULATIONS ARE MADE'
3450  PRINT '     ASSUMING A LINEAR STRESS DISTRIBUTION'
3460  PRINT
3470  G9=SQR((R1*R1)-((R1-D2)*(R1-D2)))
3480  L=ATN(G9/(R1-D2))
3490  L0=SIN(L)
3500  L1=(1-COS(L))
3510  L2=COS(2*L)
3520  L3=SIN(2*L)
3530  L4=(1-L2)/4
3540  L5=(L/2)-(L3/4)
3550  L6=(L5*L0-L1*L4)
3560  L7=(L*L5-L1*L1)
3570  L8=(L*L4-L0*L1)
3580  C0=0
```

```
3590   T=0
3600   V=0
3610   HO=0
3620   FOR I=2 TO Z-1
3630   IF B(I)<0 GOTO 3680
3640   CO=CO+1
3650   T=G(I)+T
3660   V=T(I)+V
3670   HO=F(I,3)+HO
3680   NEXT I
3690   T=T/CO
3700   V=V/CO
3710   HO=-HO/CO
3720   J9=(L6*T*1000)+(V*R1*L8)+(HO*R1*L7)
3730   J8=(HO*R1*L8)-(V*R1*L7)
3740   J7=L6*T*1000
3750   EO=J8*J8
3760   E1=4*J9*J7
3770   KO=(SQR(EO-E1))/(2*J9)
3780   M=KO-(J8/(2*J9))
3790   MO=-KO-(J8/(2*J9))
3800   PRINT
3810   S1=(V*(L1-(MO*LO)))-(HO*((MO*L1)+LO))
3820   S2=((L1*L4)-(LO*L5))*(1+(MO*MO))
3830   S3=S1/(S2*W*R1*V1*60)
3840   S4=(V*(L5-(MO*L4)))-(HO*((MO*L5)+L4))
3850   S5=L6*(1+(MO*MO))
3860   S9=S4/(S5*W*R1)
3870   Q9=S9+(S3*Z8)
3880   Q8=MO*Q9
3890   Q7=MO*S9
3900   Q6=MO*S3
3910   P8=(Q7+((2*(Q8-Q7))/3))/(2*(Q7+((Q8-Q7)/2)))
3920   Q=(P8*R1*Z8)/(V1*60)
3930   X7=SQR((R1*R1)-(Q*Q))
3940   X6=(ATN(Q/X7))
3950   X5=X6/L
3960   PRINT 'MAX. NORMAL STRESS IS ';Q9;'N/MM2'
3970   PRINT
3980   PRINT 'NORMAL STRESS AT ZERO MNIFR. IS ';S9;'N/MM2.'
3990   PRINT
4000   PRINT 'MAX. TANGENTIAL STRESS IS ';Q8;'N/MM2.'
4010   PRINT
4020   PRINT 'RUBBING STRESS IS ';Q7;'N/MM2 '
4030   PRINT
4040   PRINT 'THEORETICAL POSITION OF THE RESULTANT IS ';X5
4050
4200
4210   END
```

Appendix Fig. 7.2

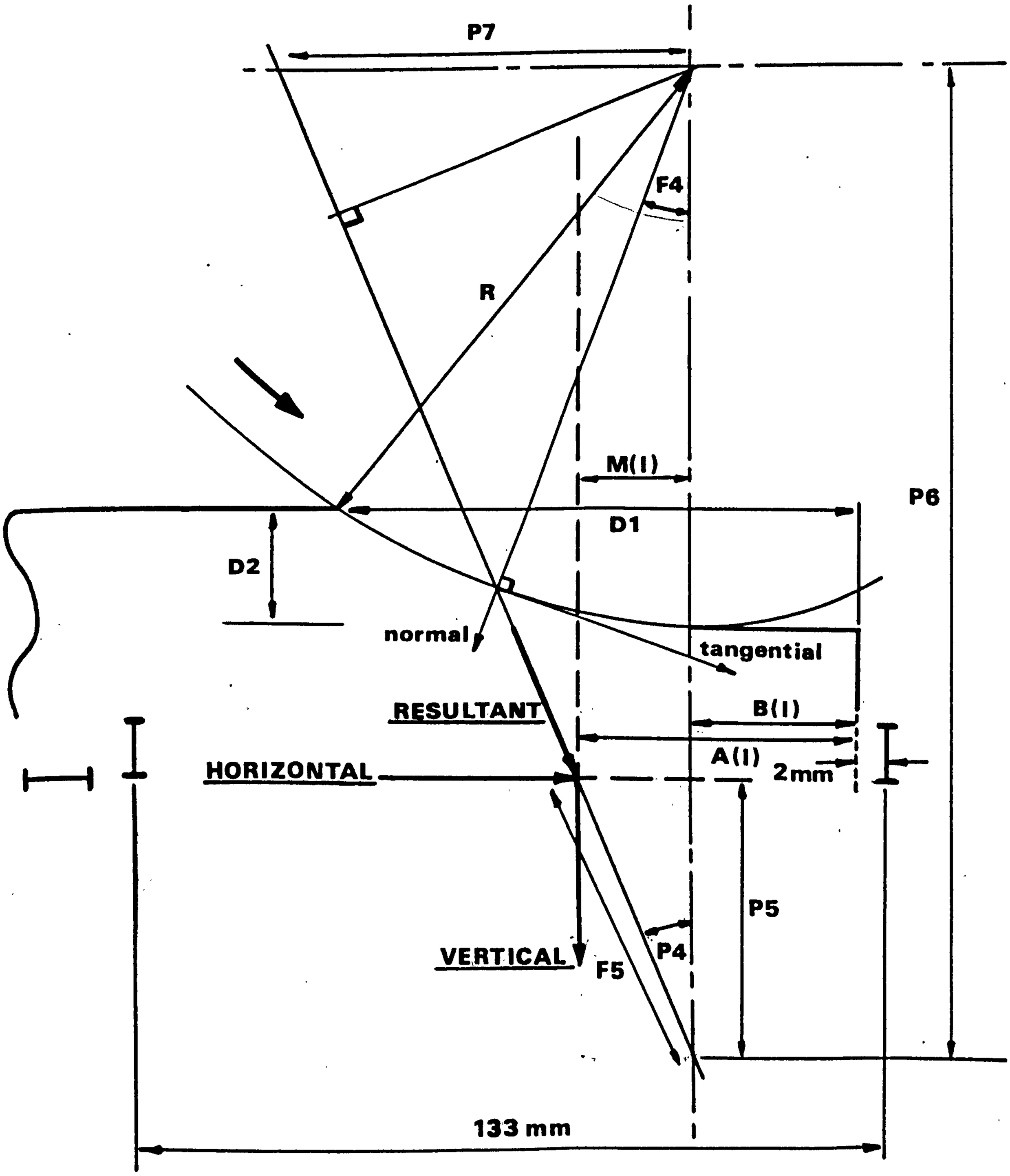

THE ALPHA-NUMERIC CHARACTERS SHOWN IN THE FIGURE REFER TO THOSE USED IN THE COMPUTER PROGRAM - APPENDIX 7.1.